University of Ghana http://ugspace.ug.edu.gh

DESIGN, CONSTRUCTION AND DOSIMETRIC CONSIDERATIONS OF CERROBEND COMPENSATOR FOR HIGH ENERGY PHOTON BEAM

By

AINADINE EBRAIMO MOMADE

(10435644)

This thesis/dissertation is submitted to the University of Ghana, Legon in partial fulfillment of the requirement for the award of

MPhil Medical Physics degree

July, 2015

University of Ghana http://ugspace.ug.edu.gh

DESIGN, CONSTRUCTION AND DOSIMETRIC CONSIDERATIONS OF CERROBEND COMPENSATOR FOR HIGH ENERGY PHOTON BEAM

By

AINADINE EBRAIMO MOMADE

(10435644)

This thesis/dissertation is submitted to the University of Ghana, Legon in partial fulfillment of the requirement for the award of

MPhil Medical Physics degree

July, 2015

University of Ghana http://ugspace.ug.edu.gh

DECLARATION

This thesis is the result of research work undertaken by Ainadine Ebraimo Momade in the Department of Medical Physics, University of Ghana, under the supervision of Prof. A. W. K. Kyere, Prof. J. H. Amuasi and Mr. S. N. Tagoe.

Ainadine Ebraimo Momade

(Student)

Prof. A. W. K. Kyere

(Principal Supervisor)

Prof. J. H. Amuasi

(Co-Supervisor)

Mr. Samuel Nii Adu Tagoe.

(Co-Supervisor)

University of Ghana http://ugspace.ug.edu.gh

DEDICATION

With all the love and affection I dedicate my work to my parents Ebraimo Momade and Muachumo Omar, to my wife Idalina Constâncio Nhaca, my children, Ibraimo Ainadine Momade, Akil Ainadine Momade, Denilson Ainadine Momade and Tamara Ainadine Momade.

University of Ghana http://ugspace.ug.edu.gh

ACKNOWLEDGMENT

It is a pleasure for me to recognize my dependence on many who, in one way or the other, have contributed to this work. First I acknowledge God who has guided and protected me and then thank my parents, Ebraimo Momade and Muachumo Omar, to whom I owe everything I am or long to be one day. I also wish to acknowledge the International Atomic Energy Agency (IAEA) and the Government of Mozambique for the financial assistance throughout my studies. I thank all my professors and lecturers who, over the two years of the course, and with great sacrifice and generosity have imported to me their knowledge in medical Physics. I thank also my supervisors, Prof. Kyere, Prof. Amuasi and Mr. Tagoe, for the way they gave their support and for everything they have done for this work to be ready. I thank Mr. Tesfaldet Habtemariam Teclehaimanot and Molalgn Gebresenbet Woldemariyam whose comments and suggestions were rewarding and well received. My collogue Elio Mendicinho De Aguiar Mendicinho Malela for the good company during the first year in this country. I thank my colleagues Philip Odonkor and Yaa Akomah Asenso for their good company during the times of phantom road construction. I keep a sense of gratitude to my brothers and my wife Idalina for the unconditional support to my fellow course mater and their day-to-day helpful practical comments. I leave here with a very special gratitude to my friend Dr. Lucilio Dos Santos for his unconditional support in providing me with the important references for the work. I thank the staff of Medical Physics department and the library staff for facilitating access to bibliographic material during my academic period and the thesis write up. I acknowledge all the workers of the Korle-Bu teaching hospital in particular for the National Center for Radiotherapy and Nuclear Medicine for their patience, for SGMC for providing their ionization chamber for my data collection. I thank the people of Ghana for the hospitality they have given me

University of Ghana http://ugspace.ug.edu.gh

during the two years of staying in the country. Without mentioning names, I want to thank all those who were directly or indirectly connected to me and wished me success.

University of Ghana http://ugspace.ug.edu.gh

TABLE OF CONTENTS

University of Ghana http://ugspace.ug.edu.gh

University of Ghana http://ugspace.ug.edu.gh

University of Ghana http://ugspace.ug.edu.gh

University of Ghana http://ugspace.ug.edu.gh

University of Ghana http://ugspace.ug.edu.gh

LIST OF TABLES

University of Ghana http://ugspace.ug.edu.gh

LIST OF FIGURES

University of Ghana http://ugspace.ug.edu.gh

University of Ghana http://ugspace.ug.edu.gh

University of Ghana http://ugspace.ug.edu.gh

University of Ghana http://ugspace.ug.edu.gh

University of Ghana http://ugspace.ug.edu.gh

LIST OF PLATES

University of Ghana http://ugspace.ug.edu.gh

LIST OF ABBREVIATIONS

IMRT	Intensity Modulated Radiotherapy
MLC	Mult-Leaf Collimator
TPS	Treatment Planning System
EBT	External Beam Radiotherapy
ICRU	International Commission on Radiological Units
PTV	Planning Target Volume
CT	Computer Tomography
PET	Positron Emission Tomography
MRI	Magnetic Resonance Imaging
KBTH	Korle-Bu Teaching Hospital
LINAC	Linear Accelerator
2D	Two Dimensions
3-D CRT	Three-Dimension Conventional Radiotherapy
QA	Quality Assurance
SSD	Source-Surface Distance
SAD	Source-Axis Distance
HVL	Half Value Layer

University of Ghana http://ugspace.ug.edu.gh

MSF	Mult State Field
DMLC	Dynamic Multleaf Collimator
OARs	Organs at Risk
MU	Monitor Unit
QC	Quality Control
3-DRTP	Tree-Dimension Radiation Treatment Planning
CD-ROM	Compact Disc Read-Only Memory
DICOM	Digital Imaging and Communication in Medicine
SGMC	Sweden Ghana Medical Center
TRS	Technical Report Series
NCRNM	National Center for Radiotherapy and Nuclear Medicine
SDD	Source-Detector Distance
BEV	Beam Eye View
IBA	Ion Beam Applications
dpi	dots per inch

University of Ghana http://ugspace.ug.edu.gh

ABSTRACT

In external beam radiotherapy (EBRT), dose optimization is achieved by conforming the dose distribution to the shape of the intended target whilst minimizing radiation to normal tissues in close proximity to the target. This can be achieved by modulating the intensities of the radiation across the radiation portals forming the irradiation geometry used for the treatment. Compensators may be used to achieve the above effect based on intensity fluence map generated with inverse planning for the irradiated region. For Treatment planning systems (TPSs) without inverse planning capabilities, bolus placed on the surface of the patient at point of beam entrance may be used to provide the required intensity modulation of the beam. During treatment, compensating filters (compensators) placed at distance from the patient's skin are used to mimic the dosimetric effects of the radiation within the irradiated region produced with the bolus to preserve the skin sparing effect of the radiation. The shape of the compensating filters needs to be adjusted for beam divergence and reduction of scatter contribution to the deposition of dose within the patient Procedures for the design and construction of cerrobend compensator had been developed and proposed for a cobalt- 60 beam and Prowess Panther version 4.6 TPS without inverse planning capabilities. Transmission measurements were done with the compensator (in the form of cerrobend slabs) mounted on a tray within the beam for various treatment depths and field sizes in a full scatter water phantom and the same measurements repeated with the tray, but without the compensator such that the thicknesses of the phantom were adjusted to get the same doses as before. These measurements were used to develop and propose algorithm for the conversion of bolus thickness to compensator thickness which would produce the same dosimetric effect as the appropriate bolus thickness. Correction

University of Ghana http://ugspace.ug.edu.gh

factors were introduced into the algorithm to account for the effects of field size, treatment depth and variation in the thickness of the compensating filter on the dose distribution within the irradiated region. To check the efficacy of the developed and proposed method and also, a number of compensators, some in the form of step wedges were designed and constructed based on the developed and proposed procedure for various treatment depths and field sizes. The constructed compensators on trays were mounted on the accessory holder of Equinox 100 cobalt - 60 teletherapy machine and the dose distribution beneath the compensator measured in a solid water phantom with a Farmer type ionization chamber and Gafchronic films at the appropriate treatment depth. The doses obtained were compared with corresponding dose distributions generated with the TPS for the solid water phantom with the bolus on the surface of phantom. Percentage deviation of the doses ranges from $\pm 1.69\%$ to $\pm$ 16.36% with a mean of $\pm 9.51\%$ and standard deviation of $\pm 5.64\%$. Though most of the deviations were within the tolerance of ± 5% required for external beam radiotherapy, there were significant number of the deviations beyond the tolerance due to inherent errors associated with the manual fabrication of the mould for the cerrobend, which needs to be streamlined.

University of Ghana http://ugspace.ug.edu.gh

CHAPTER I

1.0. INTRODUCTION

1.1. BACKGROUND

Cancer is a significant health care problem. On average about half of all cancer patients are treated with radiation therapy worldwide (IAEA TRS430, 2004).

Radiotherapy, also referred to as radiation therapy, radiation oncology or therapeutic radiology is one of the three modalities used in the management of malignant disease (cancer), the other two being chemotherapy and surgery (Suntharalingamn et al, 2005). Radiotherapy uses ionizing radiation to eradicate cancerous cells with the least possible damage to normal tissues.

The first therapeutic use of ionizing radiation was demonstrated in 1897 by Wilhelm Alexander Freud, a German surgeon before Vienna Medical Society when he demonstrated the disappearance of a hairy mole following treatment with x-ray (Hall, 2000). The first recorded experiment in radiobiology was also performed by Becquerel when he advertently left a radium container in his vest pocket and subsequently described the skin erythema two weeks later (Hall, 2000).

The modalities of radiotherapy are divided into two types, tele-therapy and brachytherapy. Brachytherapy is a method of treatment in which sealed radiation sources are placed into the tumour or in close proximity to the tumour by interstitial, intracavitary or surface application to deliver radiation at short distances (Khan, 2010). Tele-therapy is a treatment modality in which the source of radiation is remote from the target being treated. Heavy charged particles or ions may also be used for this type of treatment. With reference to the mode of application of the radiation this type of radiation therapy is referred to as external

University of Ghana http://ugspace.ug.edu.gh

beam radiation therapy or radiotherapy (EBRT). In EBRT, the methodology of treatment depends on different factors, which may include the shape and size of the tumour to be treated within the patient, sparing of normal tissues within the vicinity of the target from excessive irradiation, financial constraints and the quest of optimization of radiation dose to the target. In addition, the patient to be treated may also present with irregular surface topographies at the point of beam entrance and tissue heterogeneities within the irradiated region.

There are different treatment techniques ranging from 2-D conventional radiotherapy to more advanced intensity modulated radiotherapy (IMRT). IMRT is a treatment planning and delivery technique that can greatly improve the radiation dose optimization process and to conform the dose distribution to the irradiated target. This technique is also called conformal radiotherapy which uses radiation field shaping and intensity variation across the radiation field to conform the radiation dose to the irregular shaped target whilst reducing the dose to normal tissues in close proximity to or within the vicinity of the target. Implementation of this treatment technique is very capital intensive as the conventional therapy machine needs to be equipped with multileaf collimator and the TPS used in the patient treatment simulations or planning must have inverse planning functionality. In inverse planning, the planner chooses or defines the irradiation geometry and the dose distribution as well as the dose constraints required within the irradiated region, and the TPS works backward to get the most suitable beam modulations and weightings that would result in the dose distributions required or prescribed. These adaptations need to be complimented with the requisite manpower and training, which comes with additional cost. For countries with scarce resources, this can be implemented with conventional teletherapy

University of Ghana http://ugspace.ug.edu.gh

machine and forward planning treatment planning system (TPS) using compensating filter (or compensators) to modulate the intensity of the radiation across the radiation field. According to Chang (2004), a compensator, though traditional beam modifying device, can be used for effective implementation of IMRT delivery technique (referred to as compensator based IMRT).

In compensator based IMRT, the compensator is used not in the sense of compensating for missing tissue or tissue heterogeneity but as beam intensifier similar to dynamic wedges or multileaf collimators (MLC). The goal is to achieve dose uniformity throughout the whole target volume and, more importantly to spare critical structure based on dose and dose volume constraints prescribed by the clinicians for specific patient (Jiango et al., 1998). Therefore, compensators are designed to produce an optimized primary fluency profile at the patient's surface. This is achieved by modulating the intensities of the radiation across the radiation portals forming the irradiation geometry used for the treatment.

There are various methods by which compensators may be constructed. According to Williams & Thwaites (2000), the three main method in use are: grid-blocking system, contour system and a system using machined compensating filters. The first compensators made by Ellis et al. (1958) were constructed by stacking aluminum pillars or blocks. Another method reported by Lam et al. (1983) describes the construction of compensators from thin sheets of lead. Today, compensators are usually made from molts filled with molten alloy or wax. Using molds is advantageous since it results in compensators with smoother surfaces and thus greater accuracy.

To make a compensator for an IMRT practice, it is required to calculate the effective attenuation coefficient (μ_{eff}) of its materials, which is affected by various factors such as

University of Ghana http://ugspace.ug.edu.gh

field size, depth, off- axis distance, compensator thickness (Haghparast et al, 2013). A number of elements have been used to form compensators which include tungsten-epoxy mixture (Xu et al, 2002), Lucite (Khan et al, 1970), gypsum (Weeks et al, 1988), tin-wax (Van et al, 1995), tin (Chang et al, 2000), cerrobend (Waltz et al, 1973), steel (Van et al, 1995), aluminum (Ellis et al, 1959), brass (Ellis et al, 1959), lead (Leung et al, 1974; Cunningham et al, 1976; Andrew et al, 1982; Spicka et al, 1988), coper and brass (Teclehaimanot, 2014). In this study, a cerrobend compensator that mimics the dosimetric effects of bolus placed on the surface of the phanton will be constructed. Film and an ionization chamber will be used for dosimetric measurements and for verification of measured dose distribution and compared with those calculated with the Prowess Panther TPS software at Korle-Bu Teaching Hospital.

1.2. PROBLEM STATEMENT

In external beam radiotherapy (EBRT), dose optimization is achieved by conforming the dose distribution to the shape of the intended target whilst minimizing radiation to normal tissues in close proximity to the target. Most dosimetric measurements are done with normal beam incidence (on flat surface) and homogenous media, however patient usually presents with irregular surface contour at the point of beam entrance and tissue heterogeneities within irradiated region. The main aim of radiation therapy is to deliver uniform dose distribution within +7 % and –5 % of the dose prescription without exceeding the tolerance dose of the critical structure around tumor volume (*ICRU report 50, 1993)*.

University of Ghana http://ugspace.ug.edu.gh

To achieve this goal, the above irregularities should be corrected. Thus different studies suggested and implemented bolus which is a tissue equivalent material placed at the surface of the patient to compensate the missing tissue. However, this technique compromises on the skin sparing effect of megavoltage beam use in treating the patient, resulting in relatively high doses just beneath the bolus. This is because, the buildup region occurs within the bolus and the depth of maximum dose (d_{max}) may be on the skin surface. To resolve this, a compensator is used in place of the bolus, which is placed about 15 - 20 cm from the patient's skin to produce the same dosimetric effect as the bolus within the irradiated region such that the skin sparing effect of the megavoltage beam is maintained. In retrospect, compensators had been used as a means of correcting for both surface irregularity and tissue heterogeneity in external beam radiotherapy (EBRT), but currently these are achieved with MLC based IMRT.

Advanced technological innovations in anatomic and functional imaging modalities (CT, MRI, PET, and US) have led to improved visualization and the delineation of tumour. Radiation treatment planning and delivery techniques have also seen a marked improvement. Intensity modulated radiotherapy (IMRT) provides a high degree of dose conformity to the planning target volume (PTV) and the conformal avoidance of organs at risk. Therefore radiation field is not only geometrically shaped to conform to the outline of the planning target volume at the beams eye view, but is also intensity modulated.

The National Centre for Radiotherapy and Nuclear Medicine (NCRNM), of Korle-Bu Teaching Hospital (KBTH) presently uses paraffin wax for construction of a compensator and cerrobend for shielding blocks, but there is a need to implement physical compensator based IMRT using materials which are available in the Centre and is also inexpensive. This

University of Ghana http://ugspace.ug.edu.gh

research will focus on the design, construction and dosimetric considerations of cerrobend compensators to modulate the intensities of the radiation across the radiation portals forming the irradiation geometry used for the treatment.

1.3. OBJECTIVES

1.3.1. GENERAL OBJECTIVE

The general objective of this work is to design and construct a compensator using cerrobend materials and forward planning TPS.

1.3.2. SPECIFIC OBJECTIVES

- To investigate the dose contribution from scattered photons generated within the compensator on head scatter factor.
- To evaluate dosimetric accuracy and dose coverage with fabricated cerrobend compensator.
- To compare and evaluate measured dose with cerrobend compensator on block tray and planned dose with bolus on the surface of the phantom.
- To evaluate the variation of dose distribution by the compensator and with bolus on the surface of the phantom.

University of Ghana http://ugspace.ug.edu.gh

1.4. SCOPE AND LIMITATION

The scope of this thesis is in the area of the IMRT by means of physical compensators specifically using cerrobend which are manually fabricated. In most centres which are practicing IMRT, the construction of the compensator to provide the needed modulation is done by generating a fluency map of the radiation portal needed. This is done with a treatment planning system (TPS) with inverse planning capabilities or with a bolus placed on the surface of the patient at the beam entrance point. The bolus option will be used in this research as currently there is no TPS in the country that can do inverse planning. In this case, the cerrobend compensator will be used to replicate dosimetric effects of the bolus placed on the surface of the patient. According to Jiang et al (1998), the calculation of compensator thickness profile (an optimized primary fluency profile) is straightforward typically using the exponentially attenuation model. With reference to this, the shape of the compensator will be adjusted to account for beam divergence and reduction in dose contributed by scattered radiation. Thus the dosimetric considerations is part of the scope of this research.

1.5. RELEVANCE OF THE PROJECT WORK

In radiation oncology, a patient should get the best treatment option as much as possible in order to improve on the quality of life of patients. So the expected results such as correction factors to account for reduction in scatter for using the cerrobend compensator to mimic bolus would have immense contribution to scientific and technical knowledge. From this

University of Ghana http://ugspace.ug.edu.gh

work, it will be possible to implement IMRT delivery technique at National Centre for Radiotherapy and Nuclear Medicine of Korle-Bu Teaching Hospital. The clinical implementation of IMRT technique requires at least two systems (Khan, 2010), which are: treatment planning computer system that can calculate non-uniform fluence maps for multiple beams directed from different directions to maximize dose to target while minimizing dose to critical normal structures. This may be done with a treatment planning system (TPS) with inverse planning capabilities or with a bolus placed on the surface of the patient at the beam entrance point. The second one, is a system delivering a non-uniform fluence as planned, so each of these systems must be appropriately tested and commissioned before the actual clinical use. The bolus option will be used in this research as mentioned in section 1.4 and the cerrobend compensator will be used to replicate dosimetric effects of the bolus placed on the surface of the patient. Similar research was done using different materials by Teclehaimanot (2014) in which the results were not in the clinically acceptable levels, so with this work we are expecting to reach such clinical levels with deviation less than 5%.

Intensity modulated radiotherapy (IMRT) is widely used in clinical applications in developed countries, for the treatment of malignant and non-malignant diseases. This technique uses multiple radiation beams of non-uniform intensities. The beams are modulated to the required intensity maps for delivering highly conformal doses of radiation to the treatment targets, while sparing the adjacent normal tissue structures. This treatment technique has superior dosimetric advantages over 2-dimensional (2D) and conventional 3-dimensional conformal radiotherapy (3DCRT) treatments. It can potentially benefit the patient in three ways. Firstly, by improving conformity with target dose, it can reduce the

University of Ghana http://ugspace.ug.edu.gh

probability of in-field recurrence. Secondly, by reducing irradiation of normal tissue, it can minimize the degree of morbidity associated with treatment. Finally, by facilitating escalation of dose, it can improve local control (Cheung, 2006).

Compensator based IMRT has a lot of advantages over MLC, as reported by Taherkhani et al (2010), penumbra regions created by MLCs are larger than those generated by cerrobend blocks. Compensators provide more consistent dose, impose no limitations on the dose delivery rate, reduce skin surface doses, and because of the high density of the cerrobend allows improved skin sparing with low production rate of secondary electrons (Gray, 1979; Hine, 1951) and also reported by Shery (1987). Some of the advantages of the cerrobend are, continuous intensity modulation, high spatial resolution, gives room to treat large field size, easy quality assurance (QA) and shorter treatment time delivery (Chang, 2004). On the other hand some of drawbacks are: the therapist having to go to the treatment room to change the compensator in multiple fields (lack of automation) and production cost being labor intensive and time consuming (Chang, 2004). But now these drawbacks have been fixed in many developed countries by introducing a milling machine which is incorporated with the Treatment Planning System (TPS), and an automated compensator-IMRT technique (Javedan et al. 2008).

The other main advantages of using cerrobend in this research are: its low melting point of 158^0F (70^0C) which makes it easy to be recycled. It is readily available, inexpensive, high density (9.8g/cm^3) and is used as shielding blocks in EBRT where doses are reduced by 95% or 99% of their initial value.

University of Ghana http://ugspace.ug.edu.gh

As a material for compensation with high energy photons, cerrobend provides several advantages over other tissue equivalent materials (Shery, 1987). In the past, cerrobend had not been considered as an excellent compensator material despite its high density. Recently Chang et al (2004) reported that there are cerrobend filling techniques that produce smooth and accurate compensators with consistent density. Solidified cerrobend in the compensator mold becomes one of the top choices of compensator material. And it can be easily shaped to the intended form with uniform density using the technique described by (Chang, 2004).

Chang et al (2004) showed that compensator-IMRT technique has several benefits for delivering continuous intensity modulation and have shown that, the finer resolution compensator-IMRT technique can also produce dosimetry that is closer to the ideal IMRT treatment, without any delivery limitation, compared with the segmental MLC IMRT technique. From this work the patients treated at the National Centre of Radiotherapy and Nuclear Medicine will benefit from all the advantages of IMRT techniques mentioned above. Consequently patients will also get a better and inexpensive treatment option.

University of Ghana http://ugspace.ug.edu.gh

CHAPTER II

2.0. LITERATURE REVIEW

2.1. Beam Modifiers

Beam modifiers are devices use in EBRT to achieve desirable modification of the spatial distribution of radiation by the insertion of requisite material in the path of the beam. There are four main types of beam modifiers. These are wedge filters, shielding blocks, compensators and bolus. Bolus are made of tissue equivalent materials used for tissue compensation placed in contact with skin at right angle to the beam axes. This work is focuses on compensators.

2.1.1. Compensator

A compensator is a beam modifier introduced in radiotherapy to account for surface irregularities of the patients, internal tissue inhomogeneity and sometimes obliquity beam incident; such that dose distributions within the irradiated region would be similar to that of a flat surface homogeneous medium, water (Johns & Cunningham, 1983). Bolus are made from tissue equivalent materials were initially used to compensate for missing tissue by placing them in contact with the patient's skin. The use of bolus compromises on the skin-sparing properties of the megavoltage beam. Bolus are mostly replaced by compensating filters placed at some distance from the patient's skin and designed to mimic the role of the bolus (Johns & Cunningham, 1983) . This is illustrated in Figures 2.01. and 2.01. b..

University of Ghana http://ugspace.ug.edu.gh

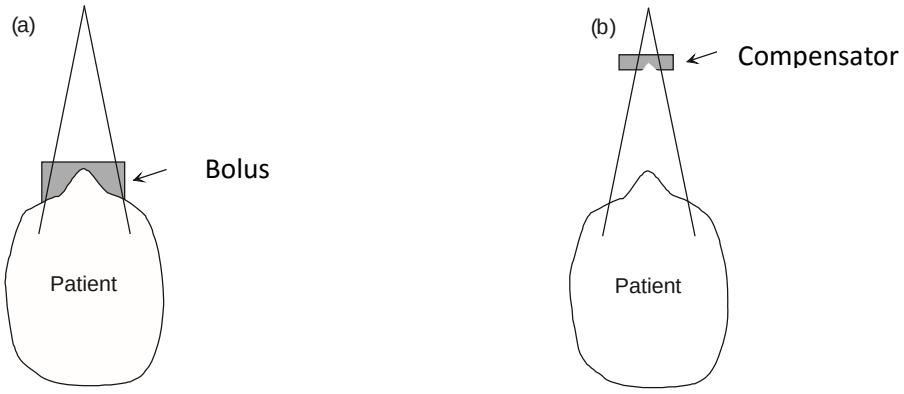

Figure 2.01. Difference between bolus and compensator filter. In a) bolus placed on the skin, producing a flat radiation distribution. Skin sparing is lost with bolus. In b) a compensator achieving the same dose distribution as in a) is constructed and attached to the treatment unit. Due to the large air gap, skin sparing is maintained (Podgorsak, 2005).

To place a compensator at some distance from the patient's skin, its dimension must be reduced in the lateral direction when compared to the bolus on the surface of the patient to account for beam divergence. Also the thickness of the compensator must be adjusted to account for attenuation and scattering properties of the compensator material which are different from that of the bolus. Therefore, the reduction of the primary beam is the most important factor but scattered radiation must be considered (Johns & Cunningham, 1983).

2.1.2. Compensator Design and Construction

There are so many factors to be considered when designing and constructing a compensator. Starting with selection of material such as high, low or middle density materials. According to Ahnesjo (1995) and Mejadden et al. (1997), the choice of the

University of Ghana http://ugspace.ug.edu.gh

elemental composition will affect the photon scattering in the filter, so the material's density will affect the thickness of the filter. A high density material will result in a smaller thickness compared to a medium density material with a smaller filter thickness. The compensator used for IMRT differs in aim from traditional compensator, where the goal is to achieve uniform dose on a specified plane within the patient (Jiang & Ayyangar, 1998). In the IMRT, the compensator is designed to produce an optimized primary fluence profile at the patient's surface (Jiang & Ayyangar, 1998) therefore, modulations with large changes in intensity must be achieved within the field resulting in drastic thickness variations across the compensator (Dimitriadis & Fallome, 2002).

The ratio of thickness (along the ray) of compensator to bolus materials is approximately the inverse ratio of the linear attenuation coefficient of the two material, but because of the altered scatter conditions, the compensator should be made 10% or so thinner than would be predicted on this basis alone. The actual ratio depends on beam size, depth of interest and the thickness of the bolus material being represented (Johns & Cunningham, 1983). Pasma et al. (1999) described a method to determine 2D thickness profile of compensator for clinical applications with accuracy of 0.5 mm using the relation bellow.

$$t_{ps} = \frac{\mu_{steel}}{\mu_{ps}} t_{steel} + \frac{\mu_{lucite}}{\mu_{ps}} t_{lucite} \qquad 2.1$$

Where $t_{steel}$the thickness of is granulate of stainless steel, t_{lucite} is the thickness of two lucite plate of the tray. μ_{steel}, μ_{ps} and μ_{lucite} the linear attenuation coefficient of the primary component of the transmission for steel, polystyrene and lucite respectively. Pasma et al. (1999) used the ratio $\frac{\mu_{steel}}{\mu_{ps}}$ for the conversion of stainless steel thickness into the equivalent polystyrene thickness.

University of Ghana http://ugspace.ug.edu.gh

Dimitiadis & Falone., (2002) reported that the thickness of a cerrobend compensator can be as much as 6 cm in some areas.

With material selection, Chang et al. (2004), presented criteria for ideal compensator material and physical form to generate smooth intensity modulation. These include large range of intensity modulation magnitude, intensity modulation of high spatial resolution; not hazardous for handling in the fabrication process; easy to form and retain the shape needed; low material cost and friendly to the environment. Compensator must be built in a way that will correct for the source to tray distance and the diverging nature of the beam reducing the lateral dimension of the compensator.

There are many ways to make a compensator. The earliest way was to make what is called an Ellis compensator (named after the British radiotherapist Frank Ellis), simply a stack of LEGO-like bricks of varying thickness. The number of bricks stacked vertically defines the dynamic range. The width of the bricks defines the spatial resolution and their height the intensity resolution (see Figure. 2.02. a). Generally, they were not focused to the source. To do so, it would have been very difficult and required several planes of bricks with the size varying from plane to plane. Another way to make a compensator is to mill a metal block to the required shape. Another way to make a compensator is to cut out sheets of lead of different shapes and to glue them together to make a pattern (see Figure.2.02. b). A fourth way is to use a hot-wire cutting device to cut a mold of the required compensator shape out of tough Styrofoam and then to fill this with either lead or tungsten balls or a hot liquid melt which cools to the required shape. The fifth technique has been to use a series of pistons to stamp a pattern in a kind of heavy alloy putty. This latter method is effectively

University of Ghana http://ugspace.ug.edu.gh

reusable. Other workers have constructed carousels with several compensators per carousel. Some compensators have been single per field.

The three main types of compensators are grid block system in which the compensator is made up of blocks of aluminum or brass from a range of standard thickness with each block having a fixed area, generally 1x1cm^2 projected to the isocentre; the contour system in which the compensator is made from sheet of a standard thickness of lead (generally 0.5-1mm); the lead sheet is cut to fit lines of equal tissue deficit interpolated from the surface measurement and the system using compensator in which the surface of the block does not have any step. These blocks are generally made by machining out the required shape in a polystyrene mold into which low melting point alloy may be poured (Aldrich and Andrew, 1982), fig.1 bellow shows the different types of compensator.

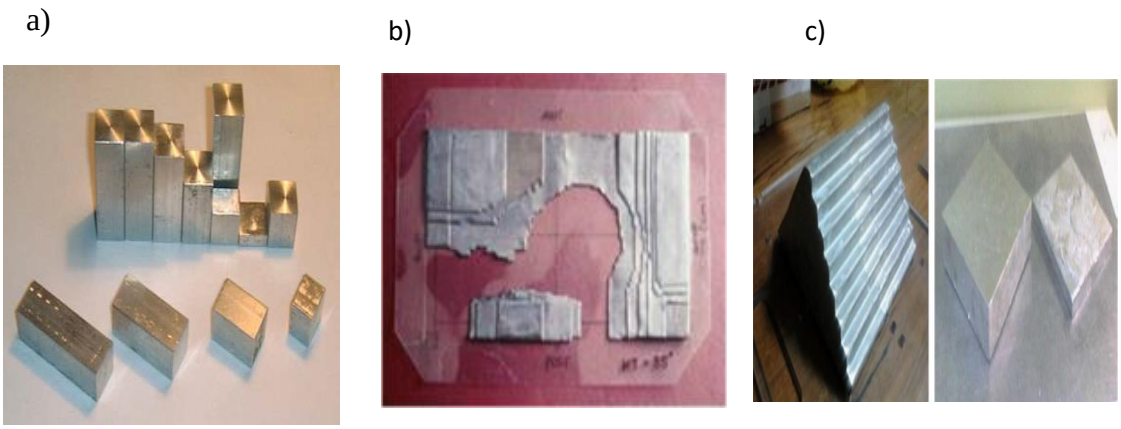

Figure 2.02. Different types of compensator. In a) the basic building blocks of an Ellis compensator with some arranged to make a 1D. In b) how a compensator was constructed from thin lead sheets glued together in order to modulate the intensity of a tangential. In c) Cerrobend alloy compensator to realize the inverse-pyramid beam. (Right) Slab compensators with various thicknesses (1.0, 2.0, 4.0, and 6.0 cm) and (left) step-wedge compensator, which the left central (Vaezzadeh et al., 2013)

University of Ghana http://ugspace.ug.edu.gh

A compensator produced for IMRT distribution involves greater thickness variation than a traditional compensator as it was mentioned earlier. In general, the compensator block making process is done using automated milling machines (Chang et al., 2004). Some studies have to proposed new ways to reduce the cost and time of this process (Nakagawa et al., 2005; Xu et al., 2002). The process of making blocks with milling machines is costly because it is usually done by a specialized company outside the hospital.

Considering the technical point of view regarding the use of cutters, compensating IMRT blocks are subject to mechanical limitations in their form during the manufacturing process (Meyer et al., 2000). The cutters operate by lateral and longitudinal movements of a drill cutting (or stick) the material of the compensator block. Regarding the type of material, less dense materials are cut faster.

Another point to be considered is that the increased spatial resolution (decrease of the drill diameter and the width of the pitch) increases the possibilities of breakage of the cutter when casting thicker materials, such as cerrobend. In the case of making IMRT blocks, Meyer et al. (2000) reported that the resolution should be such that the error does not exceed 2.5% as compared to the solution proposed by the planning system, and that it does not take a very long time.

A practical example on the limitations of milling machines can be seen in the work done by Oguchi & Obata (2009). In that study the thicknesses of IMRT blocks showed deviations of up to 0.7 cm and caused deviations of approximately 3% of the planned dose. The authors blamed the mill for the quality and the limitations of the final results of IMRT block and recommended assessment of the possibility to improve mill operating conditions. Avelino (2013) developed an alternative method to manufacture compensator block for

University of Ghana http://ugspace.ug.edu.gh

IMRT purpose from a Jaws-Only fluence map generated by a commercial treatment planning system (TPS). The fluence maps were converted into a mold, and then printed using an inkjet 3D printer. Cerrobend alloy was poured into the mold to achieve the final IMRT compensator block. The study investigated 3 different physical models (equations 2.2, 2.3 and 2.4) to create the molds which are: considering the nominal linear attenuation coefficient of Cerrobend; using the measured data to define the linear attenuation coefficient by an exponential function; and taking in consideration the effects of the field size, central-axis distance and block thicknesses in the linear attenuation coefficient. These three algorithms were assessed and the method was validated during dosimetric quality assurance test.

$$h(x,y) = -\frac{ln\left(\frac{I_{(x,y)}}{I_0}\right)}{\mu} \qquad 2.2$$

$$h(x,y) = -HVL\frac{ln\left(\frac{I_{(x,y)}}{I_0}\right)}{0.693} \qquad 2.3$$

$$h(x,y,r,S) = -\frac{ln\left(\frac{I_{(x,y)}}{I_0}\right)}{\left[kln\left(\frac{I}{I_0}\right)+a+br_{(x,y)}+cr^2_{(x,y)}\right]S} \qquad 2.4$$

In these 3 models h is the thickness of the compensator block, μ linear attenuation coefficient, k, a, b, c are constants, r is off axis distance and S the field size. In the research of Avelino (2013), the constants were calculated using least-square method and the values were k=0.017 mm^{-1}, a =0.0501 mm^{-1} and b = c = 0, the HVL value was used 1.4cm for cerrobend at 6MV energy.

University of Ghana http://ugspace.ug.edu.gh

2.2. Intensity modulated radiation therapy (IMRT)

Another use for compensator is for delivering intensity modulated radiation therapy (IMRT) beams. Intensity modulation is the process of changing beam intensity profiles to meet the goals of composite plan. The term intensity modulated radiotherapy (IMRT) refers to a radiation therapy technique in which non-uniform fluence is delivered to the patient from any given position of the treatment beam to optimize the composite dose distribution (Khan, 2010). This can be carried out in two ways by applying either multileaf collimators (MLCs) or compensator filters (Haghparast et al., 2013; Khan, 2010). As reported by Webb (2001), the planning methods have run ahead of delivery possibilities. However this situation is changing and today there are at least six methods of delivering IMRT. These are: the cast metal compensator, the use of multiple-static MLC-shaped fields (MSF/MLC), dynamic MLC techniques (DMLC), the use of the NOMOS MIMiC and the development of tomotherapy, the use of a scanning attenuating bar, and the use of swept pencils of radiation.

2.2.1. IMRT using MLC

Multleaf collimator MLC is a facility that allows beams to be shaped without the need to manufacture blocks. It consists of opposing pairs of tungsten leaves usually about 60 mm thick which can be driven independently across one axis of the beam. Typically, the primary transmission through the leaves will be about 2% and another problem is with the leakage of radiation between adjacent leaves (Willians & Twaits, 2004). The intensity

University of Ghana http://ugspace.ug.edu.gh

modulation is achieved by the movement of collimator leaves during the treatment (DMLC) or in the interval between segments (MSF-MLC), the precise control and verification of the leaf position and leaf speed are essential for accurate dose delivered, so during the treatment a real time verification mechanisms based on electronic portal imaging is essential which will prolong the treatment time.

Meanwhile, it is reported that currently available MLC based IMRT techniques have several clinical disadvantages for example: a treatment time of 10 to 30 minutes is required which is approximately 10 times more than conventional treatment, thereby leading to higher risk of involuntary movement of the PTV and OARs; a radiation leakage due to rounded leaf end is significant when employing the sliding window technique; and MU correction is difficult for a small segmented field and segmented field including a large and a small subfields (Yonda & Aoki, 2003).

2.2.2. IMRT using compensator

The metal compensator is the Cinderella of IMRT as classified by Webb (2001), somewhat overlooked but still with much potential. It relies on placing in an otherwise uniform beam an absorber of varying thickness in the direction of the ray propagation. Generally, it is made of just one material whose linear attenuation coefficient depending on energy and intensity after passing through a thickness of the compensator is modified according the attenuation law. By varying the thickness, the intensity is thus modulated.

University of Ghana http://ugspace.ug.edu.gh

Using a compensator is advantageous because there is no limitation due to the finite size of any collimator leaves. There is no limitation due to the accuracy of leaf placement. There are no tongue-and-groove artefacts. There is no quantization of fluence increment as there would be with a multiple-static-field technique. Little can go wrong. Quality assurance is straightforward (Webb, 2001). Although the compensator was invented to compensate for the fact that a patient surface is not flat, it effectively performs IMRT. Figure. 2.03. shows how the compensator modulates the intensity of the beam by varying the thickness.

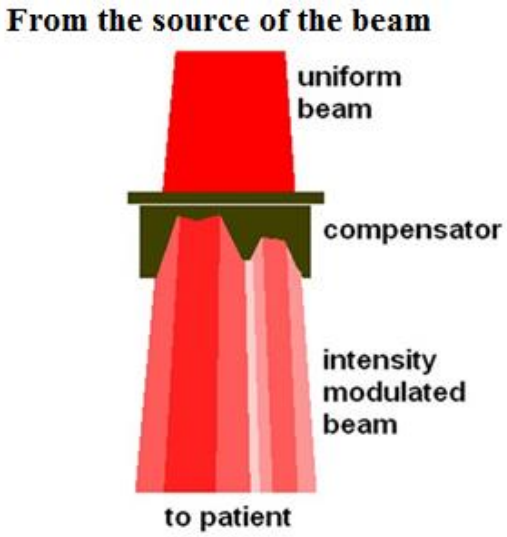

Figure. 2.03. Modulation of the intensity of the beam by the compensator with varied thicknesses

IMRT is usually accomplished by delivering sets of beam segments at different geometric angles. These segments are delivered by analysis of optimal fluence map for each gantry and angle using a leaf sequence algorithm. These fluence map in turn are delivered from an optimized process that assigns weights to beamlet will be the optimal dose for the IMRT plan. The map of the beamlet weights will correspond to the fluence maps of the field. Compensator can be used to approximate these fluence maps by appropriate attenuation of

University of Ghana http://ugspace.ug.edu.gh

individual beamlets making up the original open beam fluence (Plessis and Willemse, 2006).

2.2.3. Compensator IMRT versus MLC IMRT

Compensator has multiple advantages. The first benefit of IMRT method based on compensator is the simplicity (Chang et al., 2004). The static nature of the compensating blocks provides good reproducibility in the daily dose applied during treatment (Buckey et al., 2010). Once the IMRT block has passed the Quality Control (QC), it will be changed only in case of accident (a fall, for example). The IMRT technique based on the leaf movements of the MLC depends on the mechanical conditions of the MLC, and the technique itself contributes to the premature wear of the equipment. Furthermore, gravity can influence the movement of the MLC leaf where the leaf move vertically (Buckey et al., 2010). Other advantages of compensators include, higher resolution in the direction normal MLC leaf motion and no match line nor tongue-and-groove problems. The compensator based IMRT has advantages that all parts are irradiated simultaneously hence minimizing problems of patient movements (Vaezzadeh et al, 2013). As long as the minimum thickness is zero, the use of compensator is extremely monitor-unit (MU) efficient (Vaezzadeh et al, 2013). Chang et al. (2000) reported that a higher performance of compensator in the clinic than that both static and dynamic MLC technique because of their higher and continuous intensity modulated resolution which can be seen

University of Ghana http://ugspace.ug.edu.gh

in Figure 2.04. Compensator provide short treatment delivery time dose computation and its quality assurance (Chang et al., 2004).

Another advantage of compensator-IMRT technique is that, it can create continuously varying intensity modulation, whereas the intensity modulation created by MLC-based IMRT technique is discrete at least in one direction. One obvious drawback of most of the compensator –IMRT technique is lack of automation. Radiation therapists need to go into the treatment room and exchange customized compensators between treatment fields. Recently, methods that automate compensator exchange between treatment fields have been developed to improve the treatment delivery efficiency. Another common concern for compensator-IMRT is fabrication and assembly time, which has been reported to be extensive for some techniques.

The IMRT compensating blocks offer possibilities of fluency maps with a resolution of very high intensities, because it can generate blocks with virtually continuous forms (with deviations in the order of a few millimeters). The concern to be taken in this technique is to ascertain the attenuation caused by the maximum thickness of the block. (Chang et al., 2000). In work done by Chang et al., (2000) the maximum attenuation caused by a block of IMRT was 38.3% for photon beam with nominal energy of 6 MV. The maximum thickness of the block in this case was 5 cm and the material used was tin. Such modulation may be higher when using a thicker material or increasing the thickness of the block. Chang et al., (2000) was limited to the software solutions on the thickness of 5 cm the block to make it practical the manufacturing process. However, in the study of Chang et al. (2000), a comparison between the levels of modulation using MLC compensator block and under

University of Ghana http://ugspace.ug.edu.gh

such conditions shows that the high resolution results in the blocks closer to the ideal dose distributions (those proposed by TPS).

(a) Compensator Delivery (b) MLC Delivery

Figure 2.04. Delivered dose resolution comparison (.decimal, Inc.)

In addition, the segments of small fields in the art of IMRT are inefficient in the dosimetric point of view (Cheung, 2006), because the time required to deposit the same amount of radiation decreases with the size of the treatment field (Podgorsak, 2005). Another problem which increases the time required to deliver a dose of IMRT with MLC field is the need to split the treatment into two stages when treated area is very large (Oguchi & Obata, 2009). This division is for the MLC does not have to run large movements, which would make the solution very complex, (need for greater speed in the movements of leaves) and most likely to fail.

Among the advantages of blocks-based IMRT, two standards by clinical benefit to patients for treating disease. The IMRT blocks have dosimetric advantages and benefits for the use of this technique in treatments with moving targets (examples: lung and liver cancer). These two advantages can be considered the most relevant, to contribute in increasing the distribution (coverage) of tumour dose (greater possibility of controlling the disease) and

University of Ghana http://ugspace.ug.edu.gh

dose reduction in healthy tissues (fewer possible side effects), when compared with the technique that uses MLC.

Another dosimetric problem is that there are dose transmissions between leaves IMRT about 1.5% (Joy et al., 2012). This dose, even if provided in treatment planning systems (TPS), typically reaches a region which should be protected by the leaves. This effect does not occur in compensator IMRT because the block surface is continuous.

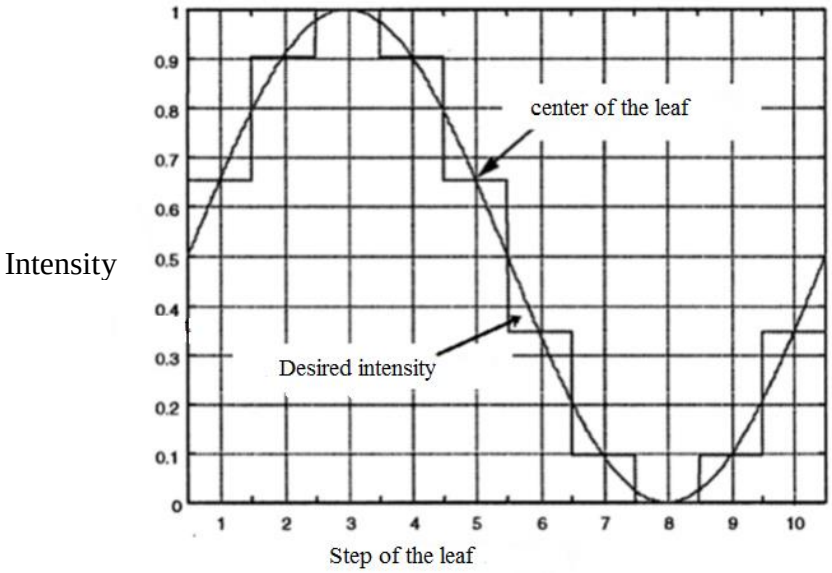

Figure 2.05. Physical limitations of MLC. The solid line represents the desired intensity profile. While the MLC performs a step-like approximation of the discrete step due to the thickness of leaf (Meyer et al., 2000).

2.3. Treatment planning system

Treatment planning is a process that involves the determination of treatment parameters considered optimal in the management of patient's disease. In radiotherapy, these parameters include target volume, dose-limiting structures, treatment volume, dose prescription, dose fractionation, dose distribution, positioning of the patient, treatment

University of Ghana http://ugspace.ug.edu.gh

machine setting and adjuvant therapies (Khan & Gerbi, 2012). This is backed up with computer hardware and software that gives complicated 3-dimensional radiation treatment planning (3-DRTP). In 3-DRTP, images are acquired via different ways such as scanners, digitizers, CD-ROM, DICOM and others. There are two types of treatment planning, namely forward and inverse treatment planning.

The principle of IMRT is to treat a patient from a number of different directions (or continuous arcs) with beams of non-uniform fluences, which have been optimized to deliver a high dose to the target volume and an acceptably low dose to the surrounding normal structures. The treatment-planning program divides each beam into a large number of beamlets and determines optimum setting of their fluences or weights. The optimization process involves inverse planning in which beamlet weights or intensities are adjusted to satisfy predefined dose distribution criteria for the composite plan.

2.3.1. Inverse treatment Planning

In the 1980s, Brahme demonstrated the potential odd beams with intensity modulated to create homogeneous and concave dose distributions (Brahme et al., 1982). Inside intensity modulated beams, the flow of radiation is not equal, but has a value that is a function of its geometric location within the cross section of the beam (Lax & Brahme, 1982). As a possible strategy to make the intensity modulated beams design feasible, Brahme introduced the concept of the inverse planning (Eklof et al., 1990).

University of Ghana http://ugspace.ug.edu.gh

In inverse planning, computational algorithms are used to convert clinically desired dose distribution in the beam intensity maps to be delivered by the processing machine.

According to (Khan, 2010) number of computational methods have been designed to calculate optimum intensity profiles. These methods, which are based on inverse planning, can be divided into two broad categories which are analytic methods and interactive methods.

Analytic methods involve mathematical techniques in which the desired dose distribution is inverted by using a back projection algorithm (Khan, 2010). According to Khan, (2010), this is a reverse of a computed tomography (CT) reconstruction algorithm where two-dimensional images are reconstructed from one dimensional intensity functions. The density or fluence distribution in the patient is obtained by deconvolving the dose kernel from desired dose distribution. These fluences can then be projected onto the beam geometry to create incident beam intensity profiles (Khan, 2010). The problem with analytical methods is that, exact analytical solutions do not exist for determining incident fluences that would produce the desired dose distribution without allowing negative beam weights (Khan, 2010). To solve these problem, some algorithms have been designed to involve both procedures, analytical and interactive (Khan, 2010).

In iterative methods, optimization techniques have been devised in which beamlet weights for a given number of beams are iteratively adjusted to minimize the value of a cost function, which quantitatively represents deviation from the desired goal (Khan, 2010). The patient input data for the inverse planning algorithm is the same as that needed for forward planning. Three-dimensional image data, image registration, and segmentation are

University of Ghana http://ugspace.ug.edu.gh

all required when planning for IMRT (Khan, 2010). For each PTV, the user enters the plan parameters such as, maximum dose, minimum dose, and a dose volume histogram. For each critical organ at risk, the program requires the desired limiting dose and a dose volume histogram.

Depending on the IMRT software, the user may be required to provide more additional information such as beam energy, beam directions, number of iterations, before proceeding to optimizing intensity profiles and calculating the resulting dose distribution (Khan, 2010). The evaluation of an IMRT treatment plan also requires the same considerations as the three-dimensional conventional radiotherapy (3-D CRT) plans, namely viewing isodose curves in orthogonal planes, individual slices, or 3D volume surfaces. The isodose distributions are usually supplemented by dose volume histograms. After an acceptable IMRT plan has been generated, the intensity profiles (or fluence maps) for each beam are electronically sent to the treatment linear accelerator fitted with appropriate hardware and software to deliver the planned intensity-modulated beams.

The treatment-planning and delivery systems must be integrated to ensure accurate and efficient delivery of the planned treatment. Because of the nature of the entire process, rigorous verification and quality assurance procedures are required to implement IMRT (Khan, 2010). Figure 2.06. shows the principle of inverse planning.

University of Ghana http://ugspace.ug.edu.gh

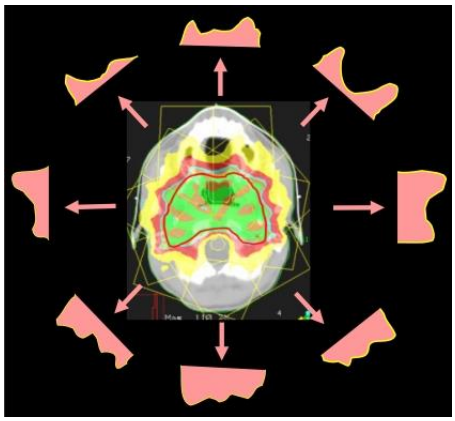

Figure 2.06. Principle of the inverse planning: The planner defines the required dose and dose distribution for the treatment and the computer can calculate and optimizes the individual characteristics of the intensity of each beam to meet the required dose (Cheung, 2006).

2.3.2. Forward Treatment Planning

The conformal radiotherapy uses direct planning and confidence in physicist's skills (planner) to decide the sizes of fields, shapes, weights and orientation of the beams, that is, trial and error technique. The planning system calculates the composition of the dose distribution by adding the contribution of each beam dose treatment. If the dose and the dose distribution are unsatisfactory, the physicist varies the parameters and beam geometry and repeat the calculation. This forward planning where the physicist optimizes the planning is the method which will be used in this research.

In forward planning, the planner selects manually all the necessary parameters such as the number of beams, beam entry directions and shapes, beam modifiers (such as compensators, wedges, blocks and bolus) and beam relative weighting. After the planner has successfully selected the parameters needed, the dose calculations and dose distributions are performed, based on the input parameters, by the TPS software. The

University of Ghana http://ugspace.ug.edu.gh

planner can also adjust manually all the input parameters till the desired dose optimization is obtained. The quality of the plan depends on the experience and skill of the planner. Even for a skilled planner, it has some limitations such as the number of degrees of freedom and the number of iterations within the given time, Figure 2.07. shows the principle of conventional forward planning.

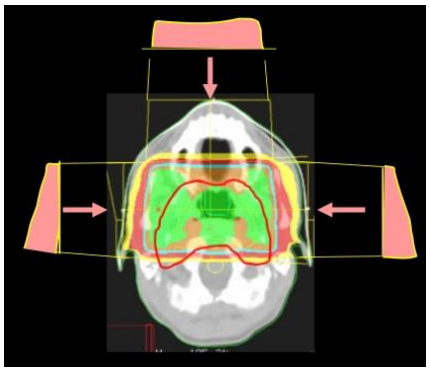

Figure 2.07. Principle of conventional forward planning: the planner (physicist) begins with a series of weights and beam profiles to obtain a plan by trial and error process (Cheung, 2006).

2.4. Photon Interaction

It is important to discuss the fundamental theory of photon interaction in compensator construction because any object placed in the path of photon beam will create scatter radiation.

The presence of a compensator would introduce spectral changes in the heterogeneous photon beam that will alter its in-phantom scatter and beam penetration (Plessis & Willemse, 2006) and therefor the way it interacts with tissue.

University of Ghana http://ugspace.ug.edu.gh

There are five major types of interaction that can cause attenuation of photon beam in the absorber. These are photo disintegration, coherent scattering, incoherent scattering (Compton), photoelectric absorption and pair production (Khan, 2010; Johns & Cunningham, 1983). Three of them are main photon interaction processes whereby scatter can occur in radiotherapy beams. These are Compton scattering, photoelectric absorption and par pair production.

2.4.1. Photoelectric absorption

In photoelectric process the photon of energy $h\nu$ will interact with an atom and eject one of bound electron (Figure 4a) from K, L, M or N shells. The ejected electron is called photoelectron and emerges with kinetic energy of $h\nu - E_b$, where E_b is a binding energy of the shell where the electron is ejected, the process varies with photon energy. After the electron has been ejected from the atom, a vacancy is created in the shell thus living the atom in excited state which can be filled by any outer orbital electron with emission of characteristic x-ray, so there is a possibility of emission of Auger electrons (Figure 2.08. a) which are monoenergetic electrons produced by the absorption of characteristic x-ray internally by the atom (Kahn, 2010; Johns & Cunningham, 1983). The probability of photoelectric absorption depends on the photon energy as illustrated in Figure 2.08. b, where the mass photoelectric attenuation coefficient is plotted as a function of photon energy (Khan, 2010).

The probability is maximum if the photon has just enough energy to knock electron from its shell and varies with atomic number of the absorber. For high Z materials the coefficient

University of Ghana http://ugspace.ug.edu.gh

per electron or per gram varies approximately by Z^3 and more nearly $Z^{3.8}$ for low Z materials (Johns & Cunningham, 1983).

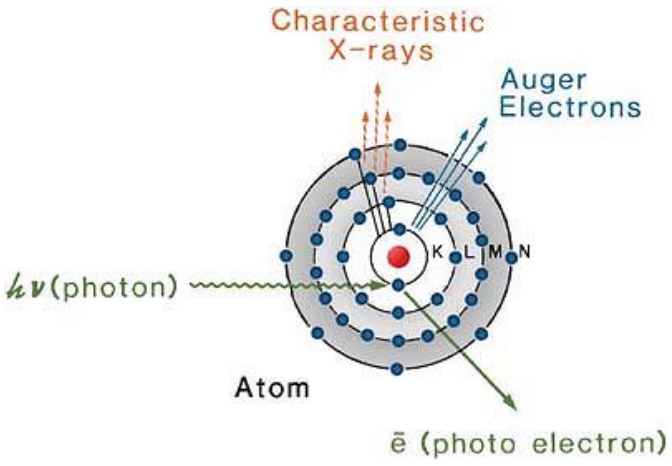

a)

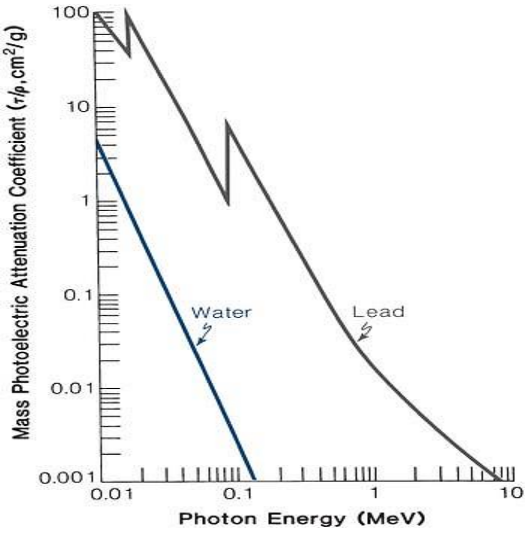

b)

Figure 2.08. In a) Illustration of the photoelectric effect in b) Mass photoelectric attenuation coefficient plotted against photon energy. Curves for water (Zeff = 7.42) and lead (Z = 82). (Khan, 2010)

University of Ghana http://ugspace.ug.edu.gh

2.4.2. Compton scattering

In the Compton process, the photon will interact with outer electron. In this interaction, the electron receives some energy from the photon and is emitted at an angle θ, (Figure. 2.09). The photon, with reduced energy is scattered at an angle φ.

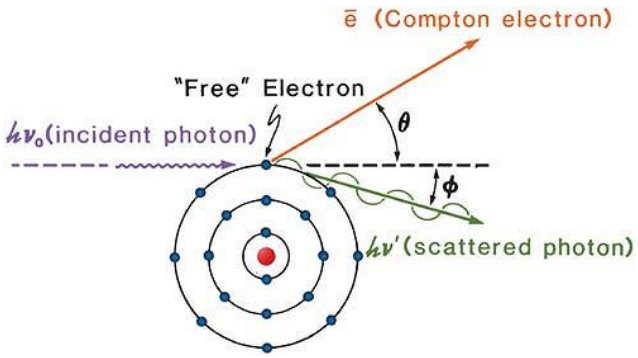

Figure.2.09. Diagram illustrating the Compton effect (Khan, 2010)

The energy given to the electron is:

$$E_e = \lambda\nu \frac{\frac{\lambda\nu}{m_e c^2}(1-\cos\phi)}{1+\frac{\lambda\nu}{m_e c^2}(1-cos\,\phi)} \qquad 2.5$$

And the energy of scattered photon is

$$\lambda\nu' = \frac{1}{1+\frac{\lambda\nu}{m_e c^2}(1-cos\,\phi)} \qquad 2.6$$

In these equations $\lambda\nu$ is the incident photon energy, $m_e c^2$ is the rest mass energy of the electron its numerical valor is 0.511MeV. The Compton mass attenuation coefficient is independent of atomic mass Z medium.

University of Ghana http://ugspace.ug.edu.gh

2.4.3. Pair production

The pair production process occurs when the energy of the incident photon is greater than 1.022 MeV (Khan, 2010; Johns & Cunningham, 1983). In the pair production process (Figure. 2.10), the photon interacts strongly with the electromagnetic field of an atomic nucleus and gives up, all of its energy in the process of creating a pair consisting of a negative electron (e^-) and a positive electron (positron) (e^+).

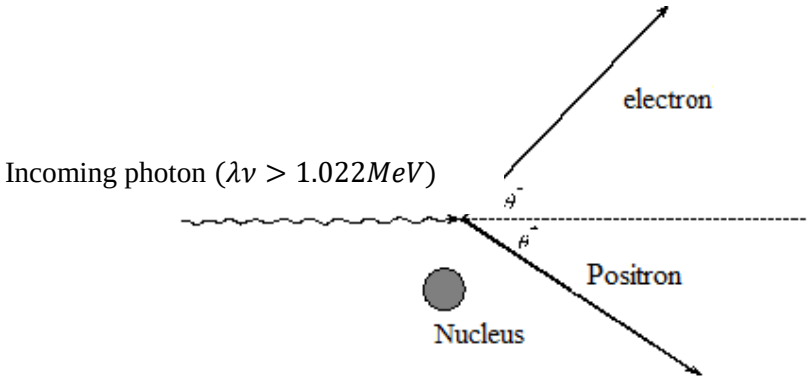

Figure. 2.10. Diagram illustrating the pair production process

The process of pair production may also occur in the field of an atomic electron (Mayles, 2007). When the photon in the field of another electron transforms into an electron - positron pair is called triplet production and the threshold energy for this process is $4m_e c^2 = 2.044MeV$ therefore for cobalt-60 gamma ray have energy photon of 1.25MeV. The triplet production does not contribute since the threshold energy is above the gamma ray photon energy (Mayles, 2007; Johns & Cunningham, 1983). The cross section for pair production in the nuclear field is zero below the threshold, it then rapidly increases with increase the energy and well above threshold varies approximately as the square of the

University of Ghana http://ugspace.ug.edu.gh

nuclear charge Z ($a^{\sigma}pair = Z^2$). For triplet production, at the energy above the threshold approximately vary as Z. the triplet production is as important as pair production in hydrogen (Z=1), but it gets increasingly less important, compared to pair production with increasing atomic number. In high atomic number media, Z dependence of these process becomes weaker because of screening of the electric field of the target entries by the surrounding atomic electrons (Mayles, 2007). Electron density of cerrobend is lower when compared with other materials like aluminum and brass, its atomic number is much higher causing the enhancement of pair production and consequently high effective linear attenuation coefficient (μ_{eff}) (Haghparast et al., 2013).

2.4.4. Relative predominance of individual effects

The relative importance of the three processes described above for different absorber materials and photon beam energy is conveniently illustrated in Figure 2.11. The curve on the left represents the energy at which photoelectric absorption and Compton scattering are equally probable as a function of the absorber atomic number and the curve on the right represents the energy at which Compton scattering and pair production are thus equally probable. The three areas are thus defined on the plot within which photoelectric absorption, Compton scattering and pair production each predominats (Podgorsak, 2005; Nkoll, 1989).

University of Ghana http://ugspace.ug.edu.gh

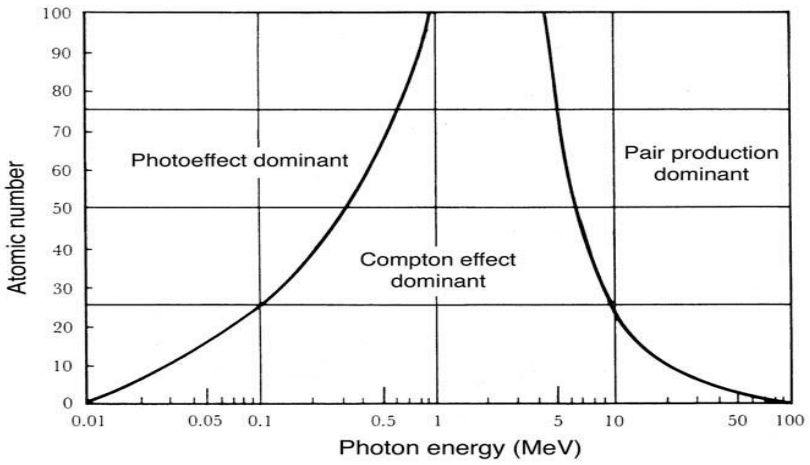

Figure. 2.11. Regions of relative predominance of the three main forms of photon interaction with matter (Podgorsak, 2005).

2.5. Beam geometry

2.5.1. Narrow beam

Narrow beam geometry refers to an experimental configuration that is designed to exclude scattered photons from being measured by the detector (Figure 2.12). It means that the relationship between the source shielding and the detector is such that almost no scatter interacts with the detector (Bushberg & Boone, 2011; Podogorsak, 2005). Therefore a reasonable distance between the attenuator and measuring device (ion chamber) to minimize the number of scattered photons reaching the detector is needed and an ionization chamber with air equivalent walls and with a flat photon energy response the spectrum of radiation comprising the beam (Podogorsak, 2005).

University of Ghana http://ugspace.ug.edu.gh

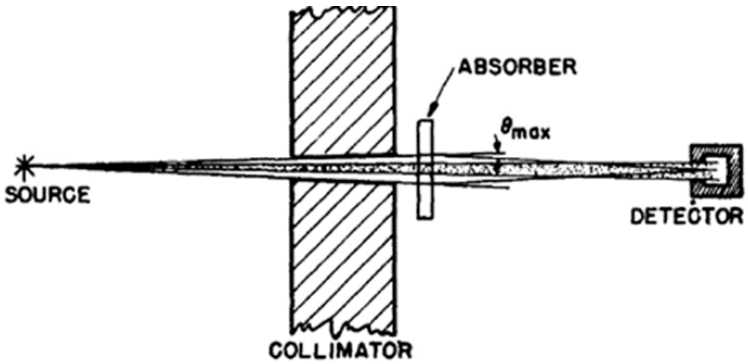

Figure. 2.12. Experimental arrangement in measuring narrow beam attenuation coefficient (Narrow geometry)

2.5.2. Broad beam

In the broad beam geometry (Figure. 2.13), the beam is sufficiently wide that a substantial fraction of the scattered photons remains in the beam. These scattered photons reaching the detector result in an underestimation of attenuation coefficient. In the broad beam geometry scattered photons may reach the detector, thus the measured attenuation is less compared with narrow beam conditions (Bushberg & Boone, 2011).

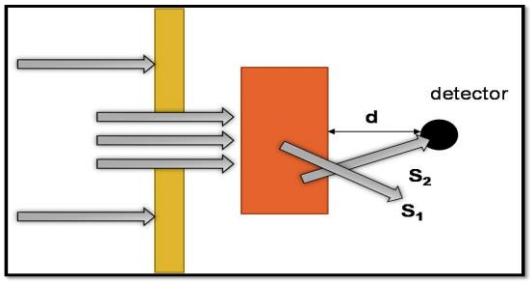

Figure. 2.13. Broad beam geometry

University of Ghana http://ugspace.ug.edu.gh

2.6. Photon beam attenuation

2.6.1. Simple attenuation model (narrow beam)

When a beam of radiation passes through matter some of the photons are absorbed and scattered by the processes discussed above. As a result of this, the number of photons and thus the total energy carried by the beam decreases. The absorption of radiation is usually accompanied by the simultaneous production of lower energy radiation in the absorber such as characteristic radiation, modified scatter and annihilation radiation which were discussed earlier. Therefore, the beam now consists of two components: the primary and the secondary lower energy component. Consider a unidirectional beam of mono-energetic photons for which the energy fluence rate (intensity) is measured by the amount of energy incident per unit time per unit area on a plane normal to the direction of propagation of the beam. For simplicity, it can be assumed that the photon fluence rate is constant from point to point across the plane normal to the direction of propagation and is constant with respect to time. For monochromatic radiation equal thicknesses of the same absorbing material would remove equal fractions of the radiation incident upon the material. Therefore, the change in the transmitted intensity with respect to the incident intensity can be expressed as a function of the change in thickness of the absorbing material as follow.

$$\frac{dI_{(x)}}{I_x} = -\mu dx \qquad 2.7$$

The negative sign follows since intensity is reduced for each addition of thickness of absorber *dx*. Solving the above differential equation will give the intensity as a function of the thickness of attenuator *x* equation 2.8.

$$I_x = I_0 e^{-\mu x} \qquad 2.8$$

University of Ghana http://ugspace.ug.edu.gh

Where I_0 is the intensity of the beam for x = 0, the initial conditions of the differential equation. Thus from this simple derivation is easy to see that the intensity of the primary radiation decreases exponentially with the thickness traversed, the rate of change of intensity is determined by the value of the total linear attenuation coefficient of the material μ. The parameter μ is the degree of attenuation per unit thickness of the absorber. The term "total" is used here because of the different processes that contribute to the reduction of intensity.

2.6.2. Total attenuation coefficient

When the photon passes through an absorber of varying thickness it will be attenuated according to the simple exponential attenuation. Each of the interaction processes removes the photon from the beam either by absorption or by scattering away from the detector's direction and can be characterized by fixed probability of occurrence per unit path length in the absorber.

The sum of this probability per unit path length that the photon is removed from the beam is called linear attenuation coefficient.

$$\mu = \tau_{(photoeleric)} + \sigma_{(Coherent\ scatter)} + \sigma_{(compton)} + k_{(pair)} \quad 2.9$$

Where:

$\tau_{(photoeleric)}$ - Linear attenuation coefficient for Photoelectric effect

$\sigma_{(Coherent\ scatter)}$- Linear attenuation coefficient for Compton Effect

University of Ghana http://ugspace.ug.edu.gh

$\sigma_{(compton)}$ – Linear attenuation coefficient for Rayleigh scattering

$k_{(pair)}$ - Linear attenuation coefficient for pair production

Figure 2.14 shows the linear attenuation coefficient of thermos-shielding material measured in 5x5 cm^2 field size and 100 SSD setup and plotted against effective photon energy along with linear attenuation coefficient of cerrobend, lead, lucite, polystyrene and water.

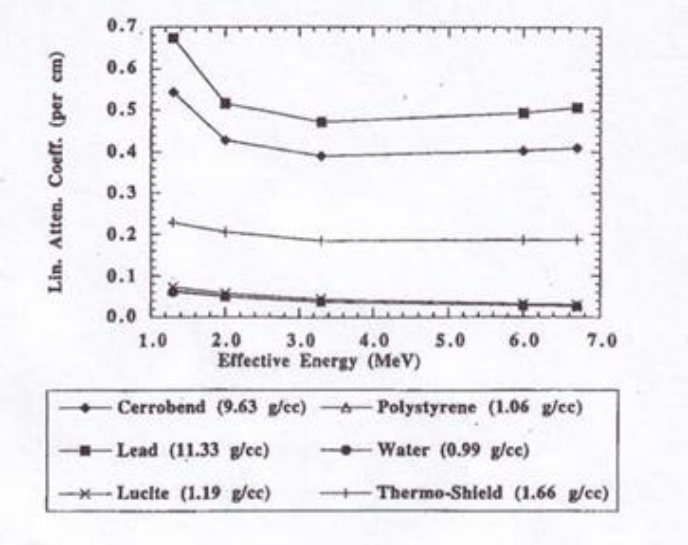

Figure.2.14. Comparison of linear attenuation coefficient of different materials Paliwal et al. (1998).

The linear attenuation coefficient is limited by the fact that it varies with the density of the absorber, even though same material will have the same density. Therefore, the mass attenuation coefficient is more widely used (Johns & Cunningham, 1983) and is defined as:

$$mass\ attenuation\ coefficient = \frac{\mu}{\rho} \qquad 2.10$$

University of Ghana http://ugspace.ug.edu.gh

Where ρ represents the density of medium

Figure 2.15 shows the mass attenuation coefficient for lead in the photon energy range from 10 keV to 100 MeV.

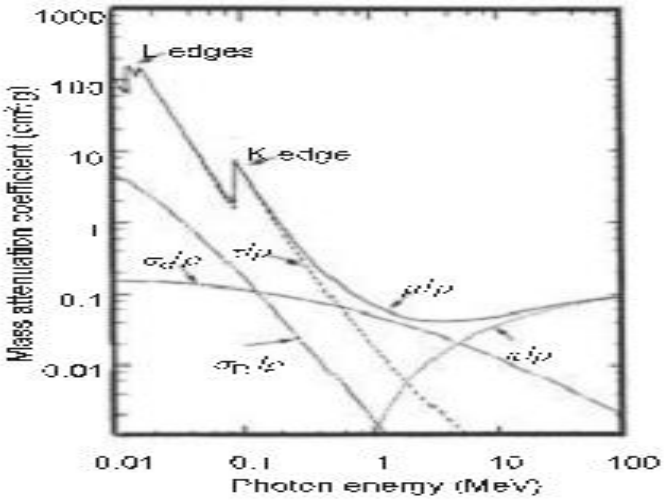

Figure. 2.15. Mass attenuation coefficient for lead in the photon energy range between 10 keV and 100 MeV. The dotted–dashed curves represent contributions of individual effects, while the solid curves represent the sum of the contributions of the individual effects (Podogorsak, 2005)

For given photon energy, the mass attenuation coefficient does not change with the physical change of a given absorber, for compound or mixture of elements can be calculated from:

$$\left(\frac{\mu}{\rho}\right) = \sum_i w_i \left(\frac{\mu}{\rho}\right)_i \qquad 2.11$$

Where:

w_i – weight fraction of element

i – the compound or mixture

University of Ghana http://ugspace.ug.edu.gh

Paliwal et al. (1998) reported that the most commonly used materials in the clinic today like lead and cerrobend have mass attenuation coefficients in the range of 4MV to 20 MV varying from 0.059 cm^2/g to 0.045 cm^2/g and 0,056 cm^2/g to 0,042 cm^2/g respectively.

2.6.3. Effective linear attenuation coefficient (broad beam)

The linear attenuation coefficient is defined for narrow beam geometry assuming only primary beam. However, use of attenuation coefficient in the construction of compensator can lead to errors since it does not account for scatter. Therefore, broad beam attenuation coefficient or effective attenuation coefficient is measured. The effective attenuation coefficient, in addition to being dependent on beam energy and the attenuatior material, has been shown to be a function of field size, depth of measurement, attenuator thickness, off-axis position and filter-patient distance (Dimitriadis & Fallone, 2002; Huang et al., 1986).

When the beam passes through an IMRT block it must be considered that the energy is not constant throughout the block and determine the linear attenuation coefficient behavior depending on the distance to the central-axis. Studies done by Yu et al. (1997) and Haghparast et al. (2013) reported that this spatial dependence can be adjusted as a second or third degree polynomial, respectively. The differences in these studies between the values of linear attenuation coefficient at central-axis and the edges of fields reached 13% (18 cm off-axis) and 8.4% (10 cm off-axis). Dimitriadis & Fallone (2002) reported that the linear attenuation coefficient is affected by the size of irradiated area in a block and

University of Ghana http://ugspace.ug.edu.gh

demonstrated that the variation between 5x5 cm^2 to 20x20 cm^2 field size is about 8% and is independent of the thickness of the material. However, Haghparast, et al. (2013) reported that the effect of varying the field size in the linear attenuation coefficient value is very small and negligible for smaller field sizes than 10x10 cm^2.

Ideally the effective attenuation coefficient used to calculate the thickness of a compensator should be measured for the conditions of each treatment and would be therefore unique to each treatment. This is impractical and therefore the effective attenuation coefficient is typically measured as a function of few variables. Variations with field size are gradual and can be ignored for small changes in field size. However significant variations in effective attenuation coefficients occur over extend of clinical field size, so it should be measured for a number of field sizes within the range of interest. The depth at which the effective attenuation coefficient is measured is a significant factor. With a bolus placed directly on the skin surface the effective attenuation coefficient will decrease at greater depth due to the increased scatter reaching the detector. When a compensator is removed from the surface of the skin secondary electrons and the scattered photons from the compensator will reach the surface of the skin and contribute to the dose. This scatter is of lower energy than the primary beam and is therefore preferentially attenuated, at greater depth the effective attenuation coefficient will increase. Although the effective attenuation coefficient is known to vary with thickness due to beam hardening, it is highly impractical to consider this effect when determining the coefficient.

University of Ghana http://ugspace.ug.edu.gh

2.7. Attenuator Scatter Contribution and Evaluation

Beam modifying filters like wedges or compensators generate scattered radiation when placed in the photon beam (Dimitriadis & Fallone, 2002; Huang et al., 1986). Huang et al. (1986) measured the magnitude of dose contribution from coper sheet for 4MV photon beam and thickness of 1 cm and found that the dose contribution was about 6% of the transmitted primary dose in a 20x20 cm^2 field size, and at edges of the beam was one-half percent. The presence of scattered photons can lead to only minor dose error in clinical applications if simple procedures are followed to account for their contribution.

Compensators are used in radiotherapy with high energy photons where the dominant interaction process is Compton effect, therefore it also produces scatter radiations, secondary electrons and scattered photons reaching the patient, electron compromise the skin sparing and at other hand scattered photons complicate the design of compensator as well as subsequent calculation of dose distribution (Huang et al., 1986). Scattering can cause changes in effective linear attenuation coefficient (μ_{eff}), for example changes in μ_{eff} with field size are attributed to the changes in the scatter radiation rate generated by the compensator (Haghparast et al., 2013).

In addition to the attenuation, the IMRT block scattered the primary beam in the linear accelerator. This scattering, however contributes very little to the dose on the surface. Even with a thick Cerrobend block (5.0 cm), the dose due to low energy photons scattered at the surface increases by about 0.3% (Jiang & Ayyangar, 1998). Concerning the electrons that are ejected out of the block, Jiang & Ayyangar (1998) said that the contamination they

University of Ghana http://ugspace.ug.edu.gh

induce to the beam increases the dose on the surface by very small amount. Regardless of the thickness of the block, the dose on the surface increases by approximately 1.0% due to the contribution of these low-energy electrons.

Some authors (Ahnesjö et al., 1995; Ahnesjö, 1994a, 1994b) have treated the problem of scatter and spectral changes in fluency by analytical models that correct for the primary and scatter fraction of the energy fluence emanating from the flattening filter, collimator and modulator, e.g. wedges and compensator. Ahnesjö & Aspradakis, (1999); Castelanos & Rosenwald (1998); Islam & Dyk (1995) and Papic & Foeze (1990), used the first based method to calculate scatter fluence from a beam modifying absorber approximation for second order scatter and semimpirical method that include sector integration. Plessis & Willems, (2006) presented a novel way of incorporating scatter and beam filtration differently with that of photon scatter kernel based method. To access possible effects of beam hardening, radiation scattering or electron contamination Srivastava and Wagter (2007) reported the relative depth dose curves in an automated water phantom using ion chamber and beam containing blocks of various thicknesses (10, 20, 30, 50 mm).

2.7.1. Scatter Evaluation

Huang et al. (1986) used broad beam geometry set up, also used by Dimitriadis & Fallone (2002) (Figure 2.16), to measure the contribution of dose from scattered photons produced by an attenuator to study the contribution of scattered photon from cerrobend compensator at 6MV photon beam energy.

University of Ghana http://ugspace.ug.edu.gh

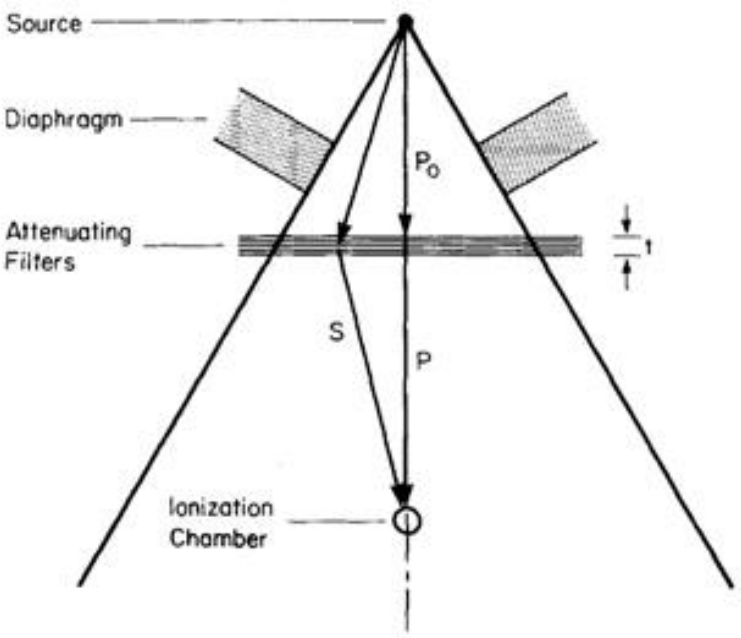

Figure.2.16. Schematic diagram of the setup used for measure the dose contribution from scattered photon produced by an attenuator filter.

In the broad beam geometry set up, as shone in Figure 2.16, the component P represents the absorbed dose produced by the beam beyond the attenuator which is smaller or equal to dose due to the primary photon generated by the source. The scatter beam component S will not be detected in the case of narrow beam geometry created by smaller field size. According to Huang et al., (1986) the scatter-to-primary dose ratio $\frac{S}{P}$ of the attenuated beam for large field size can be calculated by:

$$\frac{S}{P} = \left(\frac{S+P}{P_0}\right) \times \left(\frac{P_0}{P}\right) - 1 \qquad 2.12$$

University of Ghana http://ugspace.ug.edu.gh

If I and I_0 are the signals measured by the filter and without the filter, respectively, for finite field size and i and i_0 are measured intensities for narrow beam geometry, the scatter-to-primary dose ratio for narrow beam geometry can be expressed by:

$$\frac{S}{P} = \left(\frac{I}{I_0}\right) \times \left(\frac{i_0}{i}\right) - 1 \qquad 2.13$$

Defining effective attenuation coefficient for narrow beam geometry $\mu_0 = \frac{ln\left(\frac{i}{i_0}\right)}{t}$ and broad beam geometry $\mu_{eff} = \frac{ln\left(\frac{I}{I_0}\right)}{t}$, where i and I are electrometer reading with attenuator for narrow and broad beam geometry, respectively, and i_0, I_0 electrometer reading without attenuator for narrow and broad beam geometry t the thickness of attenuator, the scatter-to-primary dose ratio can be calculate by:

$$\frac{S}{P} = e^{(\mu_0 - \mu_{eff}) \times t} - 1 \qquad 2.14$$

According to Huang et al. (1986), this equation indicates that the influence of scattered photons produced by the beam modifying filter can be described by difference between μ_0 and μ_{eff}. Therefore, for thin filter it can be approximated by:

$$\frac{S}{P} = \left(\mu_0 - \mu_{eff}\right) \times t \qquad 14$$

Dimitriadis & Fallone (2002) reported that scattered photons may contribute to significant dose errors of up to 20% and said the exact contribution depends on the amount of materials in the beam and the field size. For a field size of 10x10 cm^2 he reported scatter of 4.6% for thickness of 6cm of cerrobend attenuator. (Shown in Figure 2.17.). The S/P was found to increase with field size and thickness of compensator. For a 20x20 cm^2 field size, the

University of Ghana http://ugspace.ug.edu.gh

percentage S/P is as high as 19.8%. The scatter contribution is of significance for IMRT compensators because the compensator can contain thicknesses of up to 6 cm.

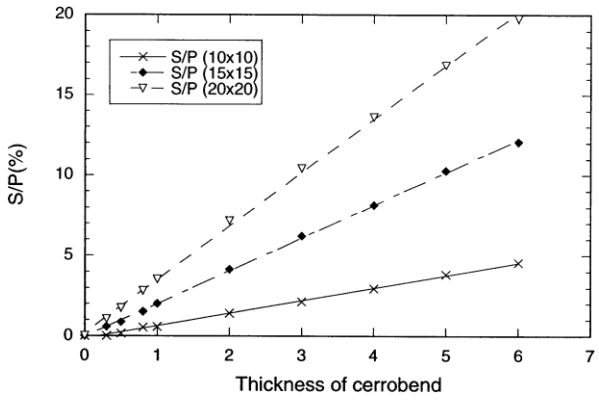

Figure. 2.17. Percentage scatter vs. thickness of filter for different field sizes (Dimitriadis & Fallone, 2002).

2.8. Beam hardening effect

Beam hardening refers to the average photon beam energy change after it goes through a high density material such as physical wedge (Cheung, 2006), in this case, the cerrobend compensator. Dimitriadis & Fallone (2002) investigated the effect of beam hardening for the purpose of intensity modulation and found that the beam hardening effect was significant, and can lead to an error of 6.2% in the transmission, for 6 cm of cerrobend in the path of the beam. Hardening effect can cause changes in effective linear attenuation coefficient. Variation of μ_{eff} with compensator thickness can be ascribed to be the hardening of the photon beam while passing through the compensator where the soft portion of x-ray spectrum is absorbed more (Haghparast et al., 2013)

University of Ghana http://ugspace.ug.edu.gh

The IMRT block acts as a filter in the poly-energetic radiation beam of linear accelerator. Photons with low energies are absorbed into the block. The consequence is that, the average beam energy increases after passing through the block. In the case of a cerrobend block with 5.0 cm thickness, the mean energy increases by approximately 50% (Jiang & Ayyangar, 1998). However, this energy modification does not influence much the percentage depth dose (PDD). For a beam of 6 MV, 10 x 10 cm^2 field with cerrobend block with 5.0 cm thickness; the dose at the surface is approximately 10% smaller and 10 cm deep, 3% higher compared to the open field beam (Jiang & Ayyangar, 1998). Therefore, the PDD is very sensitive to change in the energy spectrum. Care should be taken in relation to the change in energy of the beam by using radiation detectors with low energy dependency in that situation.

2.9. Dosimeters

A radiation dosimeter is a device, instrument or system that measures or evaluates, either directly or indirectly, the quantities exposure, kerma, absorbed dose or equivalent dose, or their time derivatives (rates), or related quantities of ionizing radiation. A dosimeter along with its reader is referred to as a dosimetry system. A radiation dosimeter also can be defined as any device that is capable of providing a reading M that is measured of dose D deposited in the dosimeter sensitive volume V by ionizing radiation (Podgorzak, 2005). In general, methods for detection of radiation can be classified into two groups: absolute dosimetry that can produce a signal from which the dose in its sensitive volume can be

University of Ghana http://ugspace.ug.edu.gh

determined without requiring calibration in a known field of radiation and relative dosimetry which requires calibration in a known radiation field. Examples of absolute dosimeters are calorimeters, Fricke dosimeters and free-air ionization chambers, while some examples of relative dosimeter include calibrated ionization chamber, film, thermoluminescent dosimeters, diodes, optical simulated luminescent detector and radio electrets (Podgorsak, 2005; Nkoll, 1989;). In this work the dosimeters used are calibrated ion chamber and film.

2.9.1. Ion chamber

Ionization chambers are used in radiotherapy and in diagnostic radiology for the determination of radiation dose. They come in various shapes and sizes depending upon the specific requirement, but all ion chambers have the following characteristics.

- Ion Chamber is basically gas filled cavity surrounded by a conductive outer wall and having a central collecting electrode. The wall and the collecting electrode are separated by a high density insulator to reduce the leakage current when polarizing voltagies applied to the chamber.
- A guard electrode is usually provided in the chamber to further reduce chamber leakage. The guard electrode intercepts the leakage current and allows it to follow to ground, bypassing the collecting electrode. It also ensures improved field uniformity in the active or sensitive volume of the chamber, with resulting advantages in charge collection.

University of Ghana http://ugspace.ug.edu.gh

- Measurements with open ionization chamber require temperature and pressure corrections to account for the change in the mass of the air in the chamber volume, which changes in the ambient temperature and pressure.

Figure 2.18. shows an example of basic design of a cylindrical ionization chamber.

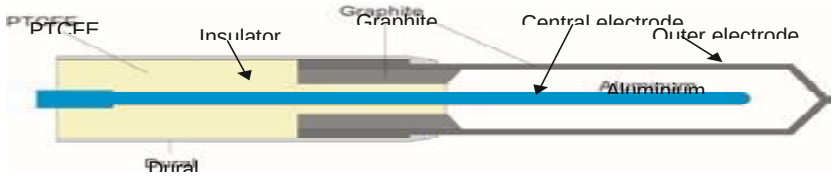

Figure. 2.18. Basic design of a cylindrical Farmer type ionization chamber.

2.9.2. Film dosimeter

Films are used for dose measurement based on optical density variation that is generally dependent on field size, depth, beam energy, processor conditions. So there are two types; silver (radiographic films) and radiochromic films (gafchromic film). Radiographic films are strongly energy dependent for photon beams but their response is relatively independent in megavoltage electron beam. They also provide opportunity to acquire planar dose maps for small field size.

Radiochromic are advantageous compared with radiographic films, they can provide excellent image resolution and are near energetic independent. Do not require chemicals processing and can be handled and prepared in room light although it is recommended to keep the light exposure minimal (Vaezzadeh et al., 2013).

University of Ghana http://ugspace.ug.edu.gh

2.10. Treatment machines

2.10.1. Cobalt-60 teletherapy machine

Treatment machines incorporating γ gamma ray for use in external beam radiotherapy are called tele-therapy machines. They are most often mounted isocentrically, allowing the beam to rotate about the patient at fixed SAD. Modern tele-therapy machines have SADs of 80 or 100cm. The most widely used tele-therapy source uses Co-60 radionuclide contained inside a cylindrical stainless steel capsule and sealed by welding. A typical diameter of cylindrical source is between 1 and 2 cm. the height of the cylinder is about 2.5cm. typical source activity are of the order 0f 5000 – 10000 Ci (185 – 370 TBq) and provide typical dose rate at 80cm from the teletherapy sources of order of 100 – 200cGy/min. The table 2.01. below shows the properties of Co^{60} radionuclide used in external beam radiotherapy.

Table 2.01: Properties of Co -60 radionuclide used in external beam radiotherapy

Half-life	5.3 years
Specific activity (Ci/g)	1100 (~250)
Photon energy (MeV)	1.17 and 1.33
Specific γ rate constant $\Gamma[Rm^2/(Ci.h)]$	1.31
Specific air kerma rate constat TAKR$[\mu Gym^2/(GBq.h)]$	309
HVL $(cm\ Pb)$	1.1
Means of production	$Co^{59} + n$; in reactor

Figure 2.19 shows Co-60 radionuclide in teletherapy source decays with a half-life of 5.26 years into Ni-60 with emission of electron (β particules) with maximum energy of 320 KeV and two γ rays with energy of 1.17 MeV and 1.33 MeV. The emitted gamma rays constitute the therapy beam; the electrons are absorbed in the cobalt source's capsule where

University of Ghana http://ugspace.ug.edu.gh

they produce relative low energy and essentially negligible bremsstrahlung x-ray and characteristic x-ray.

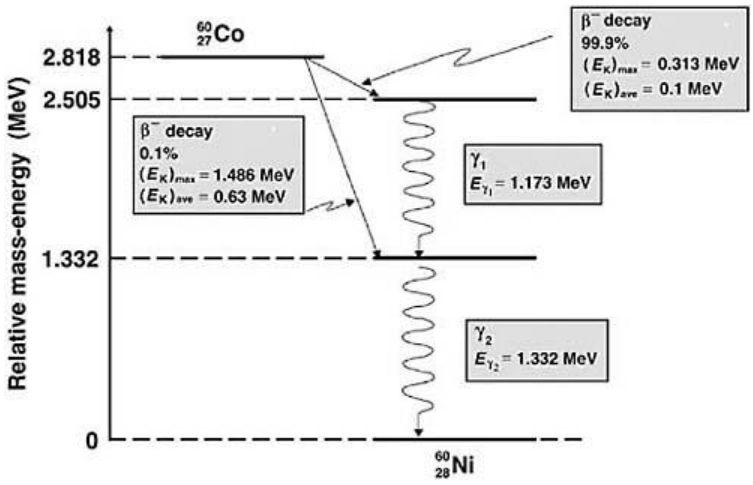

Figure 2.19. Decay scheme of cobalt-60 radionuclide

The prescribed target dose is delivered with the help of two treatment timers: primary and secondary. The primary timer actually controls the treatment timers, the second timer serves as a backup timer in the case of the primary timer failure. The set of treatment timers must incorporate the shutter error which accounts for the travel time of the source from the beam off position towards the beam on position at the start of irradiation and for the reverse travel at the end of irradiation. The collimators of tele-therapy machines provide squares and rectangular radiation fields typically ranging from 5x5cm^2 to 35x35 cm^2 at 80 cm from the source. The geometric penumbra, which result from the finite source diameter may be minimized by using small diameter source and by using penumbra trimmers as close as possible to the patient's skin.

University of Ghana http://ugspace.ug.edu.gh

2.10.2. Linear Accelerator Machine

The linear accelerator (LINAC) is a device that uses high-frequency electromagnetic waves to accelerate charged particles such as electrons to high energies through a linear tube. The high-energy electron beam itself can be used for treating superficial tumors, or it can be made to strike a target to produce x-rays for treating deep-seated tumors.

There are several types of linear accelerator designs, but the ones used in radiation therapy accelerate electrons either by traveling or stationary electromagnetic waves of frequency in the microwave region (~3,000 MHz). The difference between traveling wave and stationary wave accelerators is the design of the accelerator structure. Functionally, the traveling wave structures require a terminating, or "dummy," load to absorb the residual power at the end of the structure, thus preventing a backward reflected wave. On the other hand, the standing wave structures provide maximum reflection of the waves at both ends of the structure so that the combination of forward and reverse traveling waves will give rise to stationary waves. In the standing wave design, the microwave power is coupled into the structure via side coupling cavities rather than through the beam aperture. Such a design tends to be more efficient than the traveling wave designs since axial, beam transport cavities, and the side cavities can be independently optimized. However, it is more expensive and requires installation of a circulator (or isolator) between the power source and the structure to prevent reflections from reaching the power source. Figure 2.20. below shows the schematic linear accelerator used in medicine.

University of Ghana http://ugspace.ug.edu.gh

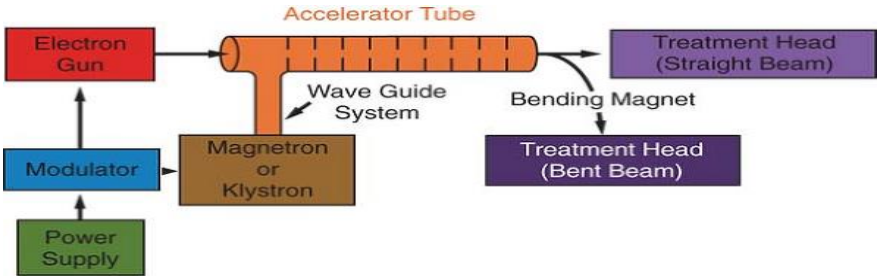

Figure. 2.20. Scheme of linear accelerator used in radiotherapy (Khan, 2010)

A power supply provides direct current power to the modulator. The modulator includes the pulse forming network. High voltage pulses from the modulator are delivered to the magnetron or klystron and simultaneously to the electron gun. Pulsed microwaves from the magnetron or klystron are injected into the accelerator tube via a waveguide system. Electrons from the electron gun are also injected into the accelerator tube in a pulsing manner. The electrons gain energy from the sinusoidal electric field. As the high energy electrons exit the accelerator structure, they are in the form of a pencil beam about three millimeters in diameter.

2.11. Cerrobend alloy material

This alloy was used because it is available in many radiotherapy departments. It is inexpensive, recyclable and can be used in applications beyond IMRT (Chang et al., 2004). This alloy which is suitable for the proposed method has low melting point, and thus can be used as a liquid to fill a mold. Another advantage is that it has high density (9.76 g / cm^2), reducing the average thickness of the IMRT blocks (Chang et al., 2004). With this,

University of Ghana http://ugspace.ug.edu.gh

the object dimensions that serves as a mould is also reduced, Table 2.02. bellow show the physical parameters of the constituents.

Table. 2.02: Physical parameters of constituents of the cerrobend (w_i is the proportion by mass of i_{th} component, A atomic mass, Z atomic number, ρ physical density and ρ_e electron density) (ElKhatib et al., 1987)

	Bismuth	Lead	Tin	Cadmium
w_i	0.5	0.267	0.133	0.1
A	208.98	207.2	118.69	1124.1
Z	81	82	50	48
$\rho(g/cm^3)$	9.78	11.36	7.30	8.65
$\rho_e(el/cm^3)$	23.3933×10^{23}	27.0709×10^{23}	18.5150×10^{23}	22.2468×10^{23}

Cerrobend is a common material used in the production of shielding blocks for irregular shaped field size in radiation therapy. It was selected in this research for constructing compensator based IMRT because it is available at National Centre for radiotherapy and Nuclear Medicine of Korle-Bu Teaching Hospital, it is easy of handle, reusable and its mechanical characteristics (strength, etc.), are well known. Plate 2.01. shows the cerrobend slabs used in the measurement of the linear attenuation coefficient. However, as a compensating material, little experience has been reported. Absorption data for cerrobend has been published only for pencil beam geometry for variety of energies (Huen et al., 1979) and for broad beam geometry with 5.7MeV x-ray.

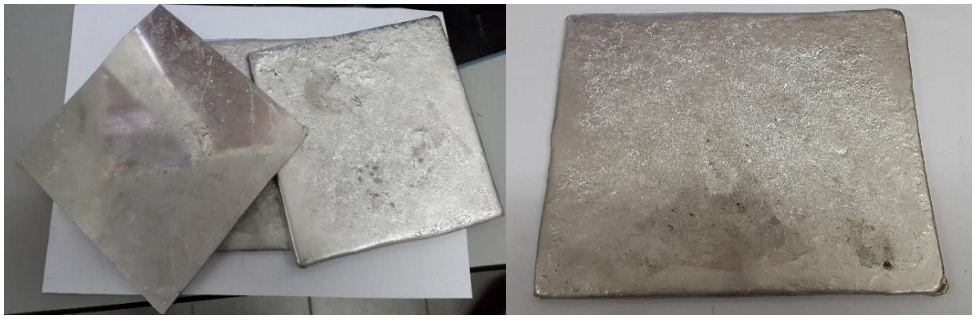

Plate. 2.01. Cerrobend slabs produced in this present research and used in the measurements for determination of linear attenuation coefficient

University of Ghana http://ugspace.ug.edu.gh

CHAPTER III

3.0. MATERIALS AND METHODOLOGY

3.1. MATERIALS

The data collection was done at National Centre for Radiotherapy and Nuclear Medicine of Korle-Bu Teaching Hospital. This Centre, has one cobalt-60 teletherapy machine (Theratron Equinox 100 cobalt-60 teletherapy unit) which was used in this research. The centre also has a mold room equipped with one block cutter (FC/1000 block cutter) for cutting the styrofoam blocks for molding and an alloy melter used for melting the cerrobend (low melting alloy material), for molding blocking blocks. These equipment were used for preparing the cerrobend slabs each with thickness of 0.5 cm on average and which were used in the measurement of the linear attenuation coefficient. They were also used for molding the compensators in molds of styrofoam block.

During the measurement of transmission through various thicknesses of the cerrobend slabs and for thicknesses volume of water in a container mounted on block tray of the head of Theratron Equinox 100 cobalt-60 teletherapy unit an ion chamber and electrometer were used. A cylindrical ion chamber with 0.125cc sensitive volume with its buildup cap on and sufficient to give electronic equilibrium connected to an electrometer was used, using source to detector distance (SDD) of 100cm.

The electrometer connected to the chamber was a PTW UNIDOS which was set to measure the intensity of transmitted radiation through the cerrobend slabs and thickness of water in the tank mounted on the block tray, in terms of charge at 60 seconds interval with bias voltage of +400V.

University of Ghana http://ugspace.ug.edu.gh

The readings were corrected for environmental conditions (temperature and pressure) using TRS 398. A barometer and digital thermometers were used to collect these parameters. For the measurements in water, 2D locally fabricated water phantom and an ionization chamber type 0.04cc with serial number 11026 manufactured by IBA Dosimetry, Germany were used. The dosimetric verifications of the compensator constructed in this research was done using gafchromic film, ionization chamber and Prowess Panther Treatment Plannig System, Epson Scanner was used for scanning the films for later readout using ImageJ software.

3.1.1. Alloy melter

Is a highly-durable alloy production melter has a heavy-gauge stainless steel inner and outer wall construction, with full-wrap ceramic heaters. The heated ball valve dispenser helps prevent nozzle blockage.

The alloy melter used in this work is shown in Plate 3.01., it is a MED-TEC, USA product with serial number 1030 and has a nominal voltage of 220volts, and intensity is 4A. It's having a digital readout to allow the operator to see the actual temperature. It can be used with either low-melt or medium-melt alloy.

Low-melting alloys start melting at 158^0 F (70^0 C) and is completely molten at 163.4^0F (73^0C) (ElKhatib et al, 1987) and medium-melt alloy at 203^0 F (95^0 C)

University of Ghana http://ugspace.ug.edu.gh

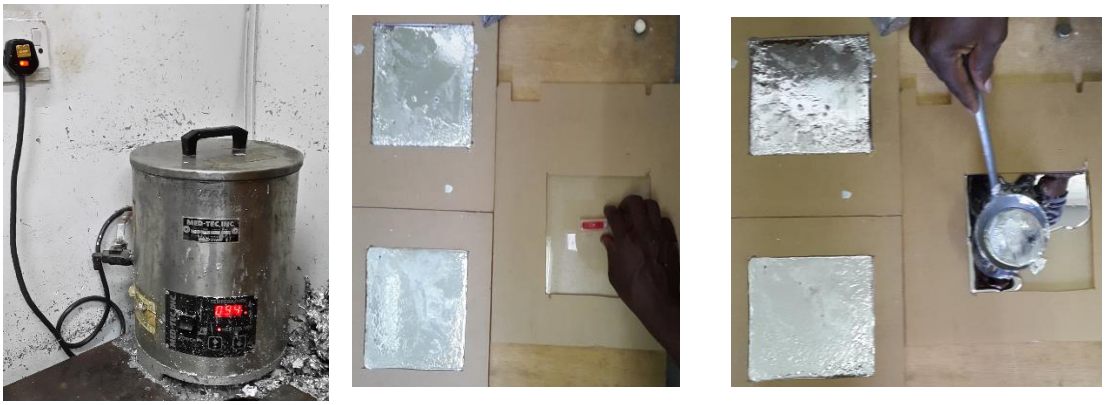

Plate 3.01. Alloy melter used in this work to melt cerrobend

3.1.2. Theratron Equinox 100 Co-60 teletherapy machine

Theratron Equinox a teletherapy treatment machine manufactured in Canada, is the machine that is available at National Centre for Radiotherapy and Nuclear Medicine at KBTH with a model number 2117. It consists of a rotatable gantry and a collimator unit head panel, hand control and a control console with a display monitor as shown in Plate 3.02.

Plate. 3.02. Theratron Equinox 100 Co-60 teletherapy machine in the treatment room at NCRNM of KBTH

University of Ghana http://ugspace.ug.edu.gh

The radiation source is a radioisotope Co-60 with 5.26 years half-life. The activity of the source and dose rate during measurement on February 22, 2014 were 370.4 TBq and 184.63 cGy/min respectively (Teclehaimanot, 2014).

The Equinox 100 is a fully computerized teletherapy machine, which may be operated either in fixed or arc mode. The following accessories are available: motorized wedge system, physical wedge filters, asymmetrical collimation, and accessories holder system for the support of beam modifying devices such as block trays and compensators. The gantry of the teletherapy machine is mounted isocentrically.

3.1.3. Prowess Panther Treatment Planning System

The Prowess treatment planning system (TPS) is a 3D radiation TPS, which uses patient data acquired from computer tomography (CT) scanners and beam data obtained during commissioning to create virtual simulation of treatment and dose calculations. It can receive information via network systems from any CT scanner using DICOM 3.0 format and from other devices such as digitizers. It is a very flexible system and may use Windows XP or Windows 7 user interface depending on the version. Prowess Panther version 4.6 uses Windows XP interface.

During simulation processes, it is possible to create digitally reconstructed radiographs (DRR) in any plane from axial CT images, which are displayed in the beam eye view phantoms with regular shapes can be created with the TPS for dosimetric studies. The TPS comes with special tools for organ and target segmentation, which make it possible for the

University of Ghana http://ugspace.ug.edu.gh

clinician to know the amount of radiation dose received per volume of organ or target delineated. This is used by the clinician to assess dose constrains of organs as well as see how good a plan is.

Radiation field shaping can be done with the TPS using custom blocks or multileaf collimators. Bolus can be added to a particular field with a click of a bottom. The bolus is made to cover the entire field with margins. Bolus can also be entered manually by using tools for organ and target segmentation. The radiological properties of bolus material are entered in terms of Hounsfield Units. When a bolus is added to the patient surface contour, the treatment depth is increased by an amount equal to the thickness of the bolus. Plate 3.03 shows the planning window of the Prowess Panther TPS.

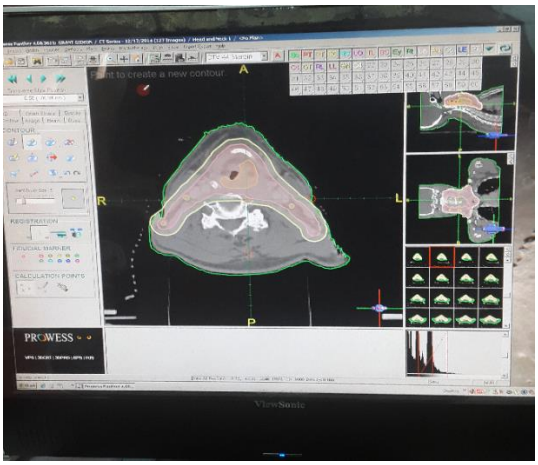

Plate. 3.03. Window of Prowess Panther treatment planning system

Patient dosimetry computer simulations are done with the aid of full 3D convolution/ super-positioning algorithm, which uses the effective path length method to account for tissue heterogeneities. The actual dose generated from beams can be displayed in real-time. The dose computation can be done in two modes i.e., fast photon and fast photon effective path

University of Ghana http://ugspace.ug.edu.gh

modes. The fast photon mode neglects tissue heterogeneities and treats the whole patient volume as water when computing patient dose distributions whilst the later corrects for tissue inhomogeneity in the dose computations.

3.1.4.System ion chambers and electrometer

An ion chamber is made up of a collecting electrode and a polarizing electrode between which there is a gas filled cavity. A potential difference is applied between the two electrodes resulting in an electric field inside the cavity. When the chamber is irradiated, secondary electrons are produced thus ionizing the gas within the cavity. The resulting positive and negative ions will move to their respective electrodes due to the presence of the electric field. The total charge collected, or the current produced at the collecting electrode is measured using an electrometer. The potential difference between the two electrodes must be set at a value low enough to minimize charge amplification whilst being large enough to avoid charge recombination.

University of Ghana http://ugspace.ug.edu.gh

Plate 3.04. An ionization chamber with an electrometer.

3.1.5. 2D FULL SCATTER WATER PHANTOM

For measurement in water a 70x70x60 cm^3 2D full scatter water phantom was modified for this research from that used by Mensah (2014) in his work to make it useful for measurements for the present work. In this research the phantom rod was redesigned using aluminum metal to allow measurements for various SSDs by reducing its size. The chamber in the phantom moves off- axis directions and depth. Plate 3.05. shows the phantom and the main components.

a)

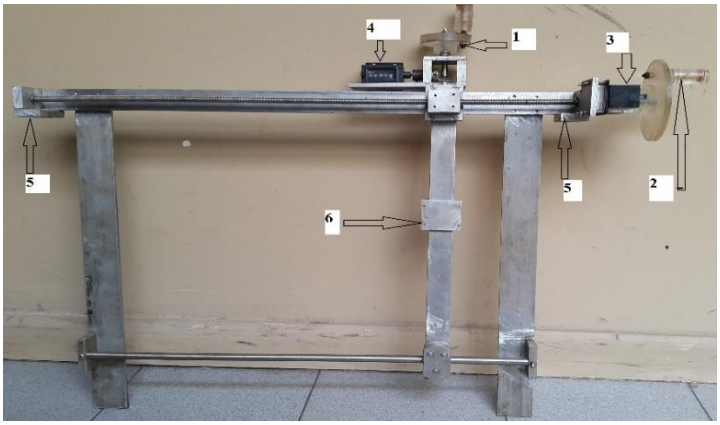

b)

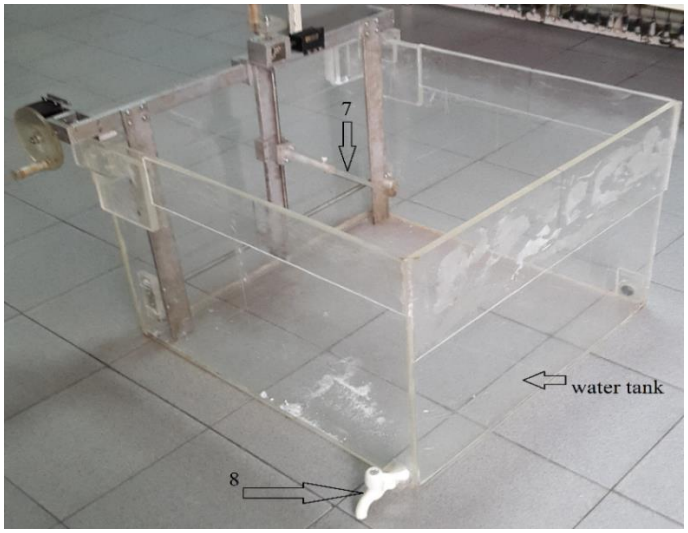

University of Ghana http://ugspace.ug.edu.gh

Plate 3.05: In a) Phantom rod showing the main components in b) water phantom with chamber holder

The function of components of the phantom in the Plate 3.05. are described below:

Components 1 and 2 are the handles, their function is to allow the operator to move the chamber during the experiment. Handle 1 allows the vertical movements of the chamber in the tank (vertical handle). Handle 2 allows movements of the chamber in the off axis directions and this is lateral handle. The components 3 and 4 are the counters, these allow the operator to read the counts that corresponds to the distance traveled by the chamber in depth and off-axis. Counter 3 is for the readings in the lateral movements of the chamber and 4 for vertical movements (depth).

Component 5 are aluminum pieces used to fix the rod on the water tank. Component 6 is where the chamber holder is fixed, 7 is the chamber holder and 8 is the pipe that allow variation of the volume of water and allow to empty the tank for later storage.

The water phantom was calibrated in such way that 70 counts readings on the counter are equivalent to 1.0 cm distance traveled by the chamber holder in the off-axis distance and in depth (vertical movements).

3.2. EXPERIMENTAL SETUP

3.2.1. Variation of transmission for cerrobend in air

The data was collected using the experimental setups in section 3.2.2 for determination of linear attenuation coefficients for cerrobend was also used to assess the percentage

University of Ghana http://ugspace.ug.edu.gh

variation of transmission with changing thickness of material and field size. Percentage of transmission was plotted against thickness of cerrobend and field size shine in Figure 4.01 a) b).

3.2.2. Determination of narrow and broad beam linear attenuation coefficients for Cerrobend

The narrow and broad-beam attenuation coefficients for cerrobend and water were determined from the transmission measured in air using a 0.125cc cylindrical ionization chamber at SDD of 100cm with a build-up cap sufficient to give electronic equilibrium. A flat filter with thickness from 0.499 cm to 4.6 cm of cerrobend was placed on a perspex frame positioned in the block-tray assembly. The output measurements were carried out for a number of field sizes (4 cm x 4 cm − 30 cm x 30 cm) and the ion chamber at 100 SDD. After the measurements, the transmissions were calculated and tabulated, graphs of natural logarithm of transmission were plotted against the thickness of cerrobend (Figures 4.02). The linear attenuation coefficient is represented by the slopes of the graphs at specific radiation field size. The narrow beam attenuation coefficient is that determined at 4 cm x 4 cm radiation field. Plate 3.06. shows the experimental setup used to measure the linear attenuation coefficient for water and cerrobend in air.

University of Ghana http://ugspace.ug.edu.gh

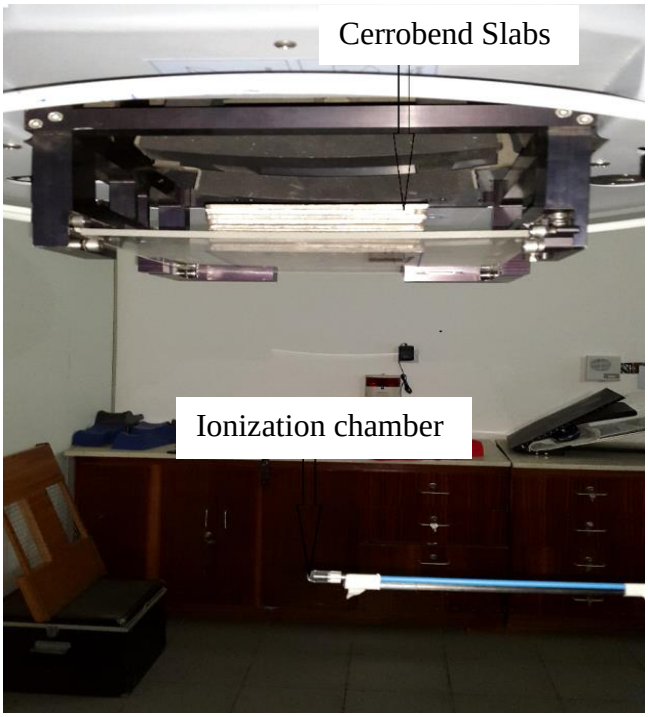

Plate. 3.06. Experimental setup for measurement of the linear attenuation coefficient in air for cerrobend

3.2.3. Determination of narrow and broad beam linear attenuation coefficients for water

The same procedure used for the measurements in section 3.2.2 for linear attenuation coefficient of cerrobend, was used for measurements of output for water. The volume of water was varied in a fabricated perspex tank with dimensions of 20x20x20 cm^3 mounted on the head of the Thermatron equinox 100 cobalt machine. The readings were collected on the electrometer and from tabulated data, graphs of transmission against of thickness of water from 2 to 14 cm (adding 2cm thickness of water at a time) were plotted, Figure 4.03. Plate 3.07 shows the experimental setup used for measurements in air.

University of Ghana http://ugspace.ug.edu.gh

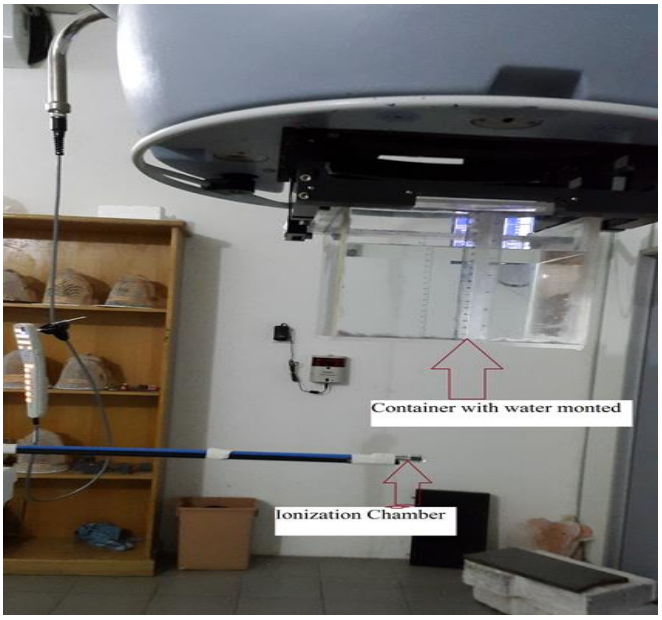

Plate. 3.07. Experimental setup for measurement of the linear attenuation coefficient in air for water

3.2.4. Assessment of scatter contribution and evaluation for cerrobend

To investigate the contribution of scattered photons generated within the cerrobend mounted on block tray, to the final dose distribution, the same set up used in 3.2.2. for the measurements and the same data used for determination of linear attenuation coefficient of cerrobend in air were used. To get the scatter-to-primary ratio dose contribution, the method described by Huang et al. (1986) described in 2.7.1. was used. From the data tabulated, graphs of S/P(%) against cerrobend thickness were generated for each field size from 4 cm x 4 cm to 30 cm x 30 cm.

University of Ghana http://ugspace.ug.edu.gh

3.2.5. Reduction in scatter for using bolus on the surface to be mimicked by compensator

To account for reduction in scatter because of using bolus on the surface of the phantom to be mimicked by cerrobend on the block tray, factors that account for the effect of thickness, field size and treatment depth were generated. The measurements were done in water using a fabricated full scatter water phantom and IBA ionization chamber type 0.04cc sensitive volume connected to PTW UNIDOS electrometer using SAD of 100 cm. The phantom was filled with water to a maximum depth of 20 cm from the detector, SSD of 80 cm. Measurements were done varying the depth by reducing the volume of water in the tank using the pip, from 20 cm to 0.5 cm as follows 20 cm, 18 cm, 15 cm, 10 cm, 6 cm, 4 cm and 0.5 cm. For each depth, readings were collected on the electrometer for open field sizes from 4 cm x 4 cm to 30 cm x 30 cm and by also varying the thicknesses of cerrobend slabs from 0.5 cm to 4.6 cm. Each volume of water that was removed from the tank was considered as a thickness of bolus. Four different depths were considered in the case of bolus on the surface of the phantom ranging from the 0.5 cm to 10 cm (0.5cm, 4cm, 6cm and 10cm with maximum error or 0.01cm) Plate 3.08 shows the experimental setup and sections 3.2.5.1, 3.2.5.2, 3.2.5.3 show the procedure to determine the equations for correction factors.

University of Ghana http://ugspace.ug.edu.gh

Plate 3.08. Experimental setup used for determination of factors to account for reduction in scatter for using bolus on the surface to be mimicked by cerrobend on block tray**.**

3.2.5.1. Thickness ratio and normalized thickness ratio correction factor with respect to thickness of water on the surface of the phantom and that of compensator on block tray determination

The output of the Theratron Equinox 100 cobalt 60 teletherapy machine using a constant radiation beam field size of 10cmx10cm was measured on the beam's central axis with 0.04cc cylindrical ionization chamber in a 70 cm x 70 cm x 60 cm locally made perspex phantom at a depth of 4 cm employing an isocentric technique. The measurements were carried out with slabs of cerrobend and a block tray in the path of the radiation beam. The ionization chamber was connected to the PTW electrometer.

Nine slabs of cerrobend having dimensions of 15 cm x 15 cm with the thicknesses of 0.5cm average, were cast from molds of 0.6 cm thick perspex and used for the measurements. The

University of Ghana http://ugspace.ug.edu.gh

measurements were done by varying the thickness of volume of water in the phantom representing thickness of bolus on the surface and thickness of cerrobend on the block tray, for each thickness of water and that of cerrobend on block tray, output of teletherapy machine were measured.

From above measurements, using the same axes, a graph of output was plotted against thickness of water on the surface of the phantom and that with cerrobend slabs mounted on block tray. From the plots, the thickness of cerrobend slab mounted on block tray that would give the same output as thickness of water on the surface of the phantom were determined for various thickness of water on the surface of the phantom. Figure 3.01 shows the graphical method used to find thickness of cerrobend (x) on the block tray that gives the same output (y) with thickness of water on the surface of the phantom.

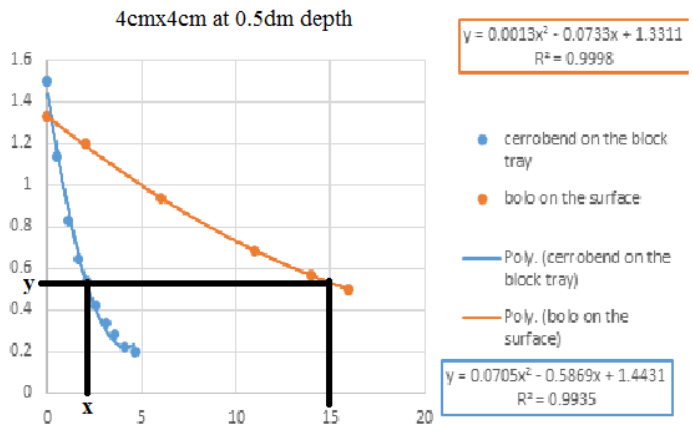

Figure 3.01. Graphical method used to find the thickness of cerrobend (x) that gives the same output (y) with bolus on the surface of the phantom

The ratio of the thicknesses of slabs of cerrobend mounted on the block tray to that of water on the surface of phantom which would give the same output were computed for each of the corresponding thickness of water on the surface of the phantom used in the above

University of Ghana http://ugspace.ug.edu.gh

measurements. A graph of the ratio and normalized ratio as a function of thickness of water on the surface of the phantom were therefore plotted, Figure 4.08 and Figure 4.09 respectively, and correlation equations of curve together with correlation coefficients, R^2 of the curve with the best fit determined.

3.2.5.2. Correction factor to account for reduction in scatter with respect to radiation field size

The procedures 3.2.5.1. were repeated for a constant thickness of cerrobend of 0.5 cm, but radiation field size was varied with square field sizes ranging from 4 cm x 4 cm to 30 cm x 30 cm, which were increased in steps of 2 cm on both coordinates until 10 cm x 10 cm and then increased 4 cm step until 30 cm x 30 cm. For each field size setting, outputs were measured with the water on the surface of the phantom and with cerrobend on block tray.

A graph of output of the teletherapy machine was plotted against one side of a square field (equivalent square) with thickness of water on the surface of the phantom and that with the cerrobend slab mounted on the block tray using the same axes, Figure 4.10. The radiation field sizes with cerrobend slab mounted on the block tray that would produce the same outputs as that with thickness of water on the surface of the phantom were determined for the various square field sizes with thickness of water on the surface of the phantom used in the measurements. The ratio of one side of the square field size with a cerrobend slab mounted on the block tray to that with the thickness of water on the surface of the phantom that would produce the same output was therefore determined for each square field size

University of Ghana http://ugspace.ug.edu.gh

with thickness of water on the surface of the phantom in the above measurements. The ratios obtained were therefore normalized to that for the $10\ cm \times 10\ cm$ field size, by dividing the various ratios with the ratio for the corresponding $10\ cm \times 10\ cm$ field size with the thickness of water on the surface of the phantom. The normalized ratios were therefore plotted against their corresponding one side of a square field with thickness of water on the surface of the phantom Figure 4.13, and the correlation equation of the curve with the best fit determined as well as the correlation coefficient, R^2, of the curve.

3.2.5.3. Correction factor to account for reduction in Scatter with respect to treatment depth

The procedures in section 3.2.5.1. were repeated again, for the 0.5 cm of cerrobend and 6 cm thickness of water on the surface of the phantom, but the depth of measurement in the phantom was varied for depths ranging from 0.5 cm to 10cm while still maintaining the isocentric treatment technique. For each depth setting, outputs of the teletherapy machine were measured with thickness of water on the surface of the phantom and also with the cerrobend slab mounted on the block tray.

A graph of output of the teletherapy machine was plotted against depth of measurement with 6cm thickness of water on the surface of the phantom and that with 0.5 cm thickness of cerrobend mounted on the block tray using the same axes shone in the Figure 4.14. The depths within the phantom with cerrobend slab mounted on the block tray that would produce the same outputs as that with the thickness of water on the surface of the phantom

University of Ghana http://ugspace.ug.edu.gh

were determined from the plots for the various depths with 6 cm thickness of water on the surface of the phantom used in the measurements. The ratio of the depth within the phantom with cerrobend slab mounted on the block tray to that with thickness of water on the surface of the phantom that would produce the same output was therefore computed for each depth of measurement within the phantom with thickness of water on the surface of the phantom in the above measurements. The ratios obtained were therefore normalized to that for the depth of 4 cm, by dividing the various ratios with the ratio for the corresponding 4 cm depth of measurement within the phantom with 6 cm thickness of water on the surface of the phantom. The normalized ratios were then plotted against their corresponding depths of measurements with thickness of water on the surface of the phantom shone on Figure 4.17, with the correlation equation of the curve with the best fit determined, as well as the correlation coefficient.

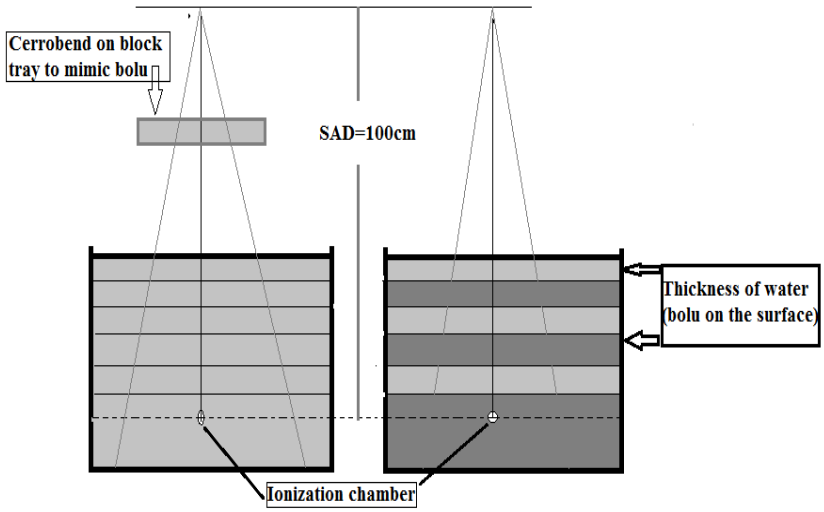

Figure 3.0.2. Schematic Diagram of experimental setup used for determination of thickness of cerrobend that produces the same output when using bolus on the surface of the phantom

University of Ghana http://ugspace.ug.edu.gh

3.2.6. Proposed method for determination of the thickness of cerrobend compensator that mimic bolus on the surface of the phantom

In the compensator design and construction, cerrobend alloy material was selected and the equation 3.01 below was used to covert the bolus thickness into the cerrobend thickness that gives the same output by using and representing the thickness ratio of the two materials cerrobend and water representing bolus on the surface which is represented in equation 3.01 by the inverse ratio of effective linear attenuation coefficient of the two materials, by applying correction factors for field size, treatment depth and the factor that accounts for variation of thickness ratio because of changing in thickness of bolus on the surface of the phantom.

$$t_c = \frac{\mu_{eff_b}}{\mu_{eff_c}} \times t_b \qquad 3.01$$

Where:

t_c - thickness of the compensator

t_b – thikness of bolus

μ_{eff_b} - effective linear attenuation coefficient of bolus

μ_{eff_c} – effective linear attenuation coefficient of compensator

Equation 3.01, in which the factor $\frac{\mu_{eff_b}}{\mu_{eff_c}}$ represents the thickness ratio, can be written as:

$$\frac{t_c}{t_b} = \frac{\mu_{eff_b}}{\mu_{eff_c}} \qquad 3.02$$

University of Ghana http://ugspace.ug.edu.gh

In this work the thickness ratio was represented as a product of thickness ratio at a reference depth and reference field size and factors that account for changes in field size and treatment depth from the reference field size and depth and normalization thickness ratio correction factor that corrects for change of thickness of bolus on the surface of the phantom. With reference of that the thickness ratio was written as the following in equation 3.03.

$$\frac{t_c}{t_b} = \frac{\mu_{eff_b}}{\mu_{eff_c}} = T_{d_r,s_r} \times F_{Tb} \times F_s \times F_d \qquad 3.03$$

Where:

d_r - Considered reference treatment depth

s_r – Considered reference field size

F_{Tb} – Normalization thickness ratio correction Factor that accounts for reduction in scatter with changes in considered reference bolus thickness on the surface of the phantom

F_d– Correction factor that account for reduction in scatter with respect to changes of considered reference treatment depth

F_s – Correction factor that accounts for changes of considered reference field size

In this work equation 3.01 that computes the thickness of cerrobend compensator that mimics bolus on the surface of the phantom can be written as follows.

$$t_c = T_{d_r,s_r} \times F_s \times F_{Tb} \times F_d \times t_b \qquad 3.04$$

University of Ghana http://ugspace.ug.edu.gh

3.2.7. Compensator construction

Styrofoam slabs with dimensions similar to that use by the oncology center to cut shielding blocks, were procured. With the FC/1000 block cutter set at the required configuration, was used to cut the outline of the radiation field in the styrofoam slabs using the magnified BEV from the TPS shone on Plate 3.09. The cut-out block was cut into steps and uniform surface according to the required shape and thickness of the compensator. The bottom piece of block removed from main styrofoam block, with the negative shape of the compensator, were re-assembled and stacked in to the orifice created in the Styrofoam block. It was ensured that the bottom of re-assembled cut-out was aligned with that of the Styrofoam block. The whole assembly was held in place by placing masking tapes on the bottom part of the slab in such a way as to seal all holes (Plate 3.10). The styrofoam slab assembly was positioned on a flat surface and held with G-clamps to apply a little bit of pressure to prevent the spilling of molten cerrobend once poured inside the created space. The styrofoam slab assembly was then filled with molten cerrobend. The content of the styrofoam slab was allowed about 45 minutes to solidify before the cerrobend was taken out and mounted on a block tray. Indentations were placed on the fabricated compensator to assist in aligning it with the beam central axis and the beam central axis marked on the block tray. Four compensators constructed with above procedures are shone in Plate 4.01. two compensators with uniform thickness and two step compensators. To verify point dose and dose distribution accuracy obtained by placing thickness of cerrobend that represents a given thickness of bolus on the surface of the phantom, four plans were generated with Prowess Panther TPS with bolus on the on the surface of the phantom and with a prescribed dose at a specific prescription point as shown in Plate 3.09 below. The thickness of bolus

University of Ghana http://ugspace.ug.edu.gh

was converted into thickness of cerrobend using equation 3.04 for a given thickness of bolus, radiation field size and treatment depth.

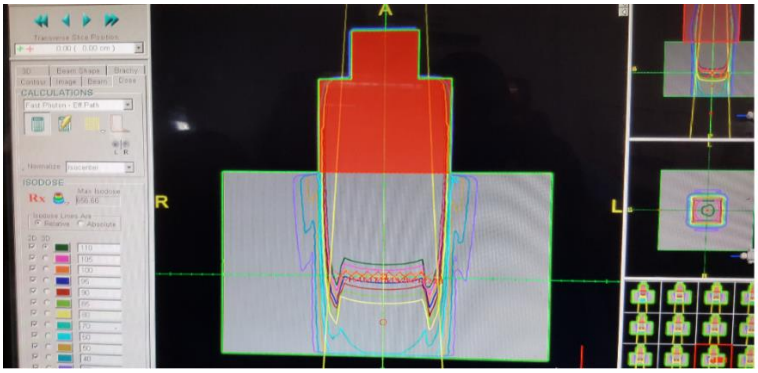

Plate 3.09. Setup bolus on the surface of the phantom in the TPS.

The cerrobend compensator that mimics bolus on the surface was reduced in the lateral dimension to account for divergence of the beam and to correct for the distance between the compensator and the phantom. To find the numerical value of the thickness of cerrobend compensator, excel spreadsheet was used to generate the values for a given thickness of bolus, radiation field size and treatment depth using Equation 3.04. The compensator was shaped in the molds of Styrofoam with respective thickness as missioned above, Plate 3.10 shows the molds prepared and used in this research for step compensator.

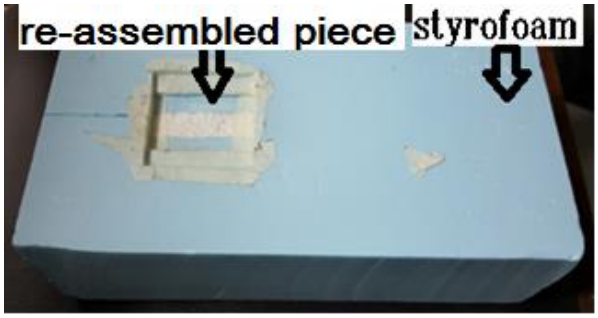

Plate 3.10. Styrofoam used to mold a step compensator

University of Ghana http://ugspace.ug.edu.gh

3.2.8. Dosimetry

3.2.8.1. Selection of the material

A phantom similar to the one used in the measurements was created with the Prowess Panther version 4.6 TPS using a slice thickness of 5 mm. And, after the outline of the phantom had been delineated on each slice with the auto-contouring tool, a plan was generated for the phantom using a single anterior beam for a given field sizes of 10 cm x 10 cm, 14 cm x 14 cm and 15 cm x 15 cm employing isocentric irradiation technique. The beam isocenter was made to coincide with the center of mass of the phantom giving a treatment depths of 4.54 cm, 6.82 cm, 11.36 cm and 8 cm. A bolus in the form of uniform and step wedge was created on the surface of the phantom for the radiation beam as shown in Plate 3.09. Using the procedures outlined above, a compensator to mimic the effect of the bolus was created with cerrobend as shown in Plate 4.01. The irradiation geometry produced with the TPS was simulated with the cobalt 60 teletherapy unit, but the bolus was replaced with the fabricated compensator. The outputs of the teletherapy machine within the phantom were measured at various points on the beam major axis across the uniform thickness and steps of the created step wedge at the beam isocenter with EBT2 gafchromic films and ionizing chamber, and the outputs compared with those of the TPS. The process was repeated for all other compensators created from the plans generated. The scanned films were digitized and gray values analyzed using imageJ software.

University of Ghana http://ugspace.ug.edu.gh

3.2.8.2. Film calibration and dose readings

EBT2 gafchromic film for dosimetry, was calibrated for dose measurement. The plan generated for the phantom in section 3.2.8.1. was used to compute treatment times for prescribed doses ranging from 50 – 350 cGy (increment of 50 cGy) using the isocenter as the normalization point without the bolus in the path of the beam. In the plans menu of the top bar menus of the TPS planning window, 'plan manager' was selected and the plan in section 3.2.8.1. was printed. After this, the bolus in the BEV was removed in beam shaping mode. The treatment times obtained from the TPS were recorded against their corresponding prescribed doses. The irradiation geometry simulated with the TPS was set up on the Theratron Equinox 100 cobalt-60 teletherapy machine with EBT2 gafchromic film sandwiched between 4 piles of perspex slabs of the phantom at equivalent a depth in water of 4.54 cm. The film was placed between the perspex slabs placed on the treatment couch, perpendicular to the beam axis. A block tray similar to the one that would be used to mount the compensator was held at the accessory holder of the teletherapy unit during the above irradiation to annul the effect of the block tray. Using the described set up, EBT2 gafchromic films were irradiated with radiation doses for treatment times obtained from the TPS with the corresponding prescribed doses inscribed on the packet of the various films for easy identification. The irradiated films were scanned within twenty-four (24) hours after irradiation and the gray values measured for digitized area using imageJ software.

The irradiated films were scanned with Epson scanner with a professional mode and the resolution to 72dpi with all color option settled off to allow the image be appropriate for imageJ software.

University of Ghana http://ugspace.ug.edu.gh

To account for warm up of the scanner, the films were scanned 5 times, and after that the mean of the gray value for the five scanners for each dose and each experiment were recorded.

Gray values were collected for each film for a particular prescribed dose and then plotted against dose using imageJ software and then generated the calibration function shone in the Figure 4.17. which was used to measure the corresponding dose for each gray value measured for the irradiated films with compensator on the block tray, for both irradiated films for calibration and for dosimetric verifications, only red channels where used. Plate 3.11 a) and b) show the image of irradiated films for calibration on imageJ red channel interface and during the scanneing process respectively.

a)

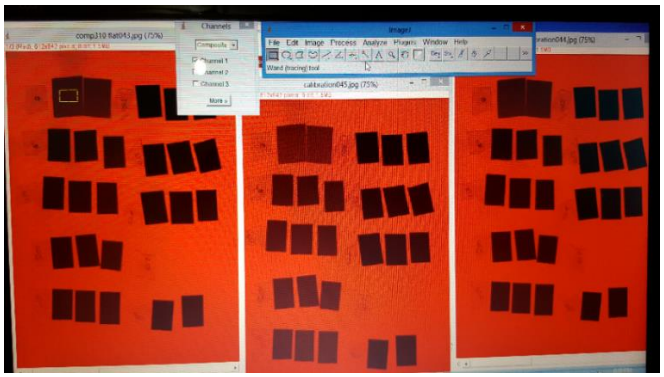

b)

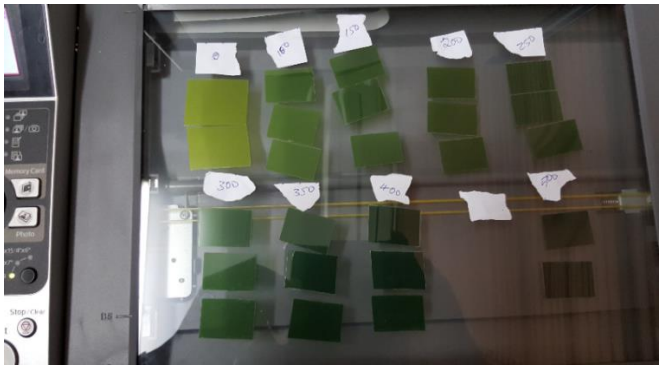

Plate 3.11. In a) Image of irradiated films during digitization ImageJ software, in b) image showing the arrangement of the films in the scanner for scanning procedure.

University of Ghana http://ugspace.ug.edu.gh

3.2.8.3. Dose measurement

To test the accuracy of delivered intensity modulated and dose distribution, and thus to verify the accuracy of the method using bolus to be mimicked by the cerrobend compensator on the block tray, tests were done using the fabricated cerrobend compensator and plastic slab phantom and EBT2 gafchromic film. For a specific treatment depth, the same planned in the TPS using bolus on the surface of the phantom, was used for a prescribed dose of 200cGy treatment time of 4.07 minutes with film at SAD of 100 cm. The same procedure that was used to scan and to analyze films for calibration, was used to measure the gray values from irradiated films with cerrobend compensator on the block tray. The compensator was constructed for specific treatment parameters (treatment depth, radiation field size) and thickness of bolus to be mimicked.

Equivalent thickness of compensator that will mimic the bolus placed on the surface of the phantom was simulated from TPS with treatment parameters and a given dose of 200cGy and then recorded the treatment time to be used for irradiation with the cobalt machine. Plate 3.12 shows the setup on the TPS and Figures 4.19, 4.20 and 4.21 show the off-axis dose profiles for each compensator constructed.

University of Ghana http://ugspace.ug.edu.gh

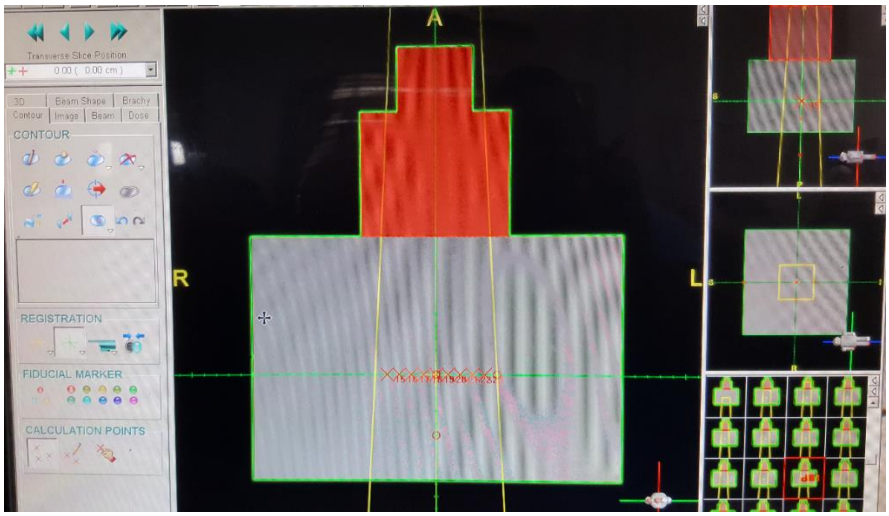

Plate 3.12. Image of bolus placed on the surface of the phantom with prescription points and radiation beam on

Three films were prepared to be irradiated with each compensator mounted on the block tray. The gray values were collected for each region of interest on the film, and then using the calibration equation in 4.4.1, the equivalent dose was measured and compared with that predicted by TPS.

3.2.8.4. Evaluation of the compensator

Copies of the plans with the bolus on the surface of the phantom were used for the dosimetry analysis. Calculation points were placed at the isocenter on the beam major axis across steps of the step wedge and uniform thickness of bolus. Starting from the beam isocenter, the calculation points were placed at 6 cm, 4 cm and 2 cm part from each other on either side of the beam central axis, 4 cm and 2 cm for uniform thickness or bolus. With prescribed doses 200 cGy normalized to the isocenter, treatment times were computed by

University of Ghana http://ugspace.ug.edu.gh

the TPS and off-axis dose profile for the calculation points obtained. The off-axis dose profiles together with their corresponding distances were recorded.

The plans produced with the TPS above were then simulated on the cobalt 60 treatment unit and the off-axis dose profile measured with EBT2 films sandwiched between piles of perspex slabs of the phantom at various depths, Figure 3.03. shows the set up for irradiating the EBT2 gafchromic films. But the bolus on the surface of the phantom were replaced with the fabricated compensators (designed to mimic the effect of the bolus), which were held on the accessory holder of the treatment unit. Indentation marks placed on the compensators helped in aligning a compensator correctly in the path of the beam. The films were irradiated for treatment times indicated by the TPS and the corresponding prescribed doses recorded on the film packet. The irradiated films which were from the same package, were scanned together with those used for the film calibration. The off-axis distances corresponding to the calculation points of the TPS were determined and marked on the paper which was scanned together with films in the correct direction. ImageJ software was then used to digitize and measure the gray values at these points along the digitized areas of the images. The measured gray values were converted to doses and compared with those of the TPS at the required off-axis distances for each prescribed dose, which can be seen in the Figures 4.22, 4.23, 4.24 and 4.25.

University of Ghana http://ugspace.ug.edu.gh

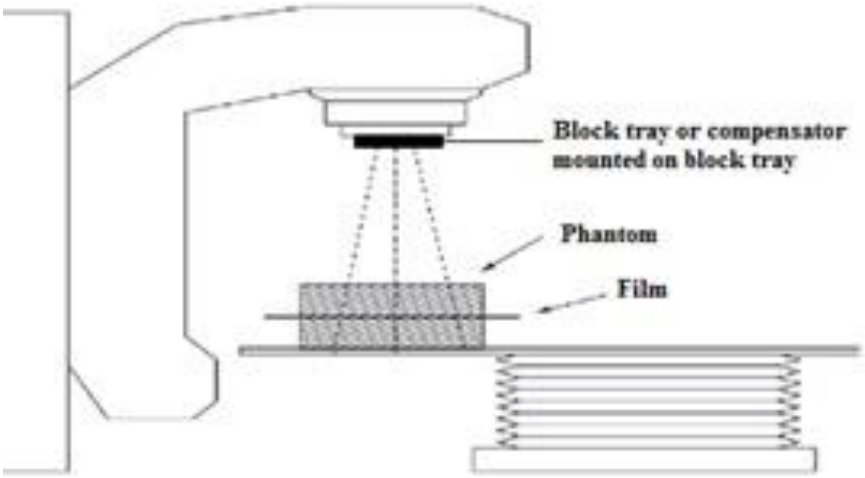

Figure 3.03. Set up for irradiating EBT2 gafchromic film

University of Ghana http://ugspace.ug.edu.gh

CHAPTER IV

4.0. RESULTS AND DISCUSSION

4.1. Variation of transmission for cerrobend

The dependence of percentage transmission of cobalt 60 beam for a particular thickness of cerrobend on collimator setting (or field size) is depicted in a) of Figure 4.01 below. The percentage of radiation transmitted by the cerrobend is plotted as function of one side of a square field size for various thicknesses of the cerrobend using the same axes. The side of a square field size is similar to equivalent square field size which is used in radiotherapy to compare dosimetric functions of irregular and rectangular field sizes to those of square field sizes, which are mostly used for dosimetry measurements. In b) of Figure 4.01, percentage radiation transmitted by the cerrobend is plotted as a function of thickness of cerrobend placed in the path of the beam for some selected field sizes (4 cm x 4cm, 10cm x 10 cm, 20cm x 20 cm and 30cm x 30cm) using the same axes. The equations of correlation and regressions (R^2) for the various curves are displayed above the curves and are distinguished from each by colours similar to that of the appropriate curve.

University of Ghana http://ugspace.ug.edu.gh

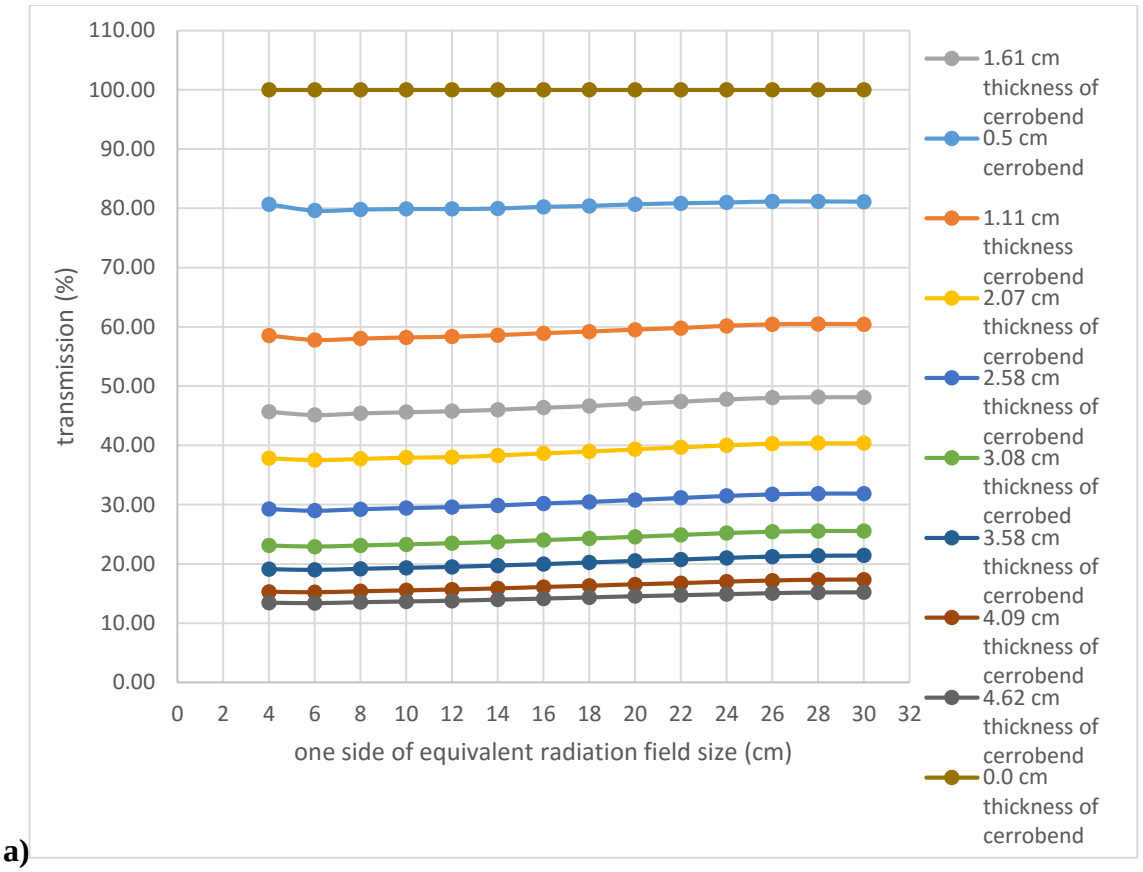

a)

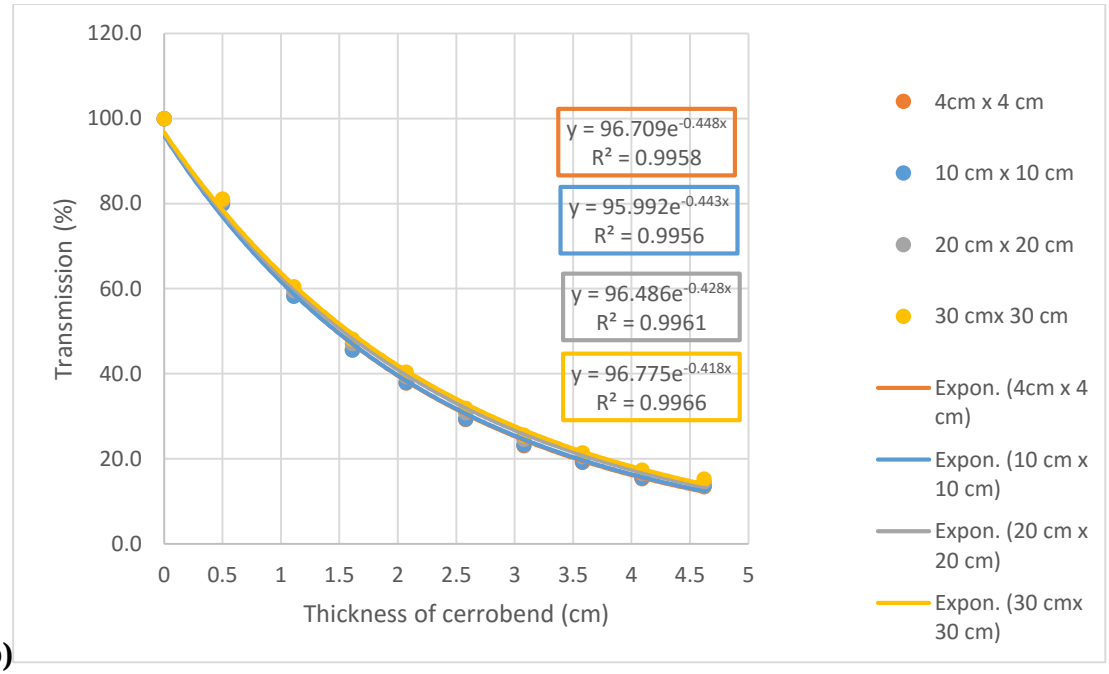

b)

Figure 4.01. Variation of percentage transmission with field size for different thicknesses of cerrobend in a) and in b) how the transmission falls with thickness o cerrobend

University of Ghana http://ugspace.ug.edu.gh

From Figure 4.01, percentage of radiation transmitted through cerrobend increases with increase in field size. As field size increases the volume of cerrobend slab traverse by the radiation increases producing more scattered radiation. The magnitude of the scattered radiation produced increases with increase in volume of cerrobend traversed by the radiation. The attenuation of the primary beam resulting from increase in the thickness of cerrobend is slightly overshadowed by the resultant scattered radiation produced by the cerrobend due to the increase in field size. Also transmission offered by the cerrobend reduces exponentially with increase in the thickness of the cerrobend traversed by the radiation for a particular field size. This reduction in transmission is influence by field size similar to or in tandem with what have been discussed. A thickness of 0.5 cm of cerrobend is able to reduce the intensity of the beam by 20 %, and thickness of 1.11 cm would reduce the intensity to about 55 %. From this analysis it is evident that a small error in the estimation of a particular thickness of cerrobend to produce a predefined dose distribution, would result in significant error in the dose distribution.

Mejadden et al. (1999) reported that an uncertainty of 0.1 mm in the thickness of cerrobend put in the path of a 6 MV beam lead to 0.5 % change in transmition dose and for 0.5 mm cerrobend with a 10 MV beam the change was 1% .

4.2. Linear attenuation coefficient of cerrobend in air

4.2.1. Linear attenuation of cerrobend

The natural logarithm of transmission is plotted as a function of thickness of cerrobend placed in the path of the beam for various field sizes using the same axes, and it is depicted

University of Ghana http://ugspace.ug.edu.gh

in Figure 4.02. The slope for a particular curve per filed size gives the linear attenuation of cerrobend for the specified collimator setting.

The equations of correlation and their corresponding regressions (R^2) are displayed on the curves for field sizes of; 4 cm x 4 cm, 6 cm x 6 cm and 30 cm x 30 cm. The linear attenuation coefficient decreases as field size increases and this is illustrated graphically in Figure 4.04 for water and cerrobend. This may be attributed to increase in the amount of scattered radiation reaching the detector as field size increases, and irradiation geometry deviating from narrow beam geometry, which is a requirement for the measurement of linear attenuation coefficient for a particular material. In the clinical environment, narrow beam geometry is not attainable, hence factors, such as irradiation geometry which would influence the linear attenuation coefficient need to be accounted for in the measurement of the linear attenuation coefficient. With reference to this, effective linear attenuation coefficient is preferred for clinical use.

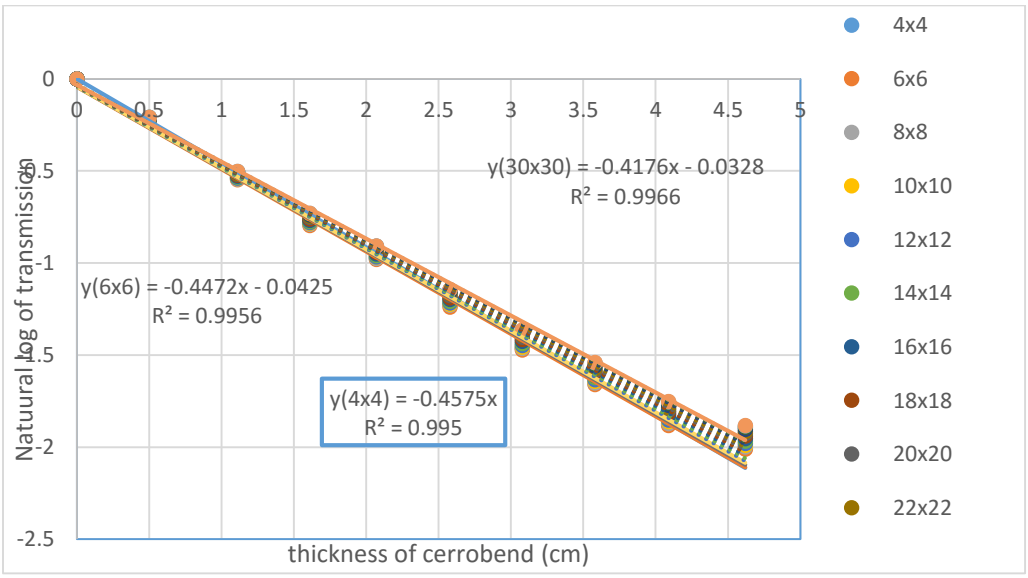

Figure. 4.02.: Relation of natural log of transmission and thickness of cerrobend

University of Ghana http://ugspace.ug.edu.gh

4.2.2. Linear attenuation of water

The natural logarithm of transmission is plotted as a function of thickness of water placed in the path of the beam for various field sizes using the same axes, and it is shown in Figure 4.03. The slope for a particular curve per filed size gives the linear attenuation coefficient of water for the specified field size.

The equations of correlation and their corresponding regressions (R^2) are displayed on the curves for field sizes of; 4 cm x 4 cm, 6 cm x 6 cm and 30 cm x 30 cm. The linear attenuation coefficient decreases as field size increases similar to what was experienced with the cerrobend. The ratios of the linear attenuation coefficient measured with a field size of 4 cm x 4 cm (presumed to be ideal narrow beam geometry) to that measured with a field size of 30 cm x 30 cm are 1.0943 and 1.2912 for cerrobend and water respectively. This shows that the dependence of field size or collimator settings on the measured linear attenuation coefficient diminishes as the density or atomic number (Z) of the absorber increases. It is therefore desirable to construct compensators from materials with densities higher than that of water Also, the beam quality needs to be considered when looking for materials to be used in the construction of compensators. For most forward planning treatment planning systems, the compensator is represented by a bolus (with density equal to that of water) during treatment planning. There is therefore the need to determine the effective linear attenuation coefficient of the compensator material relative to that of water. Hence the effect of field size cannot be ignored.

The linear attenuation coefficients measured with a filed size of 4 cm x 4 cm for cerrobend and water were 0.4575 cm^{-1} and 0.1308 cm^{-1} respectively. The values do not compare favorably with those reported by other researchers using narrow beam geometry. For

University of Ghana http://ugspace.ug.edu.gh

example Leung et al (1974) reported linear attenuation coefficient of cerrobend to be $0.81 \pm 0.3\ cm^{-1}$ for Co-60 beam using narrow beam geometry, which is different from the $0.77\ cm^{-1}$ reported by Wilks et al. (1969). El-Katib et al. (1987), also reported a linear attenuation coefficient of $0.5776\ cm^{-1}$. The discrepancies in the values of the linear attenuation coefficient compared to those stated in literature may be attributed to variations in the experimental set up used in the measurement of the linear attenuation coefficients and variations in the elemental composition of the cerrobend.

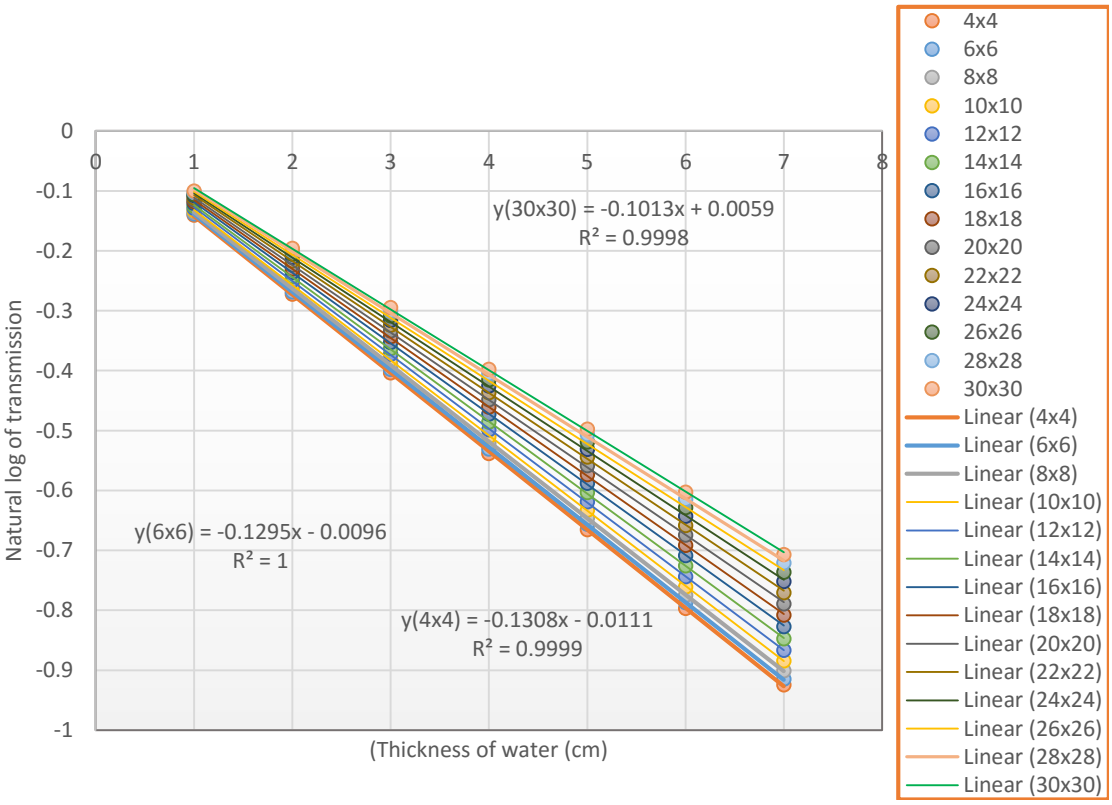

Figure. 4.03: Plot of transmission versus thickness of water

To study the dependence of the measured linear attenuation coefficient on field size, a graph of measured linear attenuation coefficient for a particular field size is plotted against corresponding field size for cerrobend and water using the same axes (this is shown in Figure 4.04). There is a linear correlation between the linear attenuation coefficient and

University of Ghana http://ugspace.ug.edu.gh

field size used for the measurement. This is in agreement with what was reported by Dimitriadis and Fallone (2002). The equations of correlation and the regressions (R^2) are displayed on the corresponding curves. From the values of regression (R^2) obtained which are approaching unity, it signifies that for any particular field size the correlation equations can be used to determine the linear attenuation coefficient with high accuracy.

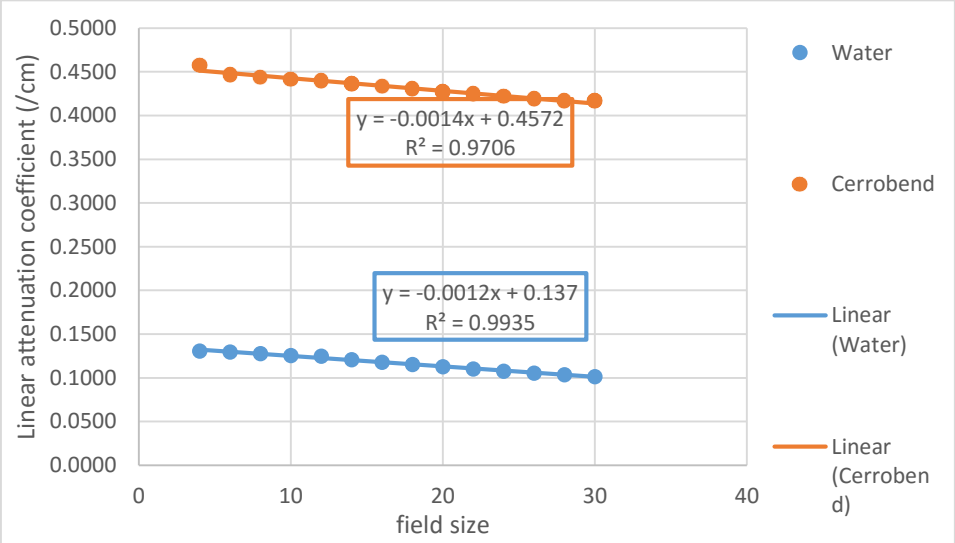

Figure. 4.04: Dependence of linear attenuation coefficient on field size for water and cerrobend

4.3. Scatter contribution and evaluation

In Table 4.01, the intensity of the beam or electrometer reading obtained during the measurements in air when a specific thickness of cerrobend is placed in the path of the beam is shown for various field sizes ranging from 4 cm x 4 cm to 30 cm x 30 cm in steps of 2 cm on both collimator settings. The intensity values increase with increasing field size

University of Ghana http://ugspace.ug.edu.gh

for a particular thickness of cerrobend, but decrease with increasing thickness of cerrobend for a particular field size. The variation with field size for a particular thickness of cerrobend placed in the path of the beam, may be attributed to the increase in the number of scattered radiation reaching the sensitive volume of the ionization chamber. The decrease in intensity is as a result of attenuation of the primary beam which tend to overwhelm the effect of the scattered radiation.

Table 4.01: Variation of the intensity of the beam with field size and thickness of cerrobend

intensity of the beam for various thicknesses of cerrobend for specific field size in air										
FS/Th(cm)	0	0.5	1.11	1.61	2.07	2.58	3.08	3.58	4.09	4.62
4	4.709	3.799	2.756	2.151	1.782	1.377	1.088	0.901	0.721	0.634
6	4.845	3.858	2.800	2.187	1.819	1.404	1.111	0.920	0.737	0.648
8	4.900	3.911	2.844	2.226	1.849	1.432	1.133	0.940	0.754	0.664
10	4.961	3.964	2.888	2.262	1.882	1.460	1.156	0.960	0.770	0.678
12	5.025	4.015	2.932	2.301	1.911	1.487	1.181	0.980	0.788	0.693
14	5.079	4.062	2.976	2.337	1.946	1.517	1.205	1.002	0.806	0.710
16	5.122	4.111	3.019	2.375	1.980	1.547	1.230	1.023	0.825	0.726
18	5.167	4.155	3.059	2.411	2.014	1.574	1.255	1.046	0.843	0.742
20	5.201	4.196	3.096	2.447	2.046	1.602	1.279	1.067	0.861	0.757
22	5.238	4.236	3.133	2.483	2.078	1.631	1.304	1.087	0.877	0.772
24	5.268	4.266	3.170	2.517	2.108	1.658	1.328	1.107	0.895	0.786
26	5.294	4.296	3.198	2.543	2.133	1.680	1.347	1.125	0.910	0.799
28	5.316	4.314	3.215	2.559	2.146	1.694	1.358	1.136	0.920	0.808
30	5.336	4.328	3.225	2.569	2.154	1.701	1.364	1.143	0.925	0.813

4.3.1. Scatter-to-primary ratio dose contribution for cerrobend

To study the effect of the scattered radiation on the primary beam, a graph of scatter-to-primary ratio dose (S/P) in terms of percentages calculated using equation 2.12 of section 2.7.1 of chapter 2 was plotted as a function of thickness of cerrobend placed in the path of

University of Ghana http://ugspace.ug.edu.gh

the beam for various field sizes using the same axes. The graph is depicted in Figure 4.05. The equations of correlation and their correlation coefficients (R^2) were determined and displayed on the various curves which are distinguished by colours. The equations of correlation follow a second order polynomial and almost all the correlation coefficients values approach unity. For a particular field size, the S/P increases with increasing thickness of absorber or cerrobend placed in the path of the beam. As the thickness of the absorber increases, and increasing the field size, S/P increases and reaches maximum and then starts decreasing. This is because of reduction in scatter rate produced in the cerrobend for large thicknesses.

The scatter contribution was found to be negligible for small field sizes. This is in line with what was experienced by Dimitriadis & Fallone (2002) using the same material for 6 MV photon beam.

University of Ghana http://ugspace.ug.edu.gh

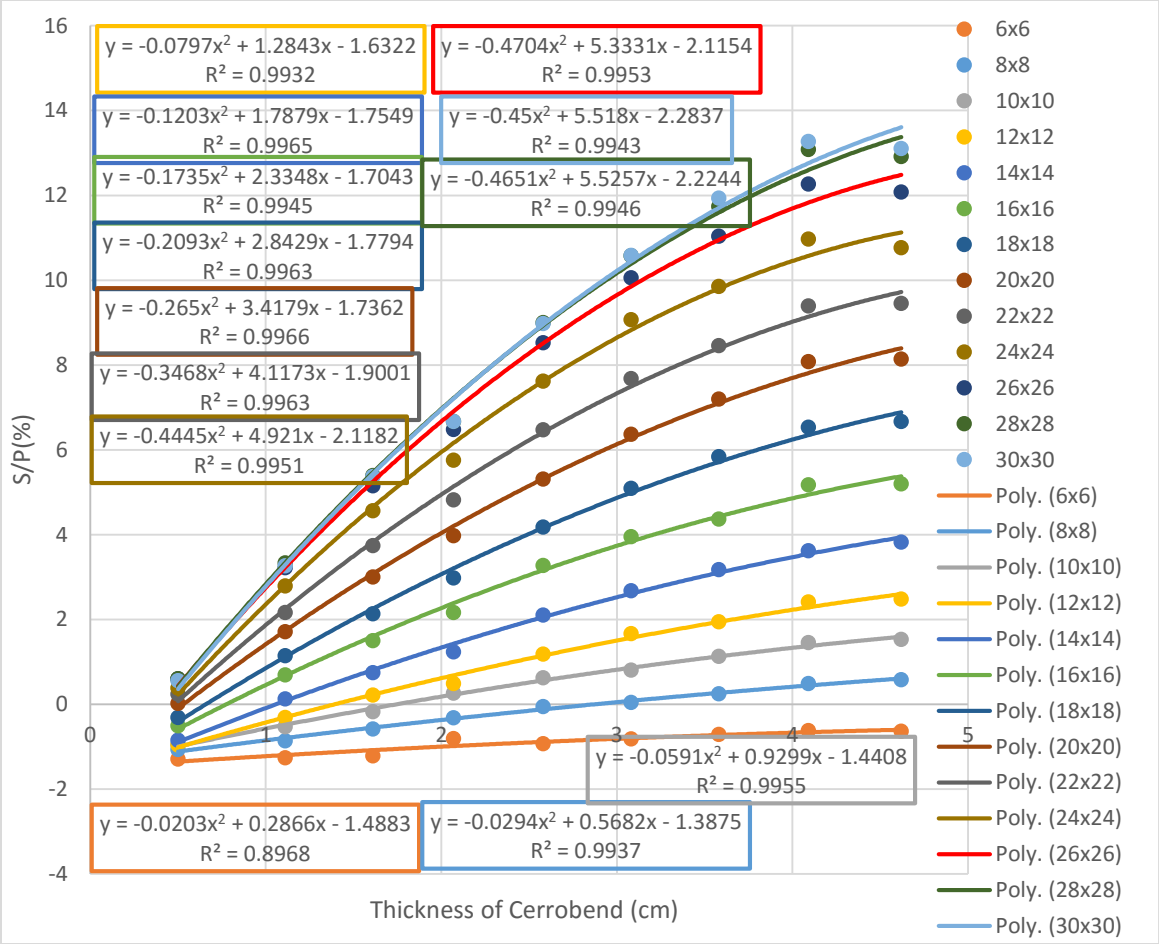

Figure. 4.05: Percentage Scatter – to –primary ratio dose contribution for cerrobend

4.3.2. Correction factors to account for reduction in scatter contribution to dose for using bolus to represent compensator

4.3.2.1. Thickness ratio and normalization thickness ratio correction Factor to account for reduction in scatter with respect to thickness of bolus

A graph of output of the teletherapy unit at a depth of 4 cm in the phantom against thickness of water on the surface of the phantom and cerrobend mounted on a block tray in the path of the radiation beam plotted on the same axes is shown in Figure 4.06. Above and below the curves are the correlation equation and coefficient of correlation, R^2 for the

University of Ghana http://ugspace.ug.edu.gh

measurement with water on the surface of the phantom and that with cerrobend mounted on a block tray respectively. The correlation between the thicknesses of water on the surface of the phantom and that with the cerrobend slab mounted on a block tray that will produce the same output as the former irradiation configuration is illustrated graphically in Figure 4.07 with the correlation equation and coefficient of correlation, R^2 displayed on the curve. Also a plot of the ratio of the thickness of cerrobend on a block tray to that with thickness of water on the surface of phantom that will produce the same output, Figure 4.08, as a function of thickness of volume of water on the surface of phantom is depicted in Figure 4.08 with the correlation equation and coefficient of correlation, R^2 displayed on the curve. The equation of best fit for the curve in Figure 4.09 represents the equation that was used to compute values for the correction factors that was used to account for reduction in scatter associated with the compensator in terms of thickness of bolus on surface of phantom in equation 3.04.

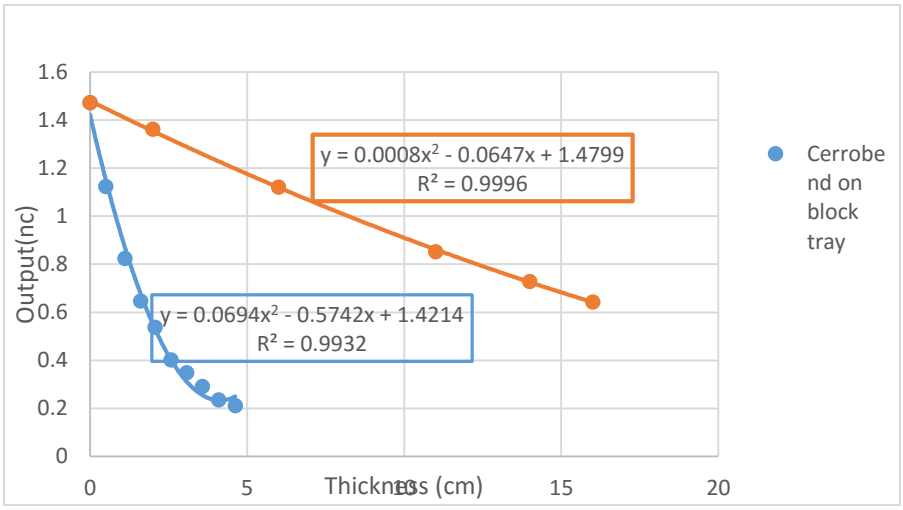

Figure 4.06 Graph of output of teletherapy unit at a depth 4cm and 10cmx10cm field size with thickness of water representing bolus on surface of the phantom and cerrobend on block tray to mimic bolus.

University of Ghana http://ugspace.ug.edu.gh

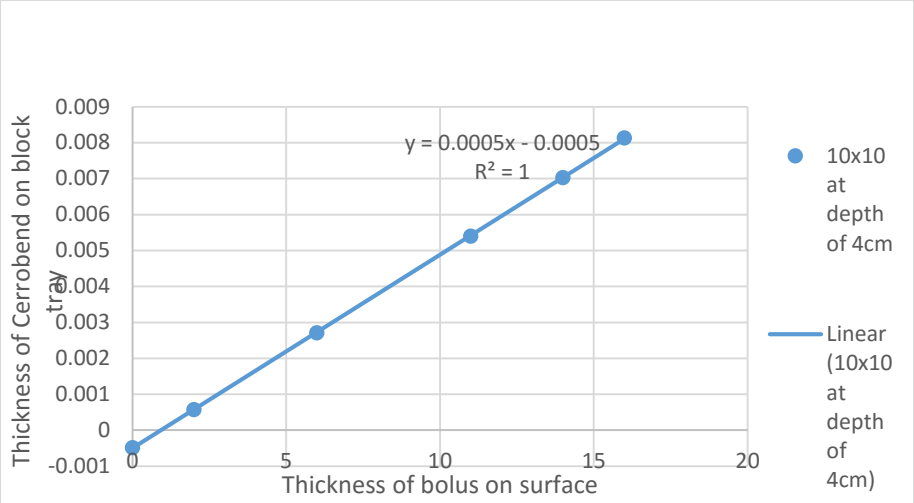

Figure 4.07 Graph of correlation between thickness of water representing bolus on surface of the phantom and thickness of cerrobend on block tray that will give the same output at a depth of 4cm and 10cmx10cm field size.

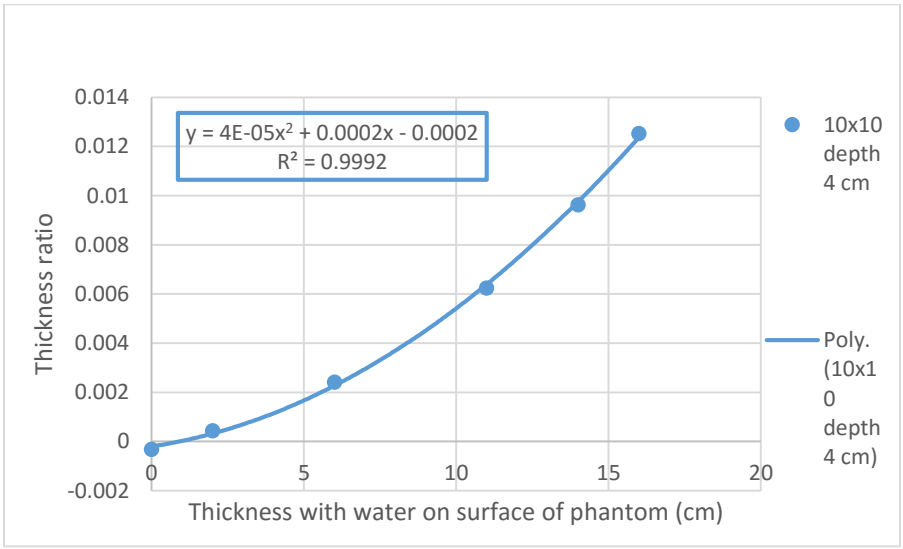

Figure 4.08 Graph of correlation between thickness ratio against thickness of water representing bolus on surface of the phantom at a depth of 4cm and 10cmx10cm field size.

University of Ghana http://ugspace.ug.edu.gh

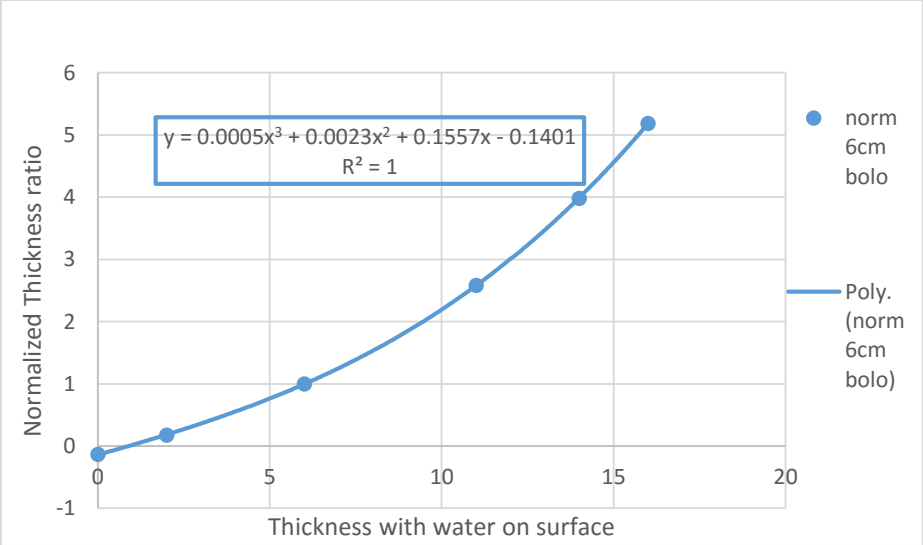

Figure 4.09 Graph of correlation between normalized thickness ratio against thickness of water representing bolus on surface of the phantom at a depth of 4cm and 10cmx10cm field size

From graph of Figure 4.08 and 4.09 the thickness ratio and normalization thickness ratio correction factor that will account for effects of changing the reference thickness of bolus on the surface of the phantom as a function of thickness of bolus on the surface of the phantom can be written as equation 4.01 and 4.02 respectively, as follows.

$$T_{d_r,s_r}(t_b) = 4e-05 \times {t_b}^2 + 0.0002 \times t_b - 0.0002 \qquad 4.1$$

$$F_{Tb}(t_b) = 0.0005 \times {t_b}^3 + 0.0023 \times {t_b}^2 + 0.1557 \times t_b - 0.1402 \qquad 4.2$$

where $\boldsymbol{t_b}$ **is** a numerical value of thickness of bolus on the surface of the phantom in centimeter.

University of Ghana http://ugspace.ug.edu.gh

4.3.2.2. Correction factor to account for reduction in scatter with respect to radiation field size

Graph of output of the teletherapy machine at a depth of 4 cm in the phantom on the beam central axis as a function of one side of a square field with 6 cm considered reference thickness of water on surface of phantom and that with 0.5 cm considered reference thickness of cerrobend slab mounted on a block tray plotted on the same axis is shown in Figure 4.10. Above and below the curves are the correlation equation and coefficient of correlation, R^2 for the measurement with thickness of volume water on the surface of the phantom and that with the cerrobend on a block tray respectively. Correlation between field sizes with thickness of volume of water on surface of phantom and that with cerrobend mounted on a block tray that will produce the same output at a depth of 4 cm in the phantom is shown graphically in Figure 4.11 with the correlation equation and coefficient of correlation, R^2 displayed on the curve. The normalized one side of a square field ratio plotted against one side of a square field with the 6 cm thickness of water on the surface of the phantom is shown in Figure 4.13. On the curve is the equation of best fit for the curve, which was used to compute the correction factors that was used to account for reduction in scatter associated with the compensator in terms of field size with the bolus on surface of phantom.

University of Ghana http://ugspace.ug.edu.gh

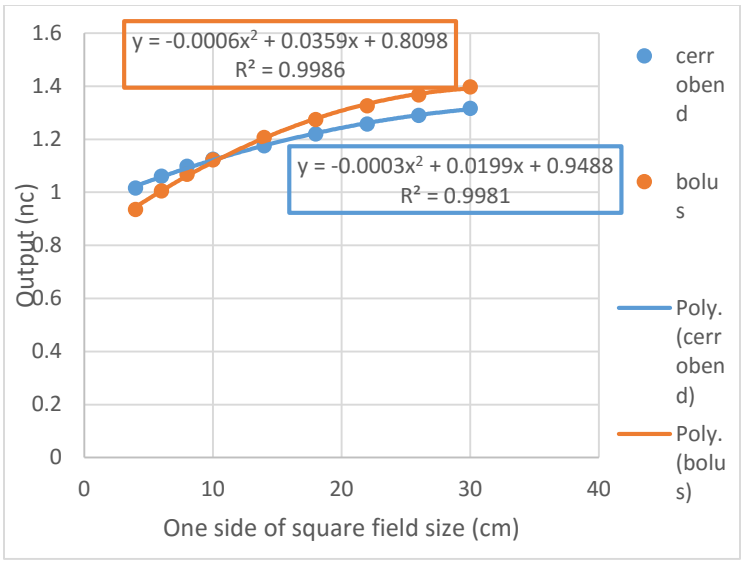

Figure 4.10 Graph of output of teletherapy unit at a depth 4cm in phantom as a funtion of field size with 6cm thickness of water representing bolus on surface of the phantom and 0.5 cm thickness of cerrobend on block tray to mimic bolus.

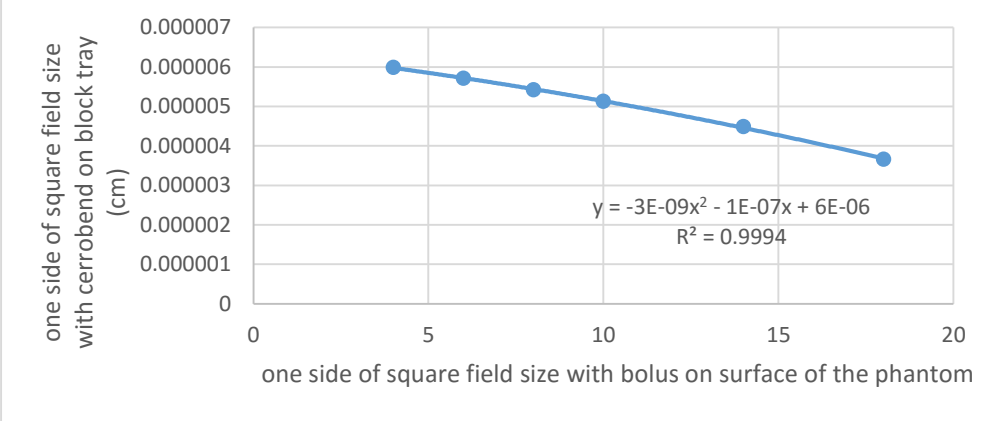

Figure 4.11 Graph of correlation between field size with 6cm thickness of water representing bolus on surface of the phantom and that with 0.5 cm thickness of cerrobend on block tray that will give the same output at a depth of 4cm.

University of Ghana http://ugspace.ug.edu.gh

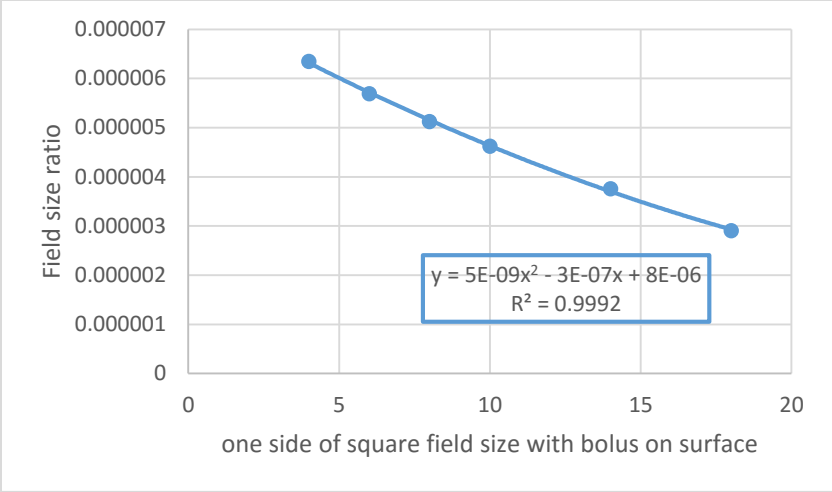

Figure 4.12 Graph of correlation between field size ratios against one side of square field size with 6 cm thickness of water representing bolus on surface of the phantom at a depth of 4cm.

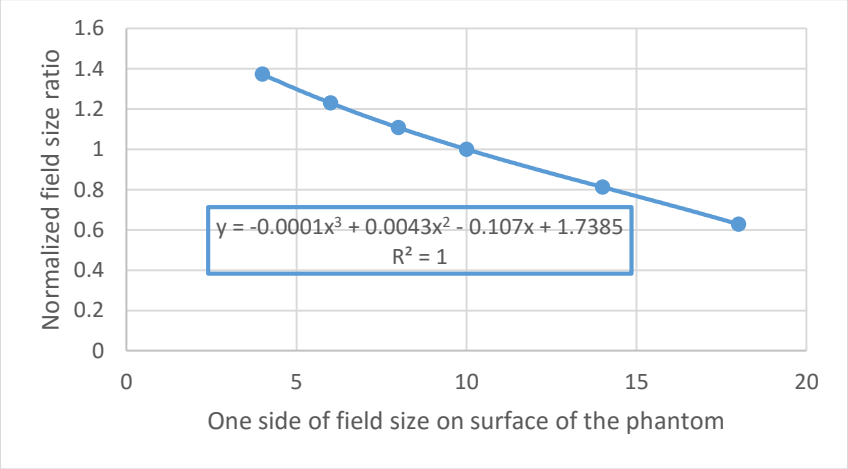

Figure 4.13 Graph of correlation between normalized field size ratios against one side of field size with 6 cm thickness of water representing bolus on surface of the phantom at a depth of 4cm.

From correlations on the graph of Figure 4.13 the correction factor that accounts for field size as a function of field size with bolus on the surface of the phantom can be written as:

$$F_{s(S)} = -0.0001 \times S^3 + 0.0043 \times S^2 - 0.107 \times S + 1.7385 \qquad 4.3$$

University of Ghana http://ugspace.ug.edu.gh

where S is numerical value of equivalent field size with bolus on the surface of the phantom.

4.3.2.3. Correction factor to account for reduction in scatter with respect to treatment depth

Figure 4.14 shows a graph of the output on the beam central axis of the teletherapy unit with thickness volume of water on the surface of the phantom and with the cerrobend mounted on a block tray as a function of depth within the phantom at which the output was measured for the 6 cm thickness of water on the surface of the phanton and 0.5 cm thickness of cerrobend slab, plotted using the same axes. Above and below the curves are the correlation equation and coefficient of correlation, R^2 for the measurement with a thickness of volume of water on the surface of the phantom and that with the cerrobend on a block tray, respectively. Correlation between the depths within the phantom with thickness volume of water on the surface of the phantom and that with the cerrobend slab mounted on a block tray that will produce the same output as the former irradiation configuration is illustrated graphically in Figure 4.15 with the correlation equation and coefficient of correlation, R^2 displayed on the curve. The normalized depth ratio plotted against depth within the phantom with the 6 cm thickness of water on the surface of the phantom is shown in Figure 4.17. On the curve is the equation of best fit for the curve, which was used to compute the correction factors that was used to account for reduction in scatter associated with the compensator in terms of treatment depth with the bolus on surface of phantom.

University of Ghana http://ugspace.ug.edu.gh

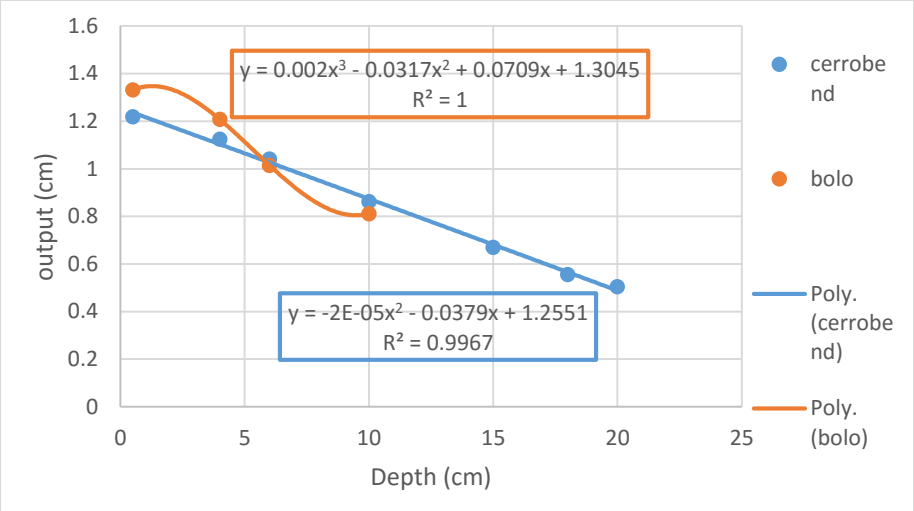

Figure 4.14 Graph of output of teletherapy unit at 10cmx10cm field size as a funtion of treatment depth with 6 cm thickness of water representing bolus on surface of the phantom and 0.5 cm thicnkess of cerrobend on block tray.

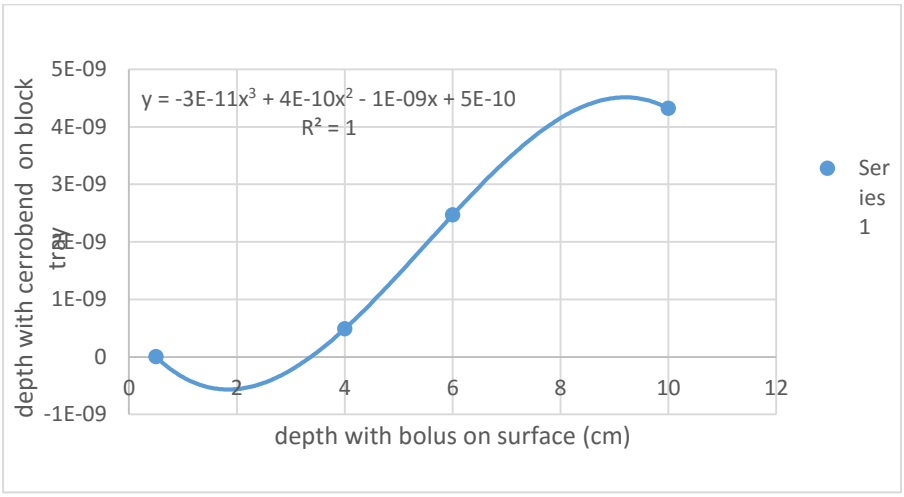

Figure 4.15 Graph of correlation between treatmet depth with 6cm thickness of water representing bolus on surface of the phantom and that with 0.5 cm thickness of cerrobend on block tray that will give the same output at 10cmx10cm field size.

University of Ghana http://ugspace.ug.edu.gh

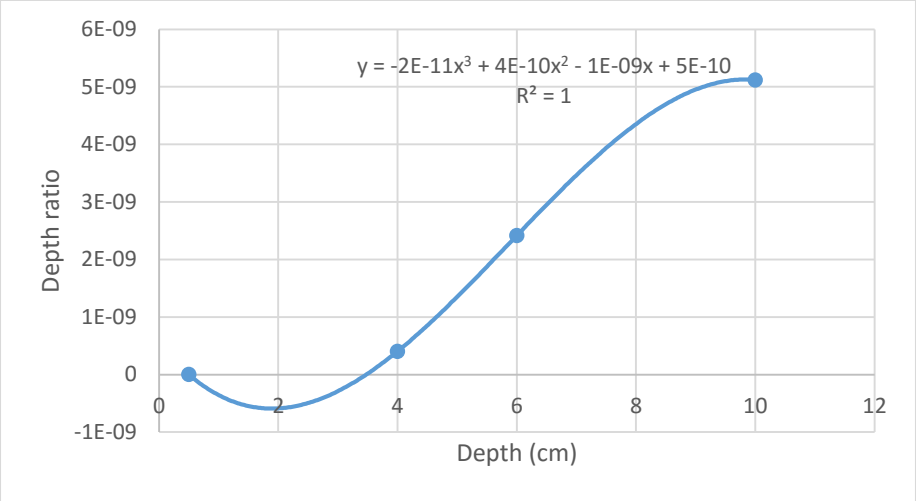

Figure 4.16 Graph of correlation between depth ratios against one side of square depth with 6 cm thickness of water representing bolus on surface of the phantom at 10cmx10cm field size.

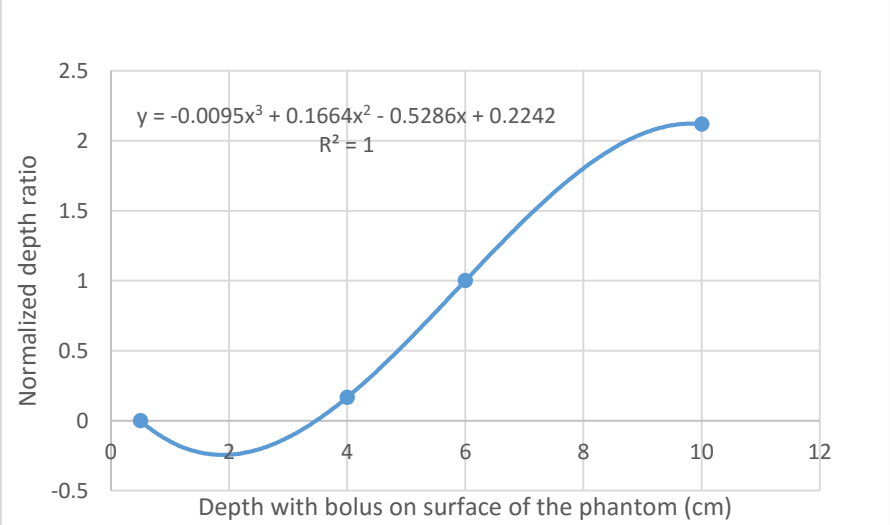

Figure 4.17 Graph of correlation between normalized depth ratios against one depth size with 6 cm thickness of water representing bolus on surface of the phantom at 10cmx10cm field size.

From correlations equations on the graph of Figure 4.17 the correction factor that account for changes in treatment depth as a function of depth with bolus on the surface of the phantom can be written as:

University of Ghana http://ugspace.ug.edu.gh

$$F_{d(d)} = -0.0095 \times d^3 + 0.1664 \times d^2 - 0.5286 \times d - 0.2242 \quad 4.4$$

where d is numerical value of equivalent treatment depth with bolus on the surface of the phantom. The equation 4.1, 4.2, 4.3 and 4.4 will be used in the equation 3.04 to calculate the thickness of required cerrobend compensator for a given thickness of bolus on the surface of the phantom, equivalent field size and treatment depth of interest.

4.4. Constructed compensator

Plate 4.01 show the cerrobend compensator that was mold in a Styrofoam block similar to that used by the center to mold shielding blocks. The compensators were constructed using equation 3.04 to find the corresponding thickness of cerrobend that mimic bolus on the surface of the phantom which take in to account the correction factors with the change in field size, treatment depth and thickness of bolus with maximum percentage error of 0.5% corresponding of $\pm 0.005cm$.

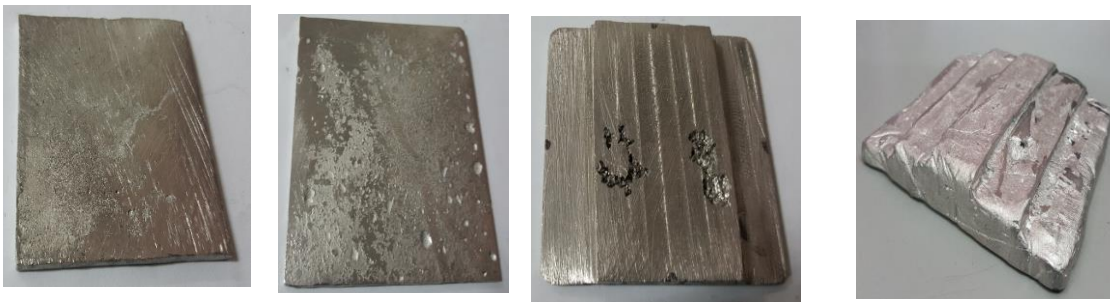

Plate 4.01. The three compensator constructed in this research flat compensator and step compensator

From the Plate 4.01 it is easy to see that it was difficult to get the same accuracy with percentage error of 0.5% when cutting the mold on the Styrofoam block because of human

University of Ghana http://ugspace.ug.edu.gh

errors. The blocks show small depressions which indicates the presence of air bubble within the constructed cerrobend compensators and irregular surface which will affect the transmission and thus the final dose distribution.

4.4.1. Dosimetry

Figure 4.18 shows calibration curve of the EBT2 gafchromic film for cobalt-60 beam with a field size of $10cm \times 10cm$ at a depth of 4.54 cm in the phantom. The curve shows the variation of gray values with dose. On the curve, the equation of correlation for the curve is displayed. This was the equation which was used to convert gray values to doses in cGy for the dosimetry work performed on the compensator. Off-axis dose profiles at a various depths in the phantom measured with the film with the fabricated compensator in the path of the beam and that determined with the TPS with the bolus in the path of the beam are shown in Figure 4.19, 4.20, 4.21, 4.22, 4.23, 4.24 and 4.25 for prescribed dose of 200 cGy. Figure 4.22, 4.23, 4.24 and 4.25 show the off-axis dose profiles at depths of 4.54 cm, 6.82 cm, 11.36 cm and 8 cm respectively in the phantom measured with the film with the fabricated compensators in the path of the beam and that determined with the TPS having the bolus in the path of beam. For the depth of 4.54 cm, the field size is 10 cm x 10 cm, depth of 6.82 cm the field size is 14 cm x 14 cm, depth of 11.36 cm the field size is 10 cm x 10 cm and for the depth of 8 cm the field size is 15 cm x 15 cm.

University of Ghana http://ugspace.ug.edu.gh

4.4.2. Calibration curve

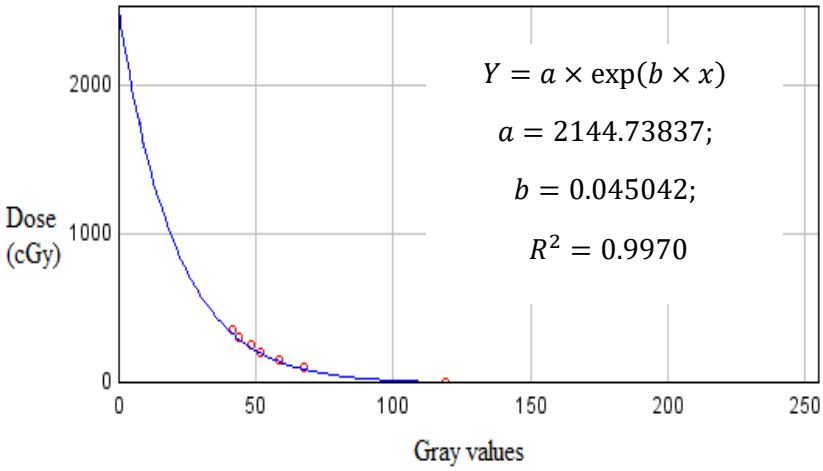

Figure 4.18 Calibration curve with

Figure 4.18 show the calibration curve with respective calibration function used to measure the dose correspondent of the gray value from the scanned films. The results showed that regardless of fluctuations, the measured mean gray valor for calibration, were in agreement with curve fitting with correlation coefficient of 0.9974. The equation generates the predicted dose for calibration with percentage error ranging from 0% to 13%. The probably source of this error is the human error during selection of region of interest to be measured the respective mean gray valor.

University of Ghana http://ugspace.ug.edu.gh

4.4.3. Dose measurements

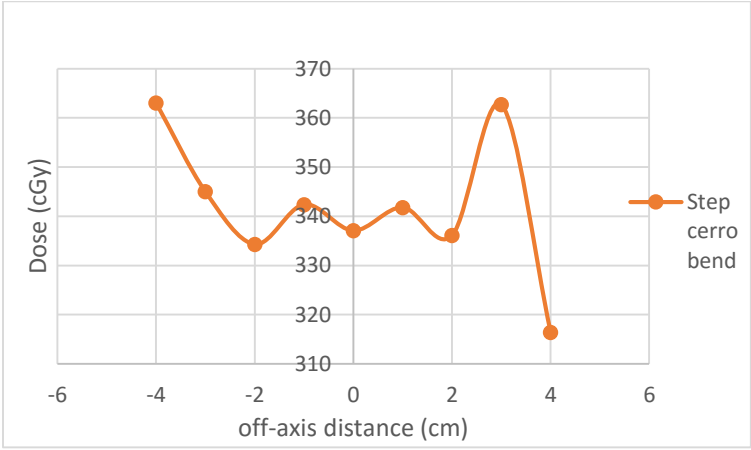

Figure 4.19. Off-axis dose profile at a depth of 11.36 in phantom with fabricated step compensator, without including the normalization thickness ratio correction factor, in the path of beam and prescribed dose of 200 cGy

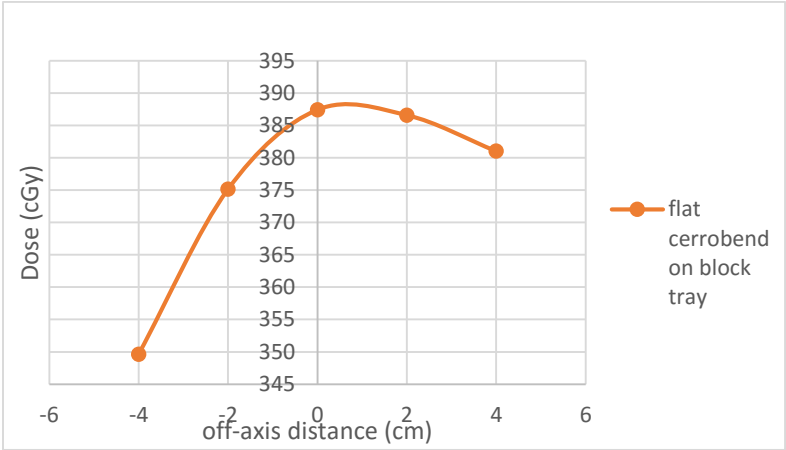

Figure 4.20. Off-axis dose profile at a depth of 4.54 in phantom with fabricated flat compensator with thickness of 1.5 mm, without including the normalization thickness ratio correction factor, in the path of beam and prescribed dose of 200 cGy

University of Ghana http://ugspace.ug.edu.gh

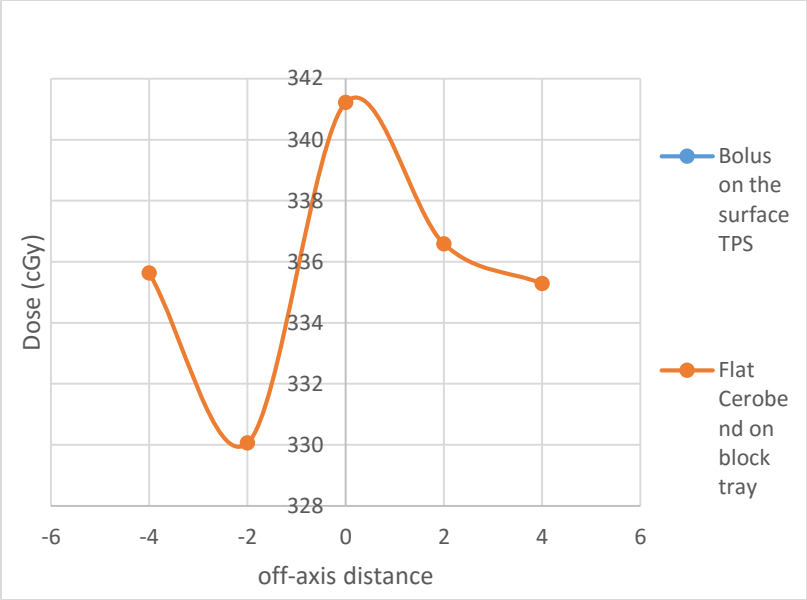

Figure 4.21. Off-axis dose profile at a depth of 6.8 in phantom with fabricated flat compensator with thickness of 4.3 mm, without including the normalization thickness ratio correction factor, in the path of beam and prescribed dose of 200 cGy

Figure 4.19, 4.20, and 4.21 are off-axis dose profiles obtained with step compensator, and 1.5mm and 4.3mm compensators with uniform thickness respectively. From the figures is easy to see the discrepancies with dose delivered caused by presence of air bubble and inaccuracy in generating a flat surface topography which are easily seen in Plate 4.01. Imprecision in production of cerrobend thickness compensator generated by the equation 3.04 which is one the most important limitation in this research and also uncertainty associated with film calibration.

University of Ghana http://ugspace.ug.edu.gh

4.4.4. Evaluation of the compensator

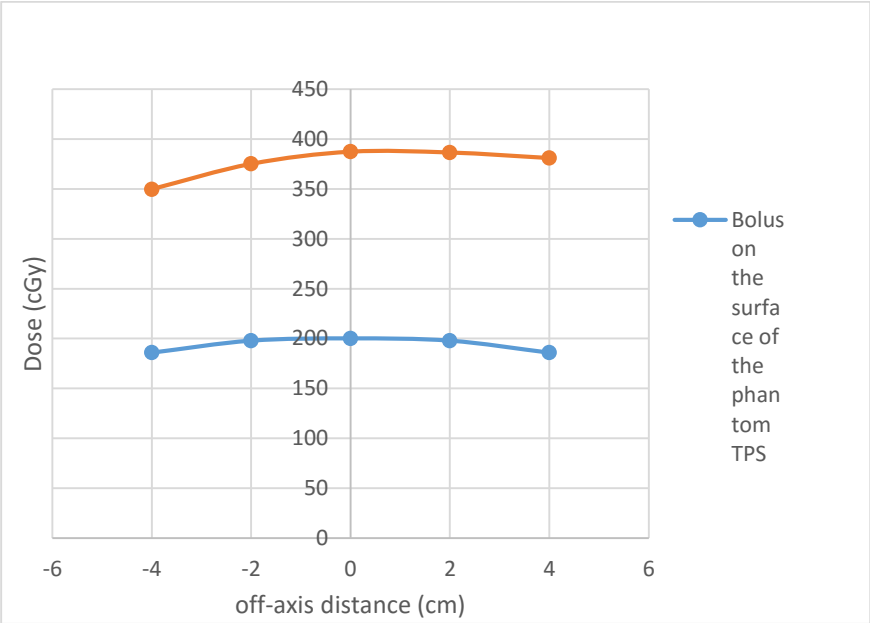

Figure 4.22 Off-axis dose profile at a depth of 4.54 cm in phantom with fabricated flat compensator, without including the normalization thickness ratio correction factor, with thickness of 1.5 mm in the path of beam and that of bolus on the surface of the phantom on the TPS, prescribed dose of 200 cGy

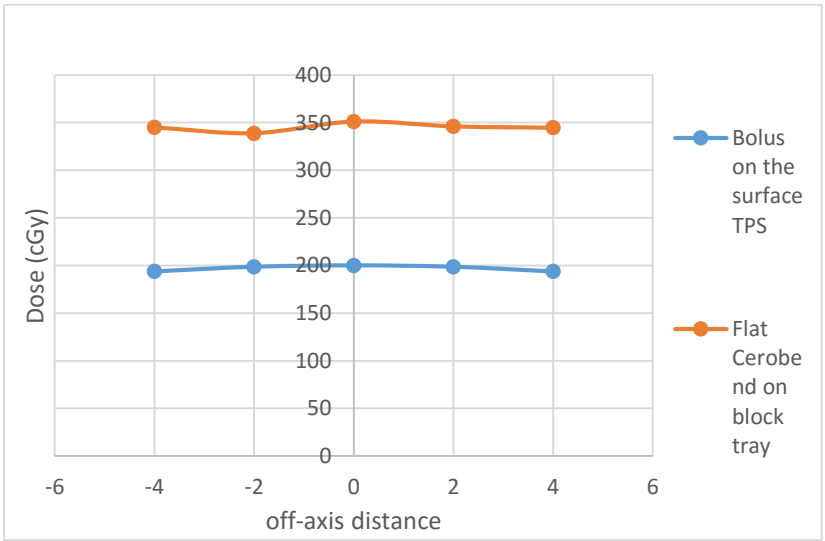

Figure 4.23. Off-axis dose profile at a depth of 6.82 cm in phantom with fabricated flat compensator, without including the normalization thickness ratio correction factor, with thickness of 4.3 mm in the path of beam and that of bolus on the surface of the phantom on the TPS, prescribed dose of 200 cGy

University of Ghana http://ugspace.ug.edu.gh

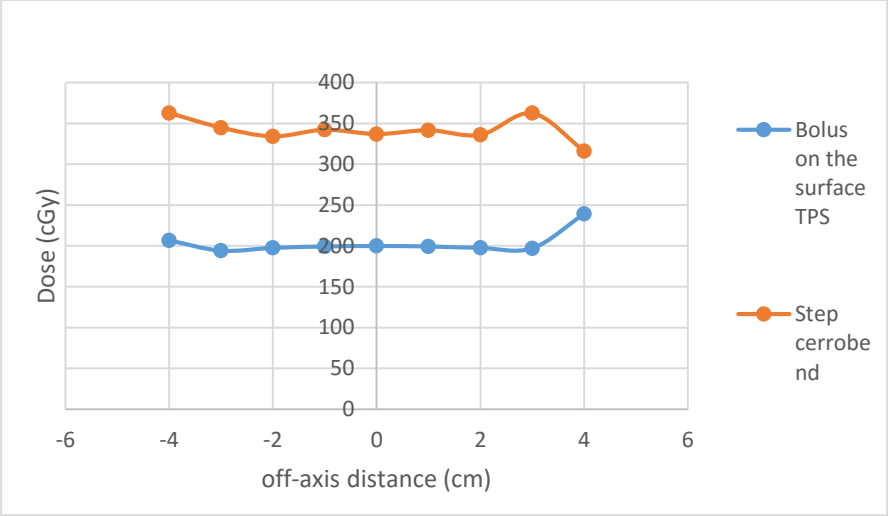

Figure 4.24. Off-axis dose profile at a depth of 11.36 in phantom with fabricated step compensator, without including the normalization thickness ratio correction factor, in the path of beam and that of bolus on the surface of the phantom on the TPS, prescribed dose of 200 cGy

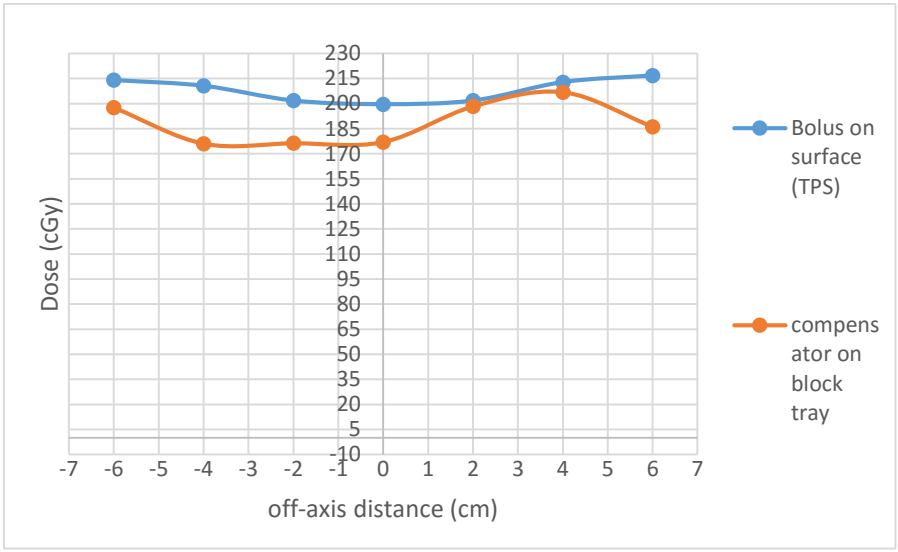

Figure 4.25. Off-axis dose profile at a depth of 8.0 in phantom with fabricated step compensator that include normalization thickness ratio correction factor in the path of beam and that of bolus on the surface of the phantom on the TPS, prescribed dose of 200 cGy

Figures 4.22, 4.23, 4.24, and 4.25 are the off-axis dose profile generated with the fabricated compensator to verify the dose and dose distribution accuracy. In figures 4.22, 4.23 and

University of Ghana http://ugspace.ug.edu.gh

4.24 the thickness of compensator was calculated using equation 3.04 without normalization thickness ratio correction factor and the discrepancies of dose with that predicted by the TPS was found to be very high, despite having an identical dose profile curve to the one given by the Prowess Panther TPS. The measured dose with constructed compensators on block tray was found to be high than that planned with bolus on the surface of the phantom. The compensators were undercompensating.

To solve these discrepancy a new step compensator was constructed including the normalization thickness ratio correction factor, the results showed improvement in accuracy. The measured dose at central axis using ionization chamber and that using EBT2 gafchromic film was found to be almost the same with absolute difference of 1.19cGy, with ionization chamber giving 178.21cGy and gafchromic film 177.02 cGy with percentage deviation of 11% with that predicted by the TPS (200cGy) for both dosimeters. The dose profile for Figure 4.25 was obtained with step compensator of 1.5 cm maximum thickness, with 3 steps of 0.5 cm each, at 8 cm treatment depth and equivalent radiation field size of 10 cm x 10 cm. For this compensator also, the results were better, but in the other hand it presents relevant discrepancy with that obtained with bolus on the surface with percentage error ranging from $\pm 1.69\%$ to $\pm 16.36\%$. These inaccuracy on dose distribution with that predicted by the Prowess Panther can be attributed to several causes. Firstly, because of scatter contribution from the cerrobend compensator as investigated in this research and which the results are presented in Figure 4.05 and also because of uncertainties associated with calibration. The effect of scatter produced in cerrobend compensator to final dose distribution was also investigated and reported by Dimitriadis & Fallone (2002) and Huang et al. (1986). Second, the presence of air bubble in the cerrobend.

University of Ghana http://ugspace.ug.edu.gh

As reported by Taherkhani et al. (2010), an air bubble with diameter large than 3.0 mm can affect beam attenuation significantly and thus the finally dose delivered. Finally, the limitations associated with production of flat surface and precise thickness as predicted by the equation 3.04, problems with limitation is obvious in these results, as reported by Mejadden et al. (1997), deviations in thickness of applied cerrobend of 0.1 mm can cause change in transmission dose of 0.5%. In this work also in figure 4.01, was demonstrated how percentage transmission changes and how rapid falls with increasing of thickness of cerrobend. In general, the measured dose with the compensator in Figure 4.2.4 was lower than that predicted by TPS. It was found to overcompensating, with absolute difference ranging from 3.41cGy to 34.52 cGy, as mentioned above, it is attributed to inaccuracy in thickness production.

University of Ghana http://ugspace.ug.edu.gh

CHAPTER V

5.0. CONCLUSIONS AND RECOMMENDATIONS

5.1. CONCLUSION

Procedures for designing and constructing a cerrobend compensator for high-energy photon beam have been outlined and proposed for cobalt-60 as high energy radiotherapy source.

To account for reduction in scatter contribution to radiation dose for using compensator to mimic bolus of the TPS, correction factors were introduced into the developed equation to account for the discrepancy in terms of field size, thickness of bolus and treatment depth respectively. Output measurements on the beam central axis in a phantom with the compensator material on the surface of the phantom and that with the compensator material on a block tray have shown that the correction factors can be equated to a third order polynomial equation by using graphical considerations.

Contribution of scattered photons generated within the cerrobend to dose, was investigated by evaluating and determining the scatter-to-primary ratio dose contribution for various thickness of cerribend.

Dosimetry analysis of dose profiles at depth of 4.54 cm, 6.82 cm, and 11.36 cm, with compensator constructed without normalized thickness ratio correction factor and at 8 cm with compensator constructed including normalization thickness ratio correction factor, in a phantom with films read by imageJ software was done. The dosimetry with compensators constructed with the normalization correction factor in the algorithm, was found to be comparable to that of the TPS in some steps along the off-axis. The deviations were ranging from $\pm 1.69\%$ to $\pm\ 16.36\%$ with a mean of $\pm 9.51\%$ and standard deviation of $\pm 5.64\%$.

University of Ghana http://ugspace.ug.edu.gh

The dose delivered with the step wedge compensator at off-axis of 4 cm and 6 cm, was found to deviate to that of TPS about $\pm 1.69\%$ and $\pm 2.80\%$ respectively which was found to be in the range of acceptable clinical levels (-5% to $+7\%$ $ICRU$ $report$ 50) . Therefore, for clinical implementation additional work needs to be done to avoid the limitations associated with these errors.

University of Ghana http://ugspace.ug.edu.gh

5.2. RECOMMENDATIONS

The acceptable discrepancy between a dose calculated by a TPS and that measured should not be more than ± 5 %. From the experimental results, it shows that a number of the doses measured with the constructed compensators compare to their calculated counterpart with the bolus by the TPS are above the threshold. This is as a result of the effects of over compensation produced by the cerrobend, and the fact that small uncertainty in the thickness of the compensator during construction may lead to significant error in the dose distribution.

A small thicknesses of a compensator constructed with the cerrobend must be represented by a relatively large thicknesses of the bolus by the TPS, which at times is problematic for the TPS to handle. With reference to these, there is the need for an alternative material to be sought for the construction of compensator for cobalt- 60 beam. The material must have density higher than that of water but lower to that of cerrobend. Nevertheless, the cerrobend can still be used for scenarios or cases where excessive compensation is required.

Also there is the need to streamline procedures used in the construction of the cerrobend compensator to enhance accuracy of the thicknesses at various part of the compensator and to ensure that the casted compensator is devoid of imperfections.

Before clinical implementation of the proposed and developed method of constructing a compensator, it is recommended to investigate and develop a fast method of verifying the compensator thickness.

University of Ghana http://ugspace.ug.edu.gh

The correction factors introduced into the algorithm used to convert a bolus thickness to compensator thickness are strongly dependent on collimator design and beam energy, and hence one has to be circumspective in the use of the algorithm. One needs to determine these correction factors for his or her teletherapy machine at the appropriate beam energy.

University of Ghana http://ugspace.ug.edu.gh

REFERENCES

Absorbed Dose Determination in External Beam radiotherapy, An international Code of practice for dosimetry based on standards of absorbed dose to water. Technical reports series No. 398. International Atomic Energy Agency, Vienna, 2000. Copy right.

Ahnesjö, A. (1994a). *Analytical modeling of photon scatter from flattening filters in photon therapy beams*. Med. Phys., 21, 1227-1235.

Ahnesjö, A. (1994b). *Collimator scatter in photon therapy beams*. Med., Phys. 22, 267-278.

Ahnesjö, A. & Aspradakis, M. M. (1999). *Dose calculations for external photon beams in radiotherapy*. Phys. Med. Biol., 44, R99-R155.

Ahnesjö, A., Weber, L. & Nilsson, P. (1995). *Modeling transmission and scatterfor photon beam attenuators*. Med. Phys., 22, 1711-1721.

Andrew, J.W & Aldrich, J.E. (1982). *A microcomputerbased system for radiotherapy beam compensator design and patient contour plotting*. Med. Phys., 9, 279–283.

Avelino, S. R. (2013). *Desenvolvimento e avaliação de um sistema baseado em impressora 3D para confecção de blocos compensadores em Radioterapia de Intensidade Modulada – IMRT*. Dissertação de mestrado, Universidade de Brasilia, Brasilia/Brasil.

Brahme, A., Roos, J E., & Lax. (1982). *Solution of an integral equation encountered in rotation therapy*. Phys. Med. Biol., 27, 1221-1229.

Buckey, C. R., Stathakis, S., & Papanikolaou, N. (2010). *The inter- and intrafraction reproducibilities of three common IMRT delivery techniques*. Med Phys, 37(9), 4854-60.

Bushberg, J.T. & Boone, J.M. (2011). *The Essential Physics of medical imaging, 3rd edition*; Lippincott Willians & Wilkins.

Castelanos, M. E. & Rosenwald, J. C. (1998). *Evaluation of the scatter field for high-energy photon beam attenuators*. Phys. Med. Biol., 43, 277-290.

University of Ghana http://ugspace.ug.edu.gh

Chang, S. (2004). *Compensator-intensity-modulated Radiotherapy—A Traditional Tool for Modern Application*, http://touchoncology.projectstatus.in/system/files/private/articles/1197/pdf/onco67301.pdf.

Chang S. X., Cullip T. J., & Deschesne, K. M. (2000). *Intensity modulation delivery techniques*: "Step & shoot" MLC auto sequence versus the use of a modulator. Med Phys, 27, 948–959.

Chang, S. X., Cullip, T. J., Deschesne, K. M., Miller, E. P. & Rosenman, J.G. (2004). *Compensators: An alternative IMRT delivery technique*. Applied Clinical Medical Physics, 5(3), 87.53Mr, 87.53Tf.

Cheung K.Y. (2006). *Intensity modulated radiotherapy: advantages, limitations and future developments*; Biomed Imaging Interv, 2(1), e19. doi: 10.2349/biij.2.1.e19.

Cunningham, J. R, Wright, D. J' Webb, H. P, Rawlinson, J. A & Leung, P. M. (1976). *A semi-automatic cutter for compensating filters*. Int J Radiat Oncol Biol Phys, 1, 355–360.

Dimitriadis, D. M. & Fallone, B. G. (2002); *Compensators For Intensity-Modulated Beams; Medical Dosimetry*, 27 (3), 215–220.

du Plessis, F. C. P. D. & Willemse, C. A. (2006); *Inclusion of compensator-induced scatter and beam filtration in pencil beam dose calculations*; Medical Physics, **33**, 2896, doi: 10.1118/1.2219777.

Eklof, A., Ahnesjo, A., & Brahme, A. (1990). *Photon beam energy deposition Kenels for inverse radiotherapy planning*. Acta Onco. 129, 447-454.

El-Khatib, E. E.; Podgorsak, E. B. & Pla, C. (1987). *Broad beam and narrow beam attenuation in Lipowitz's metal*. Medical Physics, 14, 135, doi: 10.1118/1.596100.

Ellis, F., Hall, E. J., & Oliver, R. (1959). *A Compensator for Variations in Tissue Thickness for High Energy Beams*. Radiol, 32, 421–422.

University of Ghana http://ugspace.ug.edu.gh

Gray, L. (1979). *Relative surface dose from super voltage radiation. Radiology*, 109, 437-442.

Haghparast, A., Hashemi, B., & Eivariz, M. T. (2013). *Influence of compensator thickness, field size, and off-axis distance on the effective attenuation coefficient of a cerrobend compensator for intensity-modulated radiation therapy*, American Association of Medical Dosimetrists, Medical Dosimetry, 38, 25-29.

Hall, E. J. (2000). *Radiobiology for the Radiologist; Fifth Edition*; by Lippincott Williams & Wilkins.

Henderson, S. D., Purdy, J. A., Gerber, R. L. & Mestman, S. J. (1987). *Dosmetric Consideration for a limpowitz metal Tissue compensator System*. Int.J. Radiation Oncology Biol. Phys, 13, 1107-1112.

Hine, G. J. (1951). *Scattering of secondary electrons produced by x-ray in materials of various atomic numbers*. Phys. Rev, 82, 755-756.

Huang, P., Chin, L. M. & Bjärngard, B. E. (1986); *Scattered Photon Produced By beam-modifying filter*, Med. Phys. 13: 010057-07$01.20.

Huen, A., Findley, D. O., & Skov, D. O. (1979); *Attenuation in Lipowitz's metal of x rays produced at 2, 4, 10, and 18 MV and gamma rays from cobalt-60*; Med Phys.6(2):147-8.

IAEA Technical Reports Series No.430, (October 2004), *Commissioning and Quality Assurance of Computerized Planning Systems for Radiation Treatment of Cancer*, Vienna, Austria STI/DOC/010/430.

ICRU report 50. (1993). *"Prescribing, recording and reporting photon beam therapy*", International Commission on Radiation Units and Measurements, Bethesda, MD

Islam, M. K. & Van Dyk. (1995). *Effect of scatter generated by beam modifying absorbers in megavoltage photon beams*. Med. Phys., 22, 2075-2081.

University of Ghana http://ugspace.ug.edu.gh

Javedan, K., Stevens, C. W. & Forster, W. M. (2008). *Compensator-based intensity-modulated radiation therapy for malignant pleural mesothelioma post extrapleural pneumonectomy*. Appl Clin Med Phys, 9(4), 2799.

Jiang, S. & Ayyangar, K. M. (1998). *On compensator design for photon beam intensity modulated conformal therapy, department of radiation therapy,* Medical College of Ohio, 3000 Arlington Avenue, Toledo, Ohio 43614-2598.

Johns, H. E & Cunningham, J. R. (1983). *The Physics of Radiology*; fourth edition, by Charless C Thomas Puplisher.

Joy, S., Starkschall, G., Kry, S., Salehpour, M., White, R. A., Lin, S. H., & Balter, P. (2012). *Dosimetric efects of jaw tracking in step-and-shoot intensitymodulated radiation therapy*. J Appl Clin Med Phys, 13(2),3707.

Kahn, F. M., Moore, V. C., & Burns, D. J. (1970). *The construction of compensators for cobalt therapy*. Radiology; 96, 187–192.

Khan, F. M. & Gerbi, B. J. (2012). *Treatment planning in radiation oncology*. Third edition. Lippincott Williams and Wilkins.

Khan, F. M.(2010); *Physics of Radiation Therapy*, The, 4th Edition, Lippincott Williams & Wilkins.

Lam,W. L. K., Lee, D. & O'Neill, M. J. (1983), "*Tissue compensator production using a simple photographie technique*." Radiology, 149, 322-323.

Lax, L. & Brahme, A. (1982). *Rotation therapy using a novel high gradient*. Radiology, 145, 473-478.

Leung, P. M. K., Van Dyk, J. & Robins,J. (1974). *A method of large irregular field compensation*. Br J Radiol, 47, 805–810.

Mayles, P. et al (2007); *Handbook of Radiotherapy Physics theory and Practice*; Taylor and Francis group, LLC.

Mejaddem, Y., Laxz, I. & Kz, S. A. (1997). *Procedure For Accuracy Fabrication Of Tissue Compensator With High Density Materials;* Phys. Med. Biol, 42, 415-421.

University of Ghana http://ugspace.ug.edu.gh

Meyer, J., Mills, J. A., Haas, O. C., Parvin, E. M., & Burnham, K. J. (2000). *Some limitations in the practical delivery of intensity modulated radiation therapy*. Br J Radiol, 73(872), 854-63.

Nakagawa, K., Fukuhara, N. & Kawakami, H. (2005). *A packed building-block compensator (TETRIS–RT) and feasibility for IMRT delivery*. Medical Physics, **32**, 2231, doi: 10.1118/1.1929148.

Nkoll, G. F. (1989). *Radiation Detection and masuremente, second edition*; John Willei & Sons, Inc.

Oguchi, H. & Obata, Y. (2009). *Commissioning of modulator-based IMRT with XiO treatment planning system*. Med Phys, 36(1), 261-9.

Paliwal, B.R., Rommelfanger, S., & Das R. (1998). *Attenuation Characteristics of a new compensators material: thermoshield for high energy electron and photon beam.* Med. Phys., 25(4), 0094-2405.

Papiez, E. & Froeze, G. (1990). *The calculation of transmission through a photon beam attenuator using sector integration*. Med. Mhys, 17, 281-286.

Pasma, K. L, Kroonwijk, M., van Dieren, E. B, Visser, A. G., & Heijmen, B. J. M. (1999). *Verification of compensator thicknesses using a fluoroscopic electronic portal imaging*. Medical Physics, 26, 1524, doi: 10.1118/1.598648.

Podgorsak E.B. (2005), *Radiation Oncology Physics: A Handbook for Teaccher and Students*, Viena, IAEA.

Spicka J., Fleury K., & Powers, W. E. (1988). *Polyethylene-lead tissue compensators for megavoltage radiotherapy*. Med Dosim, 13, 25–27.

Srivastava, R. P. & Wagter, C. D. (2007). *The Value of EDR2 Film Dosimetry In Compensator Based Intensity Modulated Radiation Therapy*. Phys. Med. Biol, 52, N449-N457.

University of Ghana http://ugspace.ug.edu.gh

Suntharalingamn, N., Podgorsak, E.B., & Tölli H. (2005). "*Brachytherapy: physical and clinical aspects*", in: Podgorsak E.B., Radiation Oncology Physics: A Handbook for Teaccher and Students, 1st edition, Viena, IAEA.

Taherkhani, A., Mohammad M., Saboori M. S., & Changizi V. (2010). *Evaluation of the physical characteristics of cerrobend blocks used for radiotherapy*. Iran.J. Radiat. Res, 8, 93-101.

Teclehaimanot, T. H. (2014). *Evaluation of Cooper and Brass filter compensators for High Energy Photon Beams in Prowess Panther Treatment Planning System*. MPhil Thesis, University of Ghana, Accra/ Ghana.

Vaezzadeh, S., Allahverdi, M., Nedaie, H. A., Ay, M., Shirazi, A. & Yarahmadi, M. (2013); *EBT GAFCHROMICTM™ film dosimetry in compensator-based intensity modulated radiation therapy*; Medical Dosimetry, 38, 176–183.

Van Santvoort, J. P. C, Binnekamp, D., Heijmen, B. J. M. & Levendag, P. C. (1995). *Granulate of stainless steel as a compensator material*. Radiother Oncol, 34, 78–80.

Walz, B. J., Perez, C. A, Feldmann, A., Demidecki, A. J. & Powers, W. E. (1973). *Individualized compensating filters and dose optimization in pelvic irradiation*. Radiology, 107, 611–614.

Webb, S. (2001); *Intensity-Modulated Radiation Therapy*; © IOP Publishing Ltd.

Weeks, K. J, Fraass, B. A. & Hutchins KM. (1988). *Gypsum mixtures for compensator production*. Med Phys, 15,410–414.

Wilks, R. & Casebow, M. P. (1969). Tissue compensatorwith lead for Co-60 therapy. Br. J. Radiol., 42, 452-456.

Willians, J. R. & Thwaites, D. I. (2000), *Radiotherapy Physics in Practice second edition*, Oxford University Press (reprinted 2004)

Xu, T.; Shikhaliev, P. M., Al-Ghazi, M. & Molloi, S. (2002). *Reshapable physical modulator for intensity modulated radiation therapy*. Med Phys, 29, 2222–2229.

University of Ghana http://ugspace.ug.edu.gh

Yoda, K. & Aoki, Y. (2003). *A multiportal compensator system for IMRT delivery*. Medical Physics, 30, 880, doi: 10.1118/1.1567851.

Yu, M. K., Sloboda, R. S. & Murray, B. (1997). Photon beam quality at off-axis points. Med. Phys, 24, 233-9.

University of Ghana http://ugspace.ug.edu.gh

APPENDICES

APPENDIX A

(Variation of transmission (%) with thickness of cerrobend for various field sizes)

transmission (%) for different thickness of cerrobend in air										
Th (cm)	0	0.5	1.11	1.61	2.07	2.58	3.08	3.58	4.09	4.62
Fied Size(cm)										
4	100.0	80.7	58.5	45.7	37.8	29.2	23.1	19.1	15.3	13.5
6	100.0	79.6	57.8	45.1	37.5	29.0	22.9	19.0	15.2	13.4
8	100.0	79.8	58.0	45.4	37.7	29.2	23.1	19.2	15.4	13.5
10	100.0	79.9	58.2	45.6	37.9	29.4	23.3	19.3	15.5	13.7
12	100.0	79.9	58.3	45.8	38.0	29.6	23.5	19.5	15.7	13.8
14	100.0	80.0	58.6	46.0	38.3	29.9	23.7	19.7	15.9	14.0
16	100.0	80.3	58.9	46.4	38.7	30.2	24.0	20.0	16.1	14.2
18	100.0	80.4	59.2	46.7	39.0	30.5	24.3	20.3	16.3	14.4
20	100.0	80.7	59.5	47.1	39.3	30.8	24.6	20.5	16.5	14.6
22	100.0	80.9	59.8	47.4	39.7	31.1	24.9	20.8	16.7	14.7
24	100.0	81.0	60.2	47.8	40.0	31.5	25.2	21.0	17.0	14.9
26	100.0	81.2	60.4	48.0	40.3	31.7	25.4	21.2	17.2	15.1
28	100.0	81.2	60.5	48.1	40.4	31.9	25.6	21.4	17.3	15.2
30	100.0	81.1	60.4	48.1	40.4	31.9	25.6	21.4	17.3	15.2

University of Ghana http://ugspace.ug.edu.gh

APPENDIX B

(Measurements for determination of linear attenuation coefficient and scatter contribution)

Appendix B1. Output for determination of narrow and broad beam linear attenuation coefficient and for access of scatter contributions for cerrobend, SAD= 100 cm field size from 4x4 to 30x30 cm^2 in air for cobalt-60 energy

	thickness of cerrobend									
Field Size	0.0cm input(nc)	0.5cm output (nc)	1.11cm output (nc)	1.61cm output (nc)	2.07cm output (nc)	2.58cm output (nc)	3.08cm output (nc)	3.58cm output (nc)	4.09cm output (nc)	4.62cm output (nc)
4	4.709	3.799	2.756	2.151	1.782	1.377	1.088	0.901	0.721	0.634
6	4.845	3.858	2.800	2.187	1.819	1.404	1.111	0.920	0.737	0.648
8	4.900	3.911	2.844	2.226	1.849	1.432	1.133	0.940	0.754	0.664
10	4.961	3.964	2.888	2.262	1.882	1.460	1.156	0.960	0.770	0.678
12	5.025	4.015	2.932	2.301	1.911	1.487	1.181	0.980	0.788	0.693
14	5.079	4.062	2.976	2.337	1.946	1.517	1.205	1.002	0.806	0.710
16	5.122	4.111	3.019	2.375	1.980	1.547	1.230	1.023	0.825	0.726
18	5.167	4.155	3.059	2.411	2.014	1.574	1.255	1.046	0.843	0.742
20	5.201	4.196	3.096	2.447	2.046	1.602	1.279	1.067	0.861	0.757
22	5.238	4.236	3.133	2.483	2.078	1.631	1.304	1.087	0.877	0.772
24	5.268	4.266	3.170	2.517	2.108	1.658	1.328	1.107	0.895	0.786
26	5.294	4.296	3.198	2.543	2.133	1.680	1.347	1.125	0.910	0.799
28	5.316	4.314	3.215	2.559	2.146	1.694	1.358	1.136	0.920	0.808
30	5.336	4.328	3.225	2.569	2.154	1.701	1.364	1.143	0.925	0.813

University of Ghana http://ugspace.ug.edu.gh

Appendix B.2. Output for determination of narrow and broad beam attenuation coefficient for water

	output (nc) for various Thickness of water							
FS	0.0cm	2.0cm	4.0cm	6.0cm	8.0cm	10.0cm	12.0cm	14.0cm
4	4.679	4.093	3.587	3.127	2.742	2.405	2.102	1.848
6	4.756	4.168	3.658	3.195	2.803	2.461	2.155	1.894
8	4.825	4.239	3.730	3.265	2.867	2.524	2.213	1.945
10	4.871	4.311	3.805	3.337	2.941	2.590	2.275	2.004
12	4.930	4.378	3.877	3.412	3.011	2.659	2.340	2.065
14	4.987	4.443	3.947	3.484	3.081	2.732	3.407	2.129
16	5.040	4.506	4.017	3.556	3.155	2.802	3.476	2.196
18	5.085	4.566	4.082	3.628	3.223	2.869	4.545	2.260
20	5.127	4.617	4.142	3.689	3.288	2.938	4.607	2.320
22	5.166	4.666	4.199	3.748	3.352	3.001	4.666	2.382
24	5.199	4.711	4.252	3.804	3.410	3.059	2.728	2.440
26	5.225	4.751	4.298	3.854	3.464	3.112	2.780	2.493
28	5.250	4.786	4.339	3.900	3.513	3.162	2.830	2.543
30	5.274	4.815	4.376	3.938	3.555	3.206	2.878	2.588

APPENDIX C

(Scatter to primary ratio dose contribution for cerrobend in cobalt)

	Scatter - to - primary dose contribution by cerrobend/ S/P(%)								
FS/Th (cm)	0.5	1.11	1.61	2.07	2.58	3.08	3.58	4.09	4.62
6	-1.290	-1.256	-1.213	-0.809	-0.926	-0.813	-0.707	-0.620	-0.631
8	-1.065	-0.860	-0.578	-0.315	-0.053	0.045	0.252	0.493	0.583
10	-0.942	-0.525	-0.169	0.263	0.624	0.806	1.136	1.457	1.536
12	-0.953	-0.310	0.220	0.495	1.184	1.670	1.949	2.414	2.481
14	-0.846	0.126	0.750	1.241	2.107	2.680	3.177	3.622	3.829
16	-0.503	0.698	1.504	2.166	3.275	3.951	4.370	5.177	5.201
18	-0.311	1.147	2.136	2.982	4.180	5.092	5.843	6.532	6.671
20	0.021	1.715	3.006	3.976	5.316	6.371	7.200	8.080	8.141
22	0.241	2.169	3.747	4.825	6.471	7.681	8.459	9.395	9.454
24	0.389	2.794	4.566	5.758	7.623	9.068	9.853	10.971	10.765
26	0.604	3.222	5.155	6.482	8.524	10.062	11.042	12.270	12.078
28	0.608	3.338	5.398	6.672	8.998	10.578	11.739	13.080	12.921
30	0.563	3.272	5.374	6.671	8.978	10.585	11.940	13.271	13.103

University of Ghana http://ugspace.ug.edu.gh

APPENDIX D

(Measurements for determination of correction factors)

Appendix D1. Measured output with water on the surface of the phantom

Output for different thickness of BOLO ON SURFACE (nc) (at 0.5 cm DEPTH)

	one side of equivalent radiation field size(cm)								
thickness(cm)	4	6	8	18	14	18	22	26	30
0	1.497	1.537	1.573	1.604	1.657	1.703	1.741	1.771	1.795
3.5	1.327	1.387	1.433	1.473	1.538	1.591	1.635	1.667	1.694
5.5	1.197	1.263	1.318	1.362	1.436	1.183	1.540	1.575	1.604
9.5	0.936	1.006	1.068	1.122	1.207	1.274	1.326	1.367	1.398
14.5	0.685	0.748	0.805	0.853	0.946	1.018	1.073	1.118	1.152
17.5	0.568	0.624	0.678	0.729	0.848	0.883	0.906	0.952	0.986
19.5	0.497	0.548	0.595	0.643	0.722	0.787	0.843	0.886	0.921

Output for different thickness of bolos on the surface of the phantom at 4 cm depth

	one side of equivalent radiation field size(cm)								
thickness(cm)	4	6	8	10	14	18	22	26	30
0	1.327	1.387	1.433	1.473	1.538	1.591	1.635	1.667	1.694
2	1.197	1.263	1.318	1.362	1.436	1.493	1.540	1.575	1.604
6	0.936	1.006	1.068	1.122	1.207	1.274	1.326	1.367	1.398
11	0.685	0.748	0.805	0.853	0.946	1.018	1.073	1.118	1.152
14	0.568	0.624	0.678	0.729	0.848	0.883	0.906	0.952	0.986
16	0.497	0.548	0.595	0.643	0.722	0.787	0.843	0.886	0.921

Output for different thickness of bolos on the surface of the phantom at 6.0 cm depth

	one side of equivalent radiation field size(cm)								
thickness(cm)	4	6	8	10	14	18	22	26	30
0	1.197	1.263	1.318	1.362	1.436	1.493	1.540	1.575	1.604
4	0.936	1.006	1.068	1.122	1.207	1.274	1.326	1.367	1.398
6	0.835	0.903	0.963	1.014	1.103	1.172	1.225	1.267	1.300
9	0.685	0.748	0.805	0.853	0.946	1.018	1.073	1.118	1.152
12	0.568	0.624	0.678	0.729	0.848	0.883	0.906	0.952	0.986
14	0.497	0.548	0.595	0.643	0.722	0.787	0.843	0.886	0.921

University of Ghana http://ugspace.ug.edu.gh

Output for different thickness of bolos on the surface of the phantom at 10.0 cm depth									
	one side of equivalent radiation field size(cm)								
thickness(cm)	4	6	8	10	14	18	22	26	30
0	0.936	1.006	1.068	1.122	1.207	1.274	1.326	1.367	1.398
5	0.685	0.748	0.805	0.853	0.946	1.018	1.073	1.118	1.152
6	0.646	0.707	0.763	0.811	0.913	0.973	1.017	1.062	1.097
8	0.568	0.624	0.678	0.729	0.848	0.883	0.906	0.952	0.986
10	0.497	0.548	0.595	0.643	0.722	0.787	0.843	0.886	0.921

Appendix D2. Measured output with cerrobend slabs mounted on the block tray

Output for different thickness of cerrobend (nc) at 0.5 cm treatment depth									
	one side of equivalent radiation field size(cm)								
thickness(cm)	4	6	8	18	14	18	22	26	30
0	1.497	1.537	1.573	1.604	1.657	1.703	1.741	1.771	1.795
0.5	1.138	1.168	1.192	1.218	1.263	1.303	1.335	1.364	1.393
1.11	0.830	0.854	0.880	0.899	0.930	0.965	1.004	1.030	1.047
1.61	0.648	0.666	0.687	0.705	0.732	0.762	0.795	0.819	0.846
2.07	0.536	0.549	0.571	0.583	0.609	0.635	0.667	0.690	0.718
2.58	0.418	0.430	0.444	0.456	0.477	0.499	0.525	0.545	0.569
3.08	0.332	0.337	0.366	0.374	0.391	0.409	0.438	0.454	0.472
3.58	0.279	0.288	0.306	0.313	0.328	0.345	0.368	0.381	0.396
4.09	0.223	0.230	0.245	0.251	0.259	0.275	0.297	0.311	0.323
4.62	0.200	0.205	0.218	0.224	0.234	0.247	0.264	0.275	0.285

University of Ghana http://ugspace.ug.edu.gh

Output for different thickness of cerrobend (nc) at 4. 0 cm treatment depth

	one side of equivalent radiation field size(cm)								
thickness(cm)	4	6	8	18	14	18	22	26	30
0	1.327	1.387	1.433	1.473	1.538	1.591	1.635	1.667	1.694
0.5	1.016	1.061	1.099	1.124	1.176	1.220	1.258	1.290	1.316
1.11	0.746	0.779	0.807	0.824	0.866	0.904	0.937	0.966	0.988
1.61	0.594	0.628	0.648	0.647	0.680	0.714	0.742	0.767	0.787
2.07	0.499	0.523	0.540	0.539	0.571	0.593	0.616	0.640	0.661
2.58	0.389	0.406	0.420	0.402	0.448	0.464	0.486	0.505	0.526
3.08	0.312	0.332	0.343	0.350	0.370	0.384	0.402	0.412	0.429
3.58	0.260	0.277	0.287	0.292	0.310	0.321	0.338	0.349	0.364
4.09	0.207	0.223	0.232	0.237	0.252	0.261	0.274	0.279	0.294
4.62	0.185	0.198	0.204	0.212	0.224	0.234	0.244	0.249	0.262

Output for different thikness of cerrobend (nc) at 6.0 cm treatment depth

thickness(cm)	4	6	8	18	14	18	22	26	30
0	1.197	1.263	1.318	1.362	1.436	1.183	1.540	1.575	1.604
0.5	0.918	0.968	1.008	1.042	1.100	0.906	1.185	1.216	1.242
1.11	0.672	0.711	0.743	0.777	0.813	0.665	0.890	0.918	0.936
1.61	0.534	0.563	0.587	0.609	0.640	0.526	0.705	0.730	0.748
2.07	0.442	0.467	0.489	0.509	0.534	0.436	0.591	0.615	0.634
2.58	0.344	0.363	0.383	0.398	0.419	0.339	0.467	0.486	0.505
3.08	0.286	0.302	0.315	0.328	0.345	0.281	0.385	0.402	0.422
3.58	0.237	0.248	0.264	0.274	0.290	0.231	0.324	0.339	0.356
4.09	0.192	0.203	0.212	0.220	0.234	0.190	0.261	0.273	0.289
4.62	0.171	0.175	0.189	0.197	0.209	0.164	0.232	0.243	0.258

Output for different thickness of cerrobend (nc) at 10. 0 cm treatment depth

thickness(cm)	4	6	8	18	14	18	22	26	30
0	0.936	1.006	1.068	1.122	1.207	1.274	1.326	1.367	1.398
0.5	0.722	0.776	0.822	0.862	0.928	0.988	1.030	1.046	1.073
1.11	0.535	0.574	0.610	0.636	0.688	0.736	0.772	0.800	0.817
1.61	0.432	0.449	0.479	0.502	0.543	0.596	0.626	0.634	0.658
2.07	0.366	0.379	0.398	0.419	0.448	0.501	0.526	0.523	0.548
2.58	0.285	0.291	0.312	0.324	0.351	0.392	0.415	0.416	0.438
3.08	0.228	0.239	0.254	0.266	0.289	0.321	0.339	0.332	0.348
3.58	0.191	0.200	0.213	0.224	0.243	0.269	0.283	0.277	0.297
4.09	0.152	0.161	0.170	0.181	0.196	0.216	0.229	0.224	0.241
4.62	0.135	0.144	0.152	0.161	0.174	0.192	0.201	0.193	0.210

University of Ghana http://ugspace.ug.edu.gh

Output for different thickness of cerrobend (nc) at 15. 0 cm treatment depth

thickness(cm)	4	6	8	18	14	18	22	26	30
0	0.685	0.748	0.805	0.853	0.946	1.018	1.073	1.118	1.152
0.5	0.535	0.584	0.626	0.670	0.734	0.789	0.834	0.871	0.900
1.11	0.394	0.431	0.470	0.502	0.548	0.591	0.626	0.658	0.687
1.61	0.314	0.343	0.368	0.394	0.432	0.470	0.498	0.525	0.554
2.07	0.260	0.284	0.303	0.325	0.363	0.394	0.413	0.437	0.464
2.58	0.202	0.220	0.238	0.254	0.287	0.312	0.327	0.347	0.373
3.08	0.168	0.180	0.198	0.209	0.235	0.256	0.268	0.283	0.310
3.58	0.141	0.153	0.165	0.175	0.197	0.214	0.224	0.239	0.262
4.09	0.116	0.124	0.132	0.140	0.159	0.171	0.179	0.192	0.215
4.62	0.104	0.113	0.119	0.125	0.139	0.151	0.158	0.171	0.190

Output for different thickness of cerrobend (nc) at 18. 0 cm treatment depth

thickness(cm)	4	6	8	18	14	18	22	26	30
0	0.568	0.624	0.678	0.729	0.848	0.883	0.906	0.952	0.986
0.5	0.448	0.492	0.517	0.555	0.653	0.682	0.710	0.737	0.775
1.11	0.332	0.366	0.390	0.419	0.492	0.513	0.533	0.566	0.591
1.61	0.265	0.290	0.315	0.330	0.396	0.414	0.426	0.453	0.484
2.07	0.220	0.238	0.257	0.275	0.334	0.348	0.357	0.380	0.407
2.58	0.174	0.190	0.202	0.217	0.264	0.275	0.282	0.302	0.329
3.08	0.144	0.158	0.159	0.171	0.214	0.220	0.231	0.243	0.266
3.58	0.122	0.134	0.131	0.142	0.177	0.185	0.193	0.202	0.226
4.09	0.100	0.107	0.107	0.115	0.144	0.150	0.157	0.165	0.187
4.62	0.089	0.098	0.094	0.101	0.125	0.131	0.138	0.144	0.163

Output for different thickness of cerrobend (nc) at 20. 0 cm treatment depth

thickness(cm)	4	6	8	18	14	18	22	26	30
0	0.497	0.548	0.595	0.643	0.722	0.787	0.843	0.886	0.921
0.5	0.392	0.431	0.469	0.504	0.561	0.615	0.659	0.696	0.720
1.11	0.292	0.321	0.349	0.376	0.423	0.462	0.495	0.527	0.558
1.61	0.238	0.262	0.276	0.298	0.341	0.372	0.399	0.427	0.458
2.07	0.199	0.219	0.230	0.230	0.284	0.311	0.334	0.359	0.386
2.58	0.155	0.171	0.181	0.194	0.225	0.246	0.265	0.285	0.313
3.08	0.128	0.139	0.149	0.160	0.187	0.201	0.217	0.231	0.257
3.58	0.108	0.117	0.126	0.136	0.157	0.169	0.181	0.193	0.218
4.09	0.090	0.096	0.104	0.111	0.128	0.138	0.124	0.156	0.178
4.62	0.078	0.086	0.092	0.113	0.114	0.123	0.131	0.138	0.157

University of Ghana http://ugspace.ug.edu.gh

APPENDIX E

(Measurements of gray vaor for Film calibration)

Appendix E1. Measured gray value for film calibration

	gray Valor			
dose(cGy)	RD1	RD2	RD2	mean gray valor
0	119.724	119.395	119.395	119.56
100	65.957	68.446	68.782	67.728
150	58.448	59.962	58.768	59.059
200	52.59	52.216	51.643	52.15
250	48.073	49.384	48.498	48.652
300	43.117	44.638	43.707	43.821
350	38.233	40.151	41.379	39.921

APPENDIX F

(Calculated cerrobend thickness compensators constructed for verification using equation 3.04, with and without normalization thickness ratio correction factor, in Appendixs F1, F2, F3)

Appendix F1. Flat compensator 1.5 mm cerrobend thickness

depth in pls	Thick. bolus(cm)	Depth (cm)	FS	F_S	F_d	T_{drSr}	t_c
4	20	4.54	10.00	1.00	0.37	0.02	0.15

Appendix F2. Flat compensator 4.3 mm cerrobend thickness

depth in pls	Thick. bolus(cm)	Depth (cm)	FS	F_S	F_d	T_{drSr}	t_c
6	20	6.82	14.00	0.81	1.34	0.02	0.43

Appendix F3. Step compensator (with step of 1mm and 3.0 mm) cerrobend thickness

depth in pls	Thick. bolus(cm)	Depth (cm)	FS	F_S	F_d	T_{drSr}	t_c
10	15	11.36	10	1.00	1.77	0.01	0.31
10	10	11.36	10	1.00	1.77	0.01	0.10

University of Ghana http://ugspace.ug.edu.gh

Appendix F4. Step compensator (with step of 0.5cm, 1.0cm and 1.5cm cerrobend thickness) constructed with including the normalization correction factor

dep. Plas.	Thic.(b)	Depth (cm)	FS	F_S	F_d	T_{drSr}	F_{Tb}	t_c
7	16.18	7.952	15	0.76	1.77	0.01	5.10	1.50
7	14.85	7.952	15	0.76	1.77	0.01	4.32	1.00
7	12.78	7.952	15	0.76	1.77	0.01	3.27	0.50

University of Ghana http://ugspace.ug.edu.gh

APPENDIX G

(Measurements for dosimetric verification)

Appendix G1. Off-axis dose profile for flat compensator 1.5 mm cerrobend thickness constructed without including normalization thickness ratio correction factor.

off-axis(cm)	Gray valor				Dose (cGy)		
	RD1	RD2	RD3	mean gray valor	measured	TPS	%
4	40.88	38.54	37.97	39.13	368.08	185.93	±97.97
2	38.67	38.58	39.24	38.83	373.09	197.85	±88.57
0	39.07	38.49	38.80	38.79	373.83	200.10	±86.82
-2	39.42	38.86	40.07	39.45	362.79	197.85	±83.37
-4	41.47	40.96	40.28	40.90	339.80	185.93	±82.75

Appendix G2. Off-axis dose profile for flat compensator 4.3 mm cerrobend thickness without including normalization thickness ratio correction factor

Off-axis (cm)	gray valor				DOSE(cGy)		
	RD1	RD2	RD3	mean gray value	measured	TPS	%Error
4	41.27	41.13	41.13	41.20	335.29	193.79	±73.01
2	41.87	40.36	40.36	41.12	336.58	198.57	±69.50
0	41.70	39.93	39.93	40.81	341.22	200.06	±70.56
-2	42.00	41.10	41.10	41.55	330.06	198.57	±66.22
-4	41.46	40.89	40.89	41.18	335.63	193.79	±73.19

University of Ghana http://ugspace.ug.edu.gh

Appendix G3. Off-axis dose profile for step compensator (with step of 1mm and 3.0 mm) cerrobend thickness field size 10cmx10cm at 4.54 cm treatment depth (without normalization thickness ratio correction factor)

	gray valor				DOSE(cGy)		
off-axis(cm)	RD1	RD2	RD3	mean gray value	measured	TPS	%Error
4	41.97	42.58	44.35	42.97	309.68	206.84	±49.72
3	40.01	39.68	40.76	40.15	351.56	194.22	±81.01
2	41.99	41.24	41.93	41.72	327.55	197.67	±65.71
1	41.81	40.67	41.64	41.37	332.70	199.41	±66.84
0	41.95	40.23	42.80	41.66	328.45	200.00	±64.22
-1	41.20	40.06	42.75	41.34	333.24	199.41	±67.11
-2	42.30	40.54	42.65	41.83	325.93	197.67	±64.89
-3	41.45	40.19	41.91	41.18	335.60	194.22	±72.79
-4	39.95	39.86	40.58	40.13	351.86	239.32	±47.03

Appendix G4. Off-axis dose profile for step compensator (with step of 0.5cm, 1.0cm and 1.5cm) cerrobend thickness constructed with including normalization correction factor with film dosimetry, radiation field size 10 cm x 10 cm, at treatment depth of 8 cm

	Gray valor				dose(cGy			
Off-axis (cm)	RD1	RD2	RD3	mean gray value	measured	TPS	Abs. Diff.	%Error
6	54	54.59	54.34	54.31	186.18	216.82	30.64	±14.13
4	51.87	51.16	52.88	51.97	206.86	212.82	5.96	±2.80
2	52.99	53.07	52.67	52.91	198.34	201.75	3.41	±1.69
0	54.98	55.65	55.67	55.43	177.02	199.57	22.55	±11.30
-2	55.52	55.52	55.52	55.52	176.3	201.75	25.45	±12.61
-4	54.91	54.23	57.52	55.55	176.07	210.59	34.52	±16.39
-6	51.92	52	55.05	52.99	197.62	214.04	16.42	±7.67

Appendix I1. Central-axis dose profile for step compensator (with step of 0.5cm, 1.0cm and 1.5cm) constructed with including normalization correction factor with ionization chamber dosimetry, radiation field size 10 cm x 10 cm, at treatment depth of 8 cm

P1(KPa)	P2(KPa)	AV.P(KPa)	T1	T1	ave.T	Dose(cGy)/charge(nc)
101.45	101.5	101.475	23	23	23	94.930

RD1(nc)	RD2(nc)	RD3(nc)	Av.RD (nc)	Corr.RD(nc)	Dose (cGy)		
					measured	TPS	%Error
1.861	1.861	1.861	1.861	1.877	178.208	199.57	±10.704